# Novel studies of McMurdo Dry Valleys ice-cemented permafrost cores document chemical weathering in permafrost and the timing of Plio-Pleistocene glaciations

Nicolas Cuozzo

A dissertation submitted in partial fulfillment of the requirements for the degree of

Doctor of Philosophy

University of Washington

2021

Reading Committee:

Ronald S. Sletten, Chair

Fang-Zhen Teng

Bernard Hallet

John Stone

Program Authorized to Offer Degree:

Department of Earth and Space Sciences

University of Washington

## Abstract

Novel studies of McMurdo Dry Valleys ice-cemented permafrost cores document chemical weathering in permafrost and the timing of Plio-Pleistocene glaciations

Nicolas Cuozzo

Chair of the Supervisory Committee:

Research Associate Professor Ronald S. Sletten

Department of Earth and Space Sciences

The McMurdo Dry Valleys (MDV) are a frigid, hyperarid desert of Antarctica with a landscape dominated by ice-rich permafrost. This research focuses on using two ice-rich permafrost cores collected from the MDV to study chemical processes (Beacon Valley core) and the timing of MDV Plio-Pleistocene glaciations (Victoria Valley core). In the 30-m Beacon Valley core, Mg isotopes and other geochemical data document that active weathering occurs in permafrost at temperatures well below 0°C. The weathering intensity correlates with the modeled unfrozen water content due to freezing point depression as ions are excluded and concentrated. The concept of a eutectic active zone is suggested based on the presence of unfrozen water at subzero temperatures. It is also documented that heavy Mg isotopes are fractionated into precipitating

salts, onto the cation exchange complex, and into clay minerals that form in the Beacon Valley core. Using the Mg isotopic composition and a mass balance based on the distribution of Mg in each of these reservoirs, this work reveals that chemical weathering estimations were significantly underestimated when not accounting for secondary mineral formation in the Beacon Valley core. Another noteworthy finding is that the fractionation factor determined for saponite, the dominant secondary clay mineral in the Beacon Valley core, was 0.83‰, and is lower than previously published estimates. Saponite is also the primary Mg-bearing mineral that forms during low-temperature alteration of ocean crust and helps constrain the global Mg budget. The fractionation factor determined in this study suggests that previous calculations overestimated the amount of Mg removed from the ocean during saponite formation. A separate 15-meter ice-cemented permafrost core collected in Victoria Valley provides a novel paleoenvironmental record that is used to interpret the glacial history of the MDV. The core contains three glaciogenic deposits (from bottom to top: Unit 1, 2 and 3) based on the stratigraphic record, oxidized paleosol horizons, carbonate-coated clasts, salt content and composition, and stable isotopes. Cosmogenic nuclides, $^{26}$Al and $^{10}$Be, were measured in quartz along the depth of the core. Based on forward modeling of the shielding history, the ages of the deposits and the periods of glacial cover are determined. The model suggests that glaciers covered Victoria Upper Valley for at least 3.9 Ma years before depositing Unit 1 approximately 0.7 Ma, suggesting a Plio-Pliestocene glacial event. Unit 2 was deposited ~ 0.66 Ma ago during the retreat of the glacier. During the mid-to-late Pleistocene, Victoria Upper Glacier readvanced into Victoria Upper Valley and covered Unit 2 for ~ 0.23 Ma, and finally deposited Unit 3 approximately 10,000 years ago. The deepest unit in the core, Unit 1, is interpreted as a wet-

based glacial till and provides the best age constraint for wet-based glaciation during the late Pliocene to early Pleistocene in the MDV.

# Table of Contents

## List of Figures

## List of Tables

# Chapter 1 – Introduction

## 1.1 Overview and Background

Permafrost-affected regions make up 24% of exposed land in the Northern hemisphere (Anisimov et al., 2007; Brown et al., 1997; Brown et al., 2002) and up to 25% of the Antarctic region (Bockheim, 1995). The interest in understanding chemical and geological processes in permafrost is widespread due to their ability to serve as proxy for paleoclimate (Stuiver et al., 1981), and their preservation of sediment and salt accumulation over time (Campbell and Claridge, 1987; Claridge and Campbell, 1977) . A novel place to study permafrost dynamics and processes is the McMurdo Dry Valleys. The McMurdo Dry Valleys (MDV) are one of the few ice-free and permafrost-affected regions in the Antarctic and one of the only regions on Earth where the average daily temperature rarely rises above zero degrees. The MDV were first investigated by Scott's expedition to reach the South Pole (Scott, 1907) and since then, detailed investigations have been untaken to understand long-term accumulations and distributions of salt deposits (Campbell and Claridge, 1969; Claridge and Campbell, 1968, 1977; Keys and Williams, 1981), long-term weathering processes (Claridge and Campbell, 1984; Gibson et al., 1983a; Ugolini, 1986), and the origin and timing of glacial deposits and moraines that blanket the valley's surfaces (Calkin, 1964, 1971; Denton et al., 1984; Prentice et al., 1993; Prentice et al.,

1998a; Webb et al., 1984). Here, we use deep ice-cemented permafrost cores collected from Beacon Valley and Victoria Valley to investigate the subsurface processes of these ancient environments and provide constraints on chemical weathering and the glacial history of this region.

### 1.1.1 Salt Accumulations and Magnesium Isotopes

One of the defining features of the MDV is extensive salt accumulations throughout the soil profile (Claridge and Campbell, 1977; Keys and Williams, 1981). Major anions ($Cl^-$, $SO_4^{2-}$, and $NO_3^-$) were found to be sourced from the transport of marine-derived aerosols and oxidation of reduced gaseous sulfur and nitrogen compounds. Major cations ($Ca^{2+}$, $K^+$, $Mg^{2+}$, and $Na^+$) accumulate over time from the transport of marine aerosols, and chemical weathering of ferromagnesian minerals (Bao et al., 2000; Keys and Williams, 1981; Michalski et al., 2005). Many chemical weathering studies have focused on shallow subsurface and wetter regions in the MDV, such as hyporheic zones, lake water, and streams and have provided evidence of chemical alteration of rocks. (Dickinson and Grapes, 1997; Dowling et al., 2013; Gibson et al., 1983a; Heindel et al., 2018; Jones and Faure, 1978; Leslie et al., 2014; Lyons et al., 2017; Marra et al., 2017; Maurice et al., 2002; Tamppari et al., 2012a; Wentworth et al., 2005; Witherow et al., 2010) However, there are no studies analyzing chemical weathering in deep permafrost soil profiles.

Magnesium isotopes are helpful for studying rock-water interactions (Huang et al., 2012; Liu et al., 2014; Ma et al., 2015; Opfergelt et al., 2014; Opfergelt et al., 2012; Teng et al., 2010; Tipper et al., 2012a; Tipper et al., 2010; Tipper et al., 2012b; von Strandmann et al., 2008) because of their fractionation properties (De Villiers et al., 2005; Galy et al., 2002). Large mass-

dependent fractionation can occur during low-temperature chemical reactions, including chemical dissolution, salt precipitation, cation-exchange, and clay mineral formation. Understanding the direction and degree of fractionation is critical for tracing these processes. Furthermore, the ice-cemented permafrost prevents leaching of water and holds weathering products in place, allowing for a comprehensive analysis of equilibrium fractionation of all Mg components in the system.

### 1.1.2 MDV Glacial and Climate History

The past stability of the East Antarctic Ice Sheet (EAIS) remains an important, unanswered question. Efforts to address this question are focused on EAIS stability during the Pliocene (5.33-2.58 Ma), a period characterized by $CO_2$ values comparable to today's values (Bartoli et al., 2011; Pagani et al., 2010; Seki et al., 2010) and global mean temperatures similar to those predicted for the end of the century (Austermann et al., 2015; Dowsett et al., 2012). While the marine record from the Antarctic Geologic Drilling Project (ANDRILL) and accompanying models suggest a dynamic EAIS during the Pliocene (Scherer et al., 2008; Scopelliti et al., 2013; Scopelliti et al., 2011), The McMurdo Dry Valleys (MDV) are home to some of the most well-preserved geologic records of Antarctic glaciation and are frequently used to understand past dynamics of the EAIS (Armstrong, 1978; Armstrong et al., 1968; Bockheim and McLeod, 2008; Bockheim and McLeod, 2013; Brook et al., 1993; Brown et al., 1991; Denton et al., 1971; Denton et al., 1984; Denton et al., 1993; Hall et al., 1993; Hall et al., 2002; Higgins et al., 2000; Prentice et al., 1998a; Schäfer et al., 2000; Staiger et al., 2006a; Swanger et al., 2019; Swanger et al., 2017; Swanger et al., 2011b). Providing further constraints and

providing stratigraphic context on these deposits by using deep permafrost cores can help answer the question of EAIS stability during warmer and wetter conditions.

## 1.2 Research Objectives

The two key objectives of my dissertation are to use the geochemical and sediment records preserved in ice-rich permafrost of the MDV to understand: (1) chemical weathering in subzero temperature environments, and (2) the glacial history of the MDV during warmer and wetter conditions. The three main chapters are described below.

Chapter 1 provides direct evidence of chemical weathering at subzero temperatures in a 30-meter ice-rich permafrost collected in Beacon Valley. The evidence of chemical weathering is documented in the composition of the permafrost sediment and ice, the Mg isotopic composition of the thawed permafrost ice, and pH values. The major control of chemical weathering appears to be the unfrozen water content that is modeled as a function of ionic composition and temperature.

Chapter 2 further leverages the unique environment of the MDV where weathering products are locked in the ice over potentially million-year timescales to understand the influence of secondary mineral formation on the Mg isotopic composition of the Beacon Valley core. This works reveals that secondary minerals strongly influence the Mg isotopic composition in permafrost. Furthermore, the most abundant Mg-bearing clay mineral identified in the core, saponite, is also the primary Mg-bearing mineral that forms in the oceanic crusts and acts as a sink for Mg in the global ocean budget. Therefore, the large Mg fractionation determined for saponite within the core can have implications for the global Mg budget.

Chapter 3 analyzes a 15-meter core permafrost core as a novel proxy to interpret and date glacial deposits in Upper Victoria Valley, and provides evidence of a wet-based glacial event during the late Pliocene to early Pleistocene in Victoria Valley. Using sedimentological and geochemical evidence, we interpret the depositional environment of three distinct glaciogenic deposits identified within the core. A multi-isotope ($^{26}$Al and $^{10}$Be) cosmogenic nuclide approach is used to model burial and exposures scenarios to provide age constraints of the depositional units and timing of glaciation.

# Chapter 2: Silicate Weathering in Antarctic Ice-rich Permafrost: Insights Using Magnesium Isotopes

The content of this chapter was published in

Geochimica et Cosmochemica Acta in 2020 with authors N. Cuozzo R.S. Sletten, Y. Hu, L. Liu, F.Z. Teng, and B. Hagedorn

## 2.1 Abstract

This study reports that substantial chemical weathering occurs at subzero temperatures in ice-and-salt-rich permafrost in the McMurdo Dry Valleys, Antarctica. Chemical weathering is documented in a 30.0-meter core collected in Beacon Valley by measuring the ionic composition, pH, and Mg isotopes of water extracted from thawed ice-rich sediment. Evidence of rock weathering is revealed by coinciding increases in the Mg isotopic composition and pH values. The primary factor that controls weathering is the salt content that leads to unfrozen brine; this is most apparent in the upper 7.0 meters where the salt content is high, temperatures rise above -21°C and the modeled unfrozen water reaches up to 4.0% of ice-content. In the upper 7.0 meters, up to 60% of soluble Mg in the thawed permafrost ice is sourced from Ferrar Dolerite ($\delta^{26}$Mg = -0.22 ± 0.07‰) weathering, resulting in $\delta^{26}$Mg values ranging from of -0.82 ± 0.05‰ to -0.64 ± 0.05‰. Below 7.0 meters, temperatures remain below -21°C, unfrozen water is less than 2.0% of ice-content, and on average, 5% of soluble Mg is sourced from dolerite weathering with $\delta^{26}$Mg values ranging from -1.05 ± 0.05‰ to -0.76 ± 0.05‰. Regions of the core that are modeled to have no unfrozen water show little or no evidence of chemical weathering and relatively constant $\delta^{26}$Mg values close to Taylor Glacier and Beacon Valley snowfall values

(-0.93 ± 0.06‰). This study demonstrates that significant chemical weathering occurs at subzero temperatures in permafrost where liquid brines form.

## 2.2 Introduction

The McMurdo Dry Valleys (MDV) are among the coldest and driest regions on Earth and one of the few ice-free regions in Antarctica. The environmental setting of the MDV is severe, with average summer and winter temperatures below 0°C, average precipitation less than 100 mm $yr^{-1}$ in the form of snowfall (Bromley, 1985; Doran et al., 2002; Fountain et al., 2010), no vascular plants (Alberdi et al., 2002), and landscapes dominated by ice-rich permafrost. Chemical weathering in permafrost environments such as the MDV is of interest because while permafrost is widespread, making up 24% of exposed land in the Northern hemisphere (Zhang et al., 1999) and around 25% of the Antarctic region (Bockheim, 1995; Schaefer et al., 2017), chemical weathering is not well documented in these environments, particularly in the Antarctic as it is less accessible and less studied compared to the northern hemisphere. Furthermore, they are considered one of the closest terrestrial analogs to the martian environment and can be used to better understand weathering processes occurring in similar conditions on Mars (Anderson et al., 1972; Dickinson and Rosen, 2003; Gibson et al., 1983a; Heldmann et al., 2013; Wentworth et al., 2005).

Previous studies on chemical weathering in the MDV have found extensive salt accumulations, as is common in desert landscapes. Claridge and Campbell (1977) and Keys and Williams (1981) found major cations ($Na^+$, $Ca^{2+}$, $Mg^{2+}$, and $K^+$) accumulated over time from transport and deposition of marine aerosols and chemical weathering, with Mg concentrations particularly enriched in soils formed on dolerite parent material. Major anions ($Cl^-$, $SO_4^{3-}$, and

$NO_3^-$) were found to be sourced from transport of marine aerosols and oxidation of reduced gaseous sulfur and nitrogen compounds (Bao et al., 2000; Michalski et al., 2005). Further studies have looked at solutes (Green et al., 1988; Lyons and Mayewski, 1993; Nezat et al., 2001) and isotopic composition, including Sr, Li, B, and Ca, (Dowling et al., 2013; Jones and Faure, 1978; Leslie et al., 2014; Lyons et al., 2017; Witherow et al., 2010) of lake waters, streams, and hyporheic zone sediments. These studies have suggested that silicate weathering must occur to explain the water composition in these regions. Physical evidence of rock and sediment alteration (< 1 m) in the hyporheic zone are also documented in the MDV (Dickinson and Grapes, 1997; Gibson et al., 1983b; Heindel et al., 2018; Marra et al., 2017; Maurice et al., 2002; Tamppari et al., 2012b; Wentworth et al., 2005). While most of these studies focused on weathering in wetter regions at shallow depths in the MDV (streams, lakes, and hyporheic zones), only one study (Dickinson and Rosen, 2003) has looked at weathering processes in a deep permafrost profile using oxygen isotopes and ionic composition; however, they did not quantify the degree of weathering that occurs.

Magnesium isotopes have been used to study chemical weathering in soils (Huang et al., 2012; Liu et al., 2014; Ma et al., 2015; Opfergelt et al., 2014; Opfergelt et al., 2012; Teng et al., 2010; Tipper et al., 2012a; Tipper et al., 2010; Tipper et al., 2012b; von Strandmann et al., 2008; von Strandmann et al., 2012) and they can provide an estimate on the degree of weathering because of their fractionation properties (De Villiers et al., 2005; Galy et al., 2002; Liu et al., 2014). Large mass-dependent fractionation of Mg isotopes can occur during low-temperature chemical weathering reactions, including dissolution, precipitation, and cation exchange (see review of Teng (2017) and references therein). During chemical weathering, light Mg isotopes are preferentially released from silicate rocks to river waters, which end up in the ocean. This

process results in a homogeneous and significantly lighter Mg isotopic composition of seawater ($\delta^{26}$Mg = -0.83‰ ± 0.09‰, Ling et al. (2011)), leaving variably heavier weathered residues in the upper continental crust ($\delta^{26}$Mg = -0.22‰, Li et al. (2010)). The distinct isotopic values of these two reservoirs provide a tool to look at the mixing between Mg in the MDV derived from a seawater source (snowfall and glacial ice), and a crustal silicate source (Ferrar Dolerite), and insight towards the degree of weathering.

The study presented here analyzes for Mg isotopes, pH, and ionic composition of water and sediment extracted from a thawed 30.0 m permafrost core collected in Beacon Valley. The chemical data are used to model the unfrozen water content and to quantify the contribution of Mg due to dolerite weathering in the MDV permafrost. Our results reveal that significant silicate weathering occurs in subzero salt-rich ice-cemented permafrost environments and this finding provides new insights into weathering processes in ice-cemented permafrost on Earth, as well as serving as an analog for weathering in martian permafrost.

## 2.3 Study Site

### 2.3.1 Beacon Valley, Antarctica

The MDV are a hyperarid, polar desert that remain free of ice-cover as a result of the high threshold of the Transantarctic Mountains, which divert ice from the East Antarctic Ice Sheet away from McMurdo Sound, and the Wilson Piedmont Glacier, which isolates the valleys from the Ross Sea and acts as a blockade to snow entering them (Chinn, 1990; Hall and Denton, 2002). Beacon Valley is one of the southern-most Dry Valleys, trending northeast-southwest and covering an area approximately 3 km wide and 12 km long (Figure 2.1). Average annual

temperatures are around -22.9°C (Liu et al., 2015) with less than 100 mm/yr of precipitation in the form of snowfall (Fountain et al., 2010). The lower valley on its northeast end is bounded by Taylor Glacier, an East Antarctic Ice Sheet outlet glacier. Bedrock in Beacon Valley consists of Devonian to Jurassic Beacon Group sandstones, siltstones, and shales, with sills and dikes of tholeiitic Jurassic Ferrar Dolerite (McElroy and Rose, 1987).

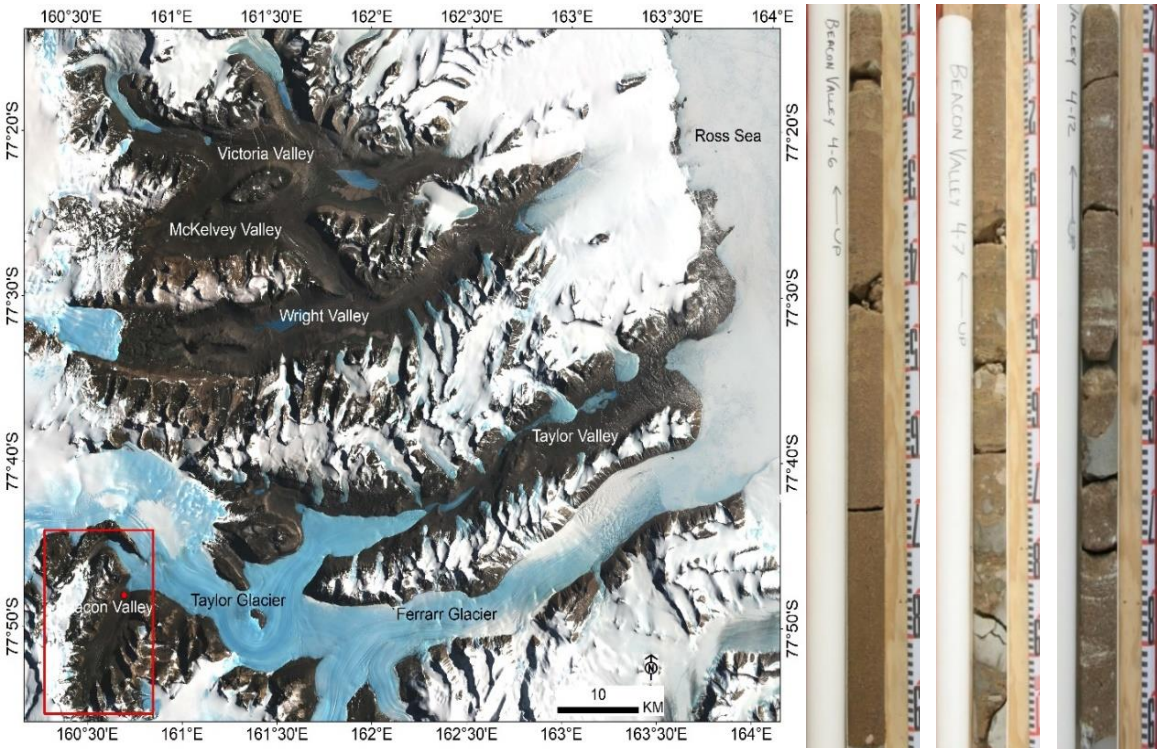


Figure 2.1: (A) Landsat Image of Mosaic of the MDV (available at http://lima.usgs.gov/), with the location of the site (red dot) where the 30-meter ice-cemented permafrost core was collected; (B) Meter sections of the ice-cemented permafrost core (6 m, 7 m, and 12 m from left to right).

The ice-cemented permafrost core analyzed in this study was collected in the lower Beacon Valley (77°48'11.4"S, 160°42'49.8"E) as described below. The surface of Beacon Valley is covered by patterned ground with polygonal diameters of 10 to 20 m and the core was collected in the center of a polygon, which is thought to be the most stable region (Linkletter et al., 1973; Sletten et al., 2003). Sediment in the Beacon Valley core is composed mostly of sand-

sized grains of quartz and dolerite that are cemented by an ice-rich matrix. Sediment is massive and shows no evidence of stratification or facies changes. The sediment is believed to be sourced from glacial deposits and aeolian processes (Bockheim et al., 2009; Diaz et al., 2018), and based on modeled sublimation rates, the sediment age is estimated to be at least 1 Ma (Liu et al., 2015).

## 2.4 Methods

### 2.4.1 Sample Collection

A 30.0-m ice-cemented permafrost core was collected in lower Beacon Valley in 2008 and stored in a -30.0°C freezer at the University of Washington, Seattle. Drilling began 0.4 m below the surface at the top of the ice-cemented permafrost. The upper 0.4 m consists of dry permafrost and was sampled separately. The permafrost core was cut into subsamples at 0.1 to 0.3 m intervals along its depth using a carbide-tipped band saw. The frozen sediment samples were then thawed overnight in a refrigerator in sealed polyethylene bags. The meltwater was extracted from the thawed sediments by centrifuging in a double-bottom centrifuge cup (a perforated cup fitted with a 0.45 μm Nucleopore filter followed by a closed cup). The total ice content of each sample was determined gravimetrically. Large clasts of dolerite were collected from the Beacon Valley surface and sampled from the core at 0.6 and 2.2 m. Taylor Glacier Ice from an archived core (Nirvana) (Pettit et al., 2014) collected near the terminus to Taylor Valley, as well as fresh Beacon Valley snowfall collected in the field were thawed and analyzed. Analyses were performed on three sets of samples: (1) water collected from thawed permafrost ice from the 30-m core, (2) permafrost sediment isolated from the 30-m core, and (3) thawed glacial ice and snow.

### 2.4.2 Compositional Analysis

The soluble salts in the thawed permafrost ice, thawed glacial ice, and thawed snow samples were analyzed for major cations ($Ca^{2+}$, $Mg^{2+}$, $Na^{+}$, $K^{+}$) using Inductively Coupled Plasma Optical Emission Spectroscopy (ICP-OES) (Perkin Elmer® Optima 3300 DV), major anions ($Cl^{-}$, $F^{-}$, $SO_4^{2-}$, $NO_3^{-}$) using Ion Chromatography (IC) (Dionex® ICS 2500), and pH using a WTW pH probe fitted with a SenTix 41 pH/temperature probe. The elemental composition of the < 2mm fraction of permafrost sediment and bulk rock samples was determined using a ThermoARL X-ray Fluorescence Spectrometer (XRF) at the GeoAnalytical Lab at Washington State University. The weathered rind of the bulk rock samples was removed and only the unweathered rock was used for analysis. The < 2mm fractions of permafrost sediment were powdered and analyzed for their mineralogy using Rigaku MiniFlex 600 benchtop X-ray diffractometer (XRD) with a D/teX high-speed detector and Co Kα radiation. Data were collected at a step size of 0.02° per minute step counting rate, from 2 to 80 degrees 2θ at 15 mA and 40kV in the X-ray Diffraction Laboratory located at NASA Johnson Space Center. Samples were prepared in aluminum holders, and the XRD instrument was operated under ambient conditions and calibrated with the National Institute of Standards and Technology (NIST) silicon standard, and a NIST lanthanum hexaboride standard is used to characterize the instruments line broadening function. Rietveld refinement was carried out using MDI Jade Software with initial structure parameters for crystalline phases from the RRUFF database. Background patterns were fit by a polynomial and peaks were modeled by a pseudo-Voigt profile function. Pattern overlays of standard phyllosilicates (Clay Mineral Repository) with known RIR and FWHM were used in Rietveld Refinements to estimate abundances of phyllosilicates in bulk samples.

### 2.4.3 Temperature measurements

A long-term record of hourly temperatures is being recorded in a polygon adjacent to the one that was cored in Beacon Valley at depths of 1.25, 2.5, 5.0, 10.0, 20.0, and 30.0 meters. The temperatures are measured using a Campbell CR10X-2M data logger with Campbell 107 thermistor temperatures probes. The yearly maximum and minimum temperature for each depth is then interpolated to create a maximum and minimum temperature at each sampling depth.

### 2.4.4 Geochemical Modeling

The equilibrium thermodynamic models, PHREEQC (Version 3 using ColdChem database) and FREZCHEM (Version 13.2), were used to model the unfrozen water content and secondary salt precipitation at each sample depth of the core based on the chemical composition of the thawed permafrost ice and using the interpolated maximum temperature. As the water freezes, ions are excluded from the ice phase and concentrate in the water, thereby depressing the freezing point of the brine (Low et al., 1968; Tice et al., 1985). PHREEQC and FREZCHEM use Pitzer equations to model these high ionic strength solutions and are capable of modeling freezing of concentrated solutions down to -70°C (Marion and Grant, 1994).

### 2.4.5 Particle Size Analysis

Particle size analysis was performed on ~ 1 g permafrost sediment samples. Samples were split using a sample splitter to avoid sampling bias and analyzed using a laser diffraction particle size analyzer (Beckman Coulter LS 13-320). Samples were dispersed using an ultrasonic probe with the addition of 5mL of 0.05% sodium bicarbonate sodium hexametaphosphate to keep the samples in suspension. Each sample was analyzed three times for reproducibility.

### 2.4.6 Magnesium Isotope Analysis

Magnesium isotopes were analyzed in water samples from the thawed permafrost ice of the core, Beacon Valley snowfall, and Taylor Glacier ice. In addition, dolerite samples collected from the core and the surface of Beacon Valley were analyzed. Rock digestion, chemical separation, and isotopic analysis were performed at the Isotope Laboratory at the University of Washington, following the methods detailed in Teng et al. (2007) and Yang et al. (2009). The rocks were sampled to avoid any weathering rinds, crushed into a powder, and dissolved sequentially using Optima-grade concentrated HF-$HNO_3$, $HNO_3$-HCl, and $HNO_3$. The water samples were evaporated to contain 5-40 µg Mg. Separation of Mg was achieved by loading 100 µL of sample dissolved in 1 N $HNO_3$ on a cation exchange chromatography column containing pre-cleaned Bio-Rad AG50W-X8 resin (200-400 mesh) and was eluted using sequential additions of 1 N $HNO_3$. This procedure is repeated twice for each sample to ensure purification.

Magnesium isotopic ratios were measured on a Nu Plasma II Multi-Collector-ICP-MS using standard-sample bracketing (alternating measurements of samples and standards) for correction of instrumental fractionation (Teng and Yang, 2014). Magnesium isotopic data are reported in delta (δ) notation, which represents parts per thousand (‰) deviations of the ratio between the sample and standard, where X refers to mass 25 or 26:

$$\delta^{x}\mathrm{Mg}\ (‰) = 1000 \times \left\{ \frac{\left( {}^{x}\mathrm{Mg}/{}^{24}\mathrm{Mg} \right)_{\mathrm{sample}}}{\left( {}^{x}\mathrm{Mg}/{}^{24}\mathrm{Mg} \right)_{\mathrm{DSM3}}} - 1 \right\}$$

The accuracy of the analysis was assessed using two in-house standards (Hawaiian Seawater and San Carlos Olivine) and two USGS rock standards (BHVO Basalt and MAG-1 Marine Mud). The results of these standards (Table 2.1) agree with recommended values (Hu et al., 2016; Teng et al., 2015).

Table 2.1: Magnesium isotopic composition of standards run between the samples

| Standard | n | $\delta^{26}$Mg | 2SD | $\delta^{25}$Mg | 2SD |
|---|---|---|---|---|---|
| Hawaii Seawater (in-house) | | -0.88 | 0.05 | -0.45 | 0.05 |
| | | -0.89 | 0.05 | -0.46 | 0.04 |
| | | -0.88 | 0.05 | -0.46 | 0.04 |
| | | -0.86 | 0.05 | -0.44 | 0.06 |
| | | -0.92 | 0.06 | -0.51 | 0.05 |
| | | -0.85 | 0.06 | -0.48 | 0.05 |
| | | -0.83 | 0.05 | -0.41 | 0.06 |
| Average | 7 | -0.87 | 0.05 | -0.46 | 0.05 |
| Ling et al. (2011) | 90 | -0.83 | 0.09 | -0.43 | 0.06 |
| San Carlos Olivine | | -0.24 | 0.05 | -0.15 | 0.05 |
| | | -0.20 | 0.05 | -0.13 | 0.05 |
| | | -0.22 | 0.05 | -0.12 | 0.04 |
| | | -0.25 | 0.05 | -0.11 | 0.06 |
| | | -0.23 | 0.05 | -0.13 | 0.06 |
| | | -0.25 | 0.03 | -0.16 | 0.04 |
| | | -0.30 | 0.06 | -0.16 | 0.07 |
| Average | 7 | -0.24 | 0.05 | -0.14 | 0.05 |
| Hu et al. (2016) | 28 | -0.24 | 0.03 | -0.12 | 0.02 |
| BHVO (USGS) | | -0.24 | 0.06 | -0.11 | 0.05 |
| Basalt, Hawaii Volcanic Observatory | | -0.27 | 0.06 | -0.14 | 0.05 |
| Average | 2 | -0.26 | 0.06 | -0.13 | 0.05 |
| Teng et al. (2015) | | -0.21 | 0.04 | -0.12 | 0.03 |
| MAG-1 (USGS) | | -0.35 | 0.06 | -0.16 | 0.05 |
| Marine Mud, Gulf of Maine | | -0.30 | 0.06 | -0.14 | 0.05 |
| Average | 2 | -0.32 | 0.06 | -0.15 | 0.05 |
| Teng et al. (2015) | | -0.25 | 0.05 | -0.11 | 0.04 |

Results of Mg standards (n = number of analyses) run between the samples. Bolded values represent the average value of the standards in each run and italicized values represent the literature values. 2SD of Mg isotopic values represents two standard deviation of the bracketing standard measurements during a full analytical session.

## 2.5 Results

Physical and chemical parameters that were measured along the core's depth are reported below, including soluble salts, temperature, ice content, modeled unfrozen water content, pH, particle size, elemental composition of bulk sediment, and Mg isotopic composition:

### 2.5.1 Ionic Composition and pH of Thawed Permafrost Ice

The thawed permafrost ice contains high concentrations of total soluble salts with an average value of 29 mmol/kg and a standard deviation (1SD) of 11.9 in the upper 7.0 m of the core and lower concentrations below 7.0 m with an average value of 19 mmol/kg (1SD = 8.1) (Figure 2.2 a and b). Two sample t-tests comparing the mean total concentrations revealed the concentrations in the two sections of the core were significantly different ($p<0.05$). Na is the most concentrated cation, followed by Ca, Mg, and K. pH values were measured starting at the ice-table at 0.4 m (Figure 2.2c). The top four samples have pH values of 6.60 and rapidly increase toward the highest measured pH of 7.70. Excluding those four samples, pH values in the upper 7.0 m are consistently higher than the lower section of the core, with a mean value of 7.29 (1SD = 0.15). At 7.0 m, pH values drop down to a pH of 7.00 and remain around 7.00 until 18.0 m. From 18.0 to 30.0 m, the pH values increase from pH of 7.00 to 7.57. Two sample t-tests also show a significant difference between the pH values of the upper and lower sections of the core ($p< 0.05$).

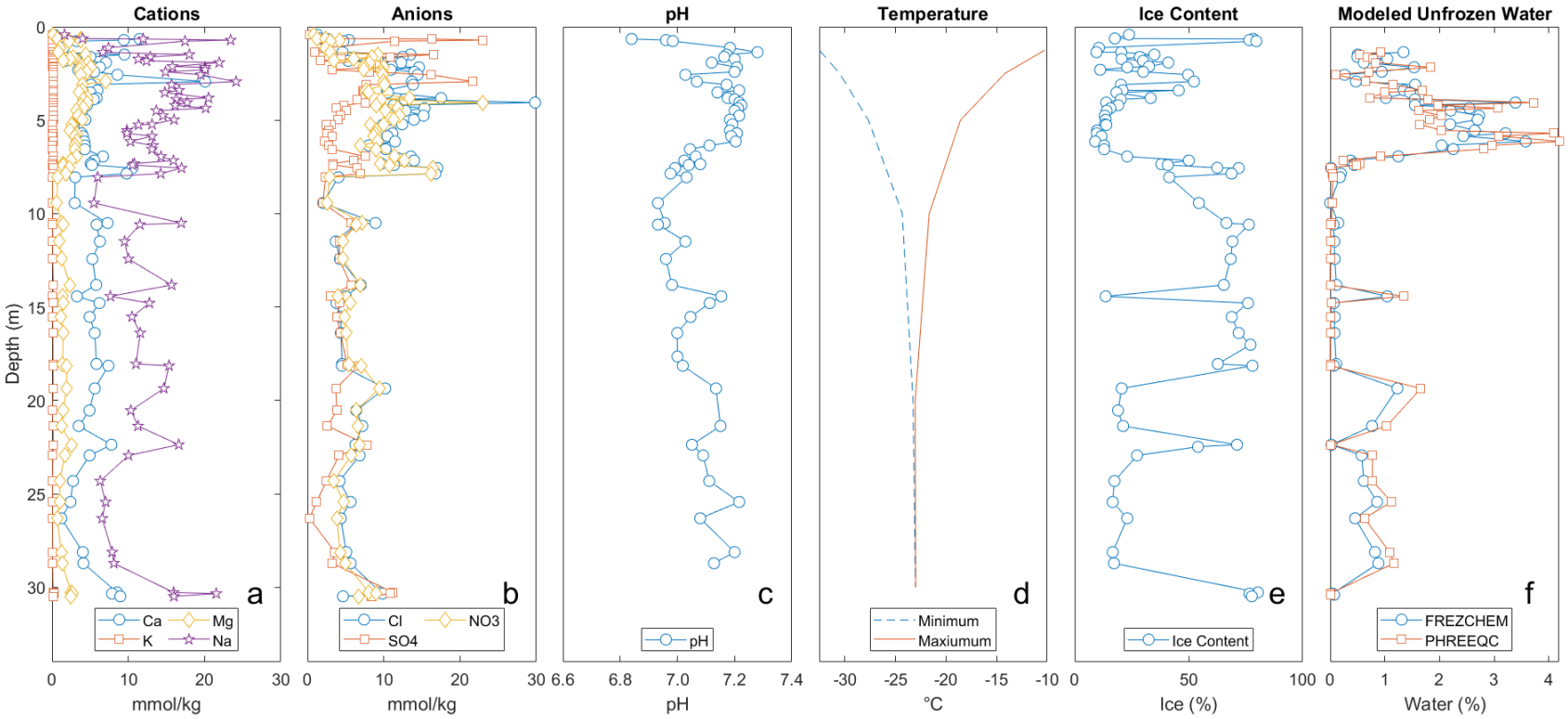


Figure 2.2: Analytical result along the depth of the 30-meter permafrost core for: (a) $Ca^{2+}$, $K^{+}$, $Mg^{2+}$, and $Na^{+}$ (mmol/kg); (b) $Cl^{-}$, $SO_4^{2-}$, and $NO_3^{-}$ (mmol/kg); (c) pH; (d) Annual maximum and minimum temperatures (°C); (e) Ice content (%) measured gravimetrically; and (f) Modeled unfrozen water content (%) using FREZCHEM and PHREEQC. Most analysis show a major shift at 7-meters depth, with cations, anions, pH, and modeled unfrozen water content higher in the upper 7-meter section, and lower in the 7-30-meter section. Temperatures have large seasonal variation in the upper 10 meters of the core, and little seasonal variation below 10 meters.

### 2.5.2 Temperature

Interpolated maximum and minimum monthly-averaged borehole temperatures in Beacon Valley remain below 0°C throughout the year with seasonal variation most prominent in the upper layers of the permafrost (Figure 2.2d). The sediment closest to the surface has the most extreme temperature highs and lows, ranging from -10°C in the summer to -35°C in the winter. Moving further down the core, these seasonal variations become less pronounced, and at 20.0 m, there is virtually no seasonal variation with temperature steady at approximately -23°C.

### 2.5.3 Ice Content

The core can be grouped into three sections based on its ice content (Figure 2.2e): 0.4-7.0 m, 7.0-18.0 m, and 18.0-30.0 m. From 0.4 to 7.0 m, the average ice content is 26.0 wt.% (1SD = 0.19). There are three outliers in the upper 7.0 m with ice content near 80 wt.% which reflect several small ice lenses in the sediment. Excluding these three values, the average ice content reduces from 26.0 to 21.7 wt.% (1SD = 0.12). At 7.0 m, there is an abrupt increase in the ice content to approximately 50 wt.%. Excluding one outlier at 14.0 m, where the ice content is 13.6 wt.%, the average ice content from 7.0-18.0 m is 62.7 wt.% (1SD = 0.13). From 18.0-30.0 m, ice content decreases to an average ice content of 23.3 wt.% (1SD = 0.11), excluding two ice lenses at 22.0 m and 30.0 m.

### 2.5.4 Modeled Unfrozen Water Content

Based on the soluble ions in the thawed permafrost and the temperature, equilibrium geochemical modeling using PHREEQC (Version 3, ColdChem database) and FREZCHEM (Version 13.2) reveal substantial unfrozen water is present in the permafrost core at various

depths (Figure 2.2f). In the upper 7.0 m of the core, the unfrozen water content generally increases with depth and reaches a maximum of 4.0% of the ice content near 7.0 m. This section of the core experiences higher summer temperatures and higher concentrations of soluble salts that depress the freezing point of water. From 7.0 to 18.0 m, most samples have less than 0.1% unfrozen water content. Average temperatures are lower and there is a lower concentration of soluble salts to depress the freezing point. From 18.0 to 30.0 m, unfrozen water content increases up to 1.7% Despite the lower average temperature, this section has higher soluble salt concentrations than 7.0 to 18.0 m. These models do not consider particle size, pore space size, or ice lens formation, which may have a small effect on the amount of unfrozen water (Anderson and Morgenstern, 1973).

### 2.5.5 Particle Size

Particle size of permafrost sediment was analyzed for the < 2mm fraction (Figure 2.3). Both the clay and silt-sized fraction (< 2 -50 μm) and the sand-sized fraction (50-2000 μm)

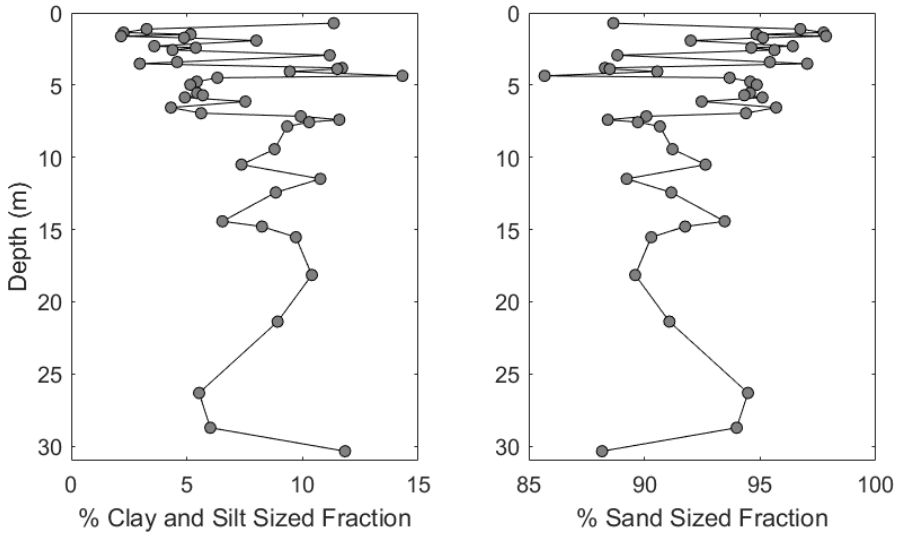


Figure 2.3: Clay-and-silt-sized fraction and sand-sized fraction of Beacon Valley core sediment. The upper 7.0 m have larger variation between samples while the lower 7.0-30.0 m have smaller variation. Sand-sized particles make up at least 85% of sediment in each sample.

display a significant difference ($p < 0.05$) between the upper 7.0 m and the lower 7.0-30.0 m. The clay and silt-sized content in the upper 7.0 m increases with depth and has an average value of 6.4% with a standard deviation of 3.3. The clay-and-silt-sized content in the lower 7.0-30.0 m has a more consistent distribution with a higher average value of 9.0% and a standard deviation of 1.9. Most of the permafrost sediment in the < 2mm fraction consists of sand-sized particles (50-2000 μm). In the upper 7.0 m, sand on average makes up 93.6% (1SD = 3.3) of the sediment, and in the lower 7.0-30.0 m, sand on average makes up 91% (1SD = 1.9) of the sediment.

### 2.5.6 Major element composition and mineralogy

XRF analysis of the < 2mm fraction of permafrost sediment and unweathered Beacon Sandstone and Ferrar Dolerite is presented in Table 2.2 as oxides in weight percent (wt.%) normalized to 100%. Beacon Sandstone is composed almost entirely of $SiO_2$ (> 99 wt.%), with little to no MgO (< 0.01 wt.%), while Ferrar Dolerite is composed primarily of $SiO_2$ (57 wt.%), $Al_2O_3$ (14 wt.%), $FeO^*$ (10 wt.%), CaO (9 wt.%), and MgO (5 wt.%). Major element composition of the permafrost sediment suggests a mixed lithology of sandstone and dolerite. XRD analysis of the permafrost sediment also suggests most of the sediment is composed of quartz, pyroxene (augite and orthopyroxene), and feldspar (andesine, anorthite, and orthoclase), with smaller amounts of gypsum (2 samples with < 1%), muscovite, kaolinite, and saponite (Table 2.3).

On average, the permafrost sediment is composed mainly of $SiO_2$ (80 wt.%, 1SD = 1.9). While the $SiO_2$ concentration varies by only a few percent, there is a statistically significant difference between the upper 7.0 m and the lower 7.0-30.0 m ($p < 0.05$). CaO and MgO concentrations are also statistically different ($p < 0.05$) in the upper and lower sections of the

core, showing a decrease in the upper 7.0 m and remaining constant in the lower 7.0-30.0 m. $K_2O$, $Na_2O$, and $Al_2O_3$ remain constant throughout the 30.0-meter core and show no statistical difference in the upper and lower sections.

Table 2.2: Elemental abundance of Beacon Core Sediment samples

| Sample Type | Sample ID | Depth (m) | XRF – LOI Normalized Major Elements (Weight %) | | | | | | | | | |
|---|---|---|---|---|---|---|---|---|---|---|---|---|
| | | | $SiO_2$ | $TiO_2$ | $Al_2O_3$ | FeO* | MnO | MgO | CaO | $Na_2O$ | $K_2O$ | $P_2O_5$ |
| Permafrost Sediment | BV4-24-27 | 0.66 | 78.69 | 0.60 | 6.90 | 5.38 | 0.10 | 2.24 | 4.16 | 0.89 | 0.95 | 0.08 |
| | BV4-105-113 | 1.49 | 75.34 | 0.86 | 7.75 | 6.47 | 0.12 | 2.50 | 4.69 | 1.03 | 1.15 | 0.08 |
| | BV4-189-192 | 2.31 | 77.26 | 0.78 | 7.21 | 5.88 | 0.11 | 2.23 | 4.32 | 1.02 | 1.11 | 0.08 |
| | BV4-269-271 | 3.10 | 81.82 | 0.46 | 6.04 | 4.28 | 0.08 | 1.94 | 3.63 | 0.79 | 0.89 | 0.06 |
| | BV4-340-343 | 3.82 | 81.15 | 0.46 | 6.68 | 4.39 | 0.08 | 1.76 | 3.44 | 0.88 | 1.08 | 0.07 |
| | BV4-395-397 | 4.36 | 78.61 | 0.53 | 7.54 | 5.03 | 0.09 | 2.01 | 3.96 | 1.00 | 1.15 | 0.08 |
| | BV4-455-460 | 4.98 | 79.58 | 0.49 | 7.30 | 4.73 | 0.09 | 1.84 | 3.72 | 1.00 | 1.17 | 0.08 |
| | BV4-529-532 | 5.71 | 79.34 | 0.52 | 7.28 | 4.86 | 0.09 | 1.89 | 3.77 | 1.00 | 1.17 | 0.08 |
| | BV4-613-618 | 6.56 | 79.30 | 0.51 | 7.45 | 4.77 | 0.09 | 1.83 | 3.70 | 1.04 | 1.24 | 0.08 |
| | BV4-653-656 | 6.95 | 79.46 | 0.51 | 7.36 | 4.75 | 0.09 | 1.79 | 3.72 | 1.04 | 1.20 | 0.08 |
| | BV4-675-677 | 7.16 | 81.52 | 0.47 | 6.60 | 4.26 | 0.08 | 1.71 | 3.34 | 0.86 | 1.07 | 0.07 |
| | BV4-744-748 | 7.86 | 81.96 | 0.43 | 6.59 | 4.08 | 0.08 | 1.64 | 3.24 | 0.83 | 1.08 | 0.07 |
| | BV4-763-768 | 8.06 | 80.51 | 0.49 | 7.06 | 4.49 | 0.08 | 1.72 | 3.49 | 0.93 | 1.14 | 0.07 |
| | BV4-1005-1016 | 10.51 | 80.68 | 0.48 | 6.93 | 4.47 | 0.08 | 1.77 | 3.49 | 0.90 | 1.13 | 0.07 |
| | BV4-1108-1110 | 11.49 | 81.04 | 0.46 | 6.99 | 4.26 | 0.08 | 1.71 | 3.38 | 0.85 | 1.16 | 0.07 |
| | BV4-1202-1204 | 12.43 | 81.35 | 0.47 | 6.80 | 4.26 | 0.08 | 1.66 | 3.36 | 0.84 | 1.11 | 0.07 |
| | BV4-1438-1440 | 14.79 | 81.57 | 0.45 | 6.63 | 4.23 | 0.08 | 1.71 | 3.32 | 0.85 | 1.10 | 0.07 |
| | BV4-2096-2098 | 21.37 | 80.81 | 0.43 | 7.01 | 4.26 | 0.08 | 1.81 | 3.58 | 0.93 | 1.02 | 0.06 |
| | BV4-2830-2833 | 28.72 | 81.93 | 0.41 | 6.44 | 4.11 | 0.08 | 1.74 | 3.44 | 0.82 | 0.97 | 0.06 |
| | BV4-3007-3010 | 30.49 | 76.55 | 0.60 | 8.43 | 5.44 | 0.10 | 2.11 | 4.31 | 1.10 | 1.28 | 0.08 |
| Bulk Rock | Dolerite 2 | 0.60 | 57.65 | 0.97 | 13.89 | 10.66 | 0.18 | 4.20 | 8.73 | 2.14 | 1.43 | 0.15 |
| | Dolerite 3 | 2.20 | 56.80 | 0.90 | 14.35 | 10.01 | 0.18 | 5.11 | 9.29 | 2.03 | 1.22 | 0.13 |
| | Beacon Sandstone 1 | surface | 99.81 | 0.02 | 0.15 | 0.02 | 0.00 | 0.02 | 0.03 | 0.00 | 0.03 | 0.01 |
| | Beacon Sandstone 2 | surface | 99.53 | 0.11 | 0.35 | 0.03 | 0.00 | 0.01 | 0.00 | 0.00 | 0.06 | 0.01 |
| | Vida Granite | surface | 69.41 | 0.34 | 15.44 | 2.93 | 0.06 | 0.39 | 1.89 | 3.68 | 5.78 | 0.07 |

Values are normalized to LOI. FeO* is total Fe represented as FeO

Table 2.3: Mineralogy of Beacon Valley core sediment

| Sample ID | XRD Analysis (% mineral) | | | | | | | | | |
|---|---|---|---|---|---|---|---|---|---|---|
| | Quartz | Andesine | Augite | OPX | Anorthite | Orthoclase | Gypsum | Muscovite | Kaolinite | Saponite |
| BV4-105-113 | 51.2 | 13.5 | 9.6 | 8.7 | 4.0 | 3.6 | 0.9 | 0.8 | 0.7 | 5.3 |
| BV4-269-271 | 62.4 | 13.8 | 7.7 | 6.3 | 4.2 | 4.2 | 0.0 | 1.4 | 0.6 | 3.4 |
| BV4-529-532 | 61.2 | 12.7 | 8.6 | 4.5 | 0.0 | 6.4 | 0.0 | 1.9 | 1.1 | 2.9 |
| BV4-763-768 | 61.5 | 15.2 | 5.8 | 8.8 | 0.0 | 0.0 | 0.5 | 1.0 | 1.7 | 4.6 |
| BV4-2096-2098 | 59.8 | 14.2 | 6.5 | 4.9 | 0.0 | 6.7 | 0.0 | 1.1 | 0.9 | 4.1 |
| BV4-2830-2833 | 62.1 | 13.4 | 5.2 | 6.9 | 0.0 | 4.6 | 0.0 | 2.0 | 0.7 | 4.9 |

### 2.5.7 Magnesium Isotopes

Magnesium isotopic ratios of the thawed permafrost ice, bulk rock samples, thawed Taylor Glacier ice, and Beacon Valley snowfall are reported in Table 2.4. There are two Mg reservoirs in Beacon Valley with distinct Mg isotopic compositions. Dolerite samples collected from the core and the surface of Beacon Valley have an average Mg isotopic composition of -0.22 ± 0.07‰ (n = 3), which is typical for basaltic rocks (Teng, 2017). Taylor Glacier/Beacon Snowfall samples have a significantly lower average Mg isotopic composition of -0.93 ± 0.06‰ (n = 4), which is close to the seawater Mg isotopic composition of -0.83 ± 0.09‰ (Ling et al., 2011). In the upper 7.0 m, the Mg isotopic composition of the thawed permafrost ice samples falls between these two end-members, and in the lower 7.0-30.0 m, Mg isotopic composition falls within the Taylor Glacier/Beacon Snowfall range (Figure 2.4).

The Mg isotopic composition in the upper 7.0 m can be further distinguished at 0.4-1.5 m and 1.5-7.0 m. At 0.4 m, the Mg isotopic composition is the highest recorded in the thawed permafrost ice with a $\delta^{26}$Mg value of -0.52 ± 0.05‰ and lies directly at the boundary between the dry permafrost and ice-cemented permafrost. Moving down towards 1.5 m, the Mg isotopic

composition decreases to a $\delta^{26}$Mg value of -0.81 ± 0.05‰. These upper samples, which are almost all heavier than the Taylor Glacier/Beacon Snowfall end member, are sampled from the section containing multiple ice lenses. From 1.5-7.0 m, Mg isotopic ratios start with a value of -0.82 ± 0.05‰, close to that of Taylor Glacier/Beacon Snowfall (-0.93 ± 0.06‰), and gradually increase to -0.64 ± 0.05‰ near 7.0 m. From 7.0-30.0 m, $\delta^{26}$Mg values are consistently lighter than above 7.0 m, averaging -0.93‰. These values in the lower section of the core are mostly within the range of the Taylor Glacier/Beacon Snowfall end member isotopic composition but show a slight increasing trend in Mg isotope composition with depth. In addition, two samples are significantly lighter than the Taylor Glacier/Beacon Snowfall end member.

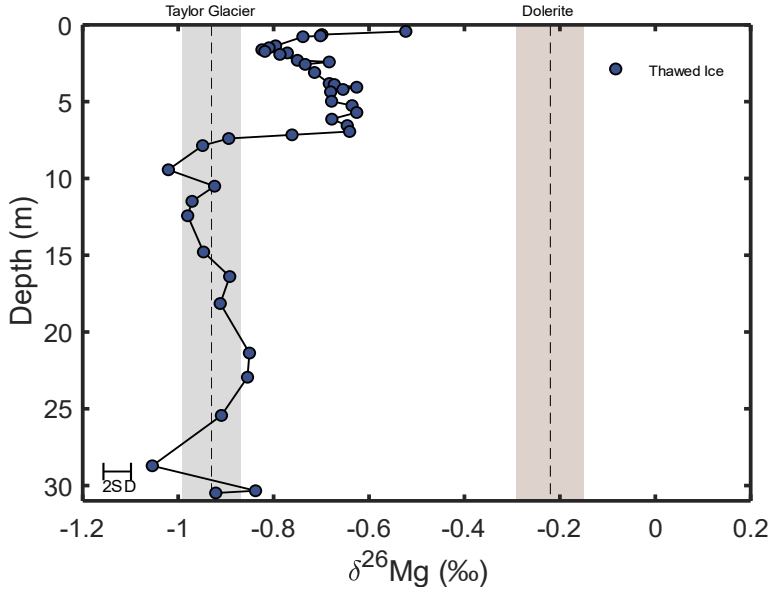


Figure 2.4: Mg isotopic analysis of the thawed permafrost ice samples, averaged dolerite rocks, and averaged Taylor Glacier/Beacon snowfall values. The Mg sources in the Antarctica Dry Valleys are shown in the shaded regions. Taylor Glacier/Beacon snowfall (gray) has an Mg isotopic composition of -0.93 ± 0.06‰ and dolerite (brown) have an average value of -0.22 ± 0.07‰. Thawed permafrost ice values are plotted as blue circles. From 0-7 meters, the Mg isotopic composition is intermediate between Taylor Glacier/Beacon snowfall and dolerite, and from 7-30 meters, the isotopic composition is near or within the range of Taylor Glacier/Beacon snowfall.

Table 2.4: Magnesium isotopic composition of Beacon valley thawed ice samples, Bulk rock samples, and Taylor Glacier/Snow samples

| Sample Type | Sample Name | Midpoint Depth (m) | $\delta^{26}Mg$ | 2SD | $\delta^{25}Mg$ | 2SD |
|---|---|---|---|---|---|---|
| Thawed Ice | BV4-0-4.5 (BV001) | 0.42 | -0.52 | 0.05 | -0.23 | 0.05 |
| | BV4-22-24 | 0.63 | -0.70 | 0.05 | -0.34 | 0.05 |
| | BV4-28-35 | 0.72 | -0.70 | 0.05 | -0.39 | 0.05 |
| | BV4-34.5-39.5 (BV002) | 0.77 | -0.74 | 0.05 | -0.38 | 0.05 |
| | BV4-93-100 | 1.37 | -0.80 | 0.05 | -0.42 | 0.05 |
| | BV4-105-113 | 1.49 | -0.81 | 0.05 | -0.44 | 0.05 |
| | BV4-120-123 | 1.62 | -0.82 | 0.05 | -0.42 | 0.05 |
| | BV4-130-135 | 1.73 | -0.82 | 0.05 | -0.44 | 0.05 |
| | BV4-142-143 | 1.83 | -0.77 | 0.05 | -0.41 | 0.05 |
| | BV4-150-154 | 1.92 | -0.79 | 0.05 | -0.42 | 0.05 |
| | BV4-189-192 | 2.31 | -0.75 | 0.05 | -0.40 | 0.05 |
| | BV4-200-203 | 2.42 | -0.68 | 0.05 | -0.34 | 0.05 |
| | BV4-215-219 | 2.57 | -0.73 | 0.05 | -0.37 | 0.05 |
| | BV4-269-271 | 3.10 | -0.71 | 0.05 | -0.39 | 0.05 |
| | BV4-340-343 | 3.82 | -0.68 | 0.05 | -0.38 | 0.05 |
| | BV4-347-350 | 3.89 | -0.67 | 0.05 | -0.35 | 0.05 |
| | BV4-364-368 | 4.06 | -0.63 | 0.05 | -0.33 | 0.05 |
| | BV4-379-382 | 4.21 | -0.65 | 0.05 | -0.34 | 0.05 |
| | BV4-395-397 | 4.36 | -0.68 | 0.05 | -0.36 | 0.04 |
| | BV4-455-460 | 4.98 | -0.68 | 0.05 | -0.37 | 0.04 |
| | BV4-483-488 (BV005) | 5.26 | -0.64 | 0.05 | -0.34 | 0.04 |
| | BV4-529-532 | 5.71 | -0.63 | 0.05 | -0.32 | 0.04 |
| | BV4-573-575 | 6.14 | -0.68 | 0.05 | -0.35 | 0.04 |
| | BV4-613-618 | 6.56 | -0.65 | 0.05 | -0.35 | 0.04 |
| | BV4-653-656 | 6.95 | -0.64 | 0.05 | -0.34 | 0.04 |
| | BV4-675-677 | 7.16 | -0.76 | 0.05 | -0.41 | 0.04 |
| | BV4-698-702 | 7.40 | -0.89 | 0.05 | -0.45 | 0.04 |

| | | | | | | |
|---|---|---|---|---|---|---|
| | BV4-744-748 | 7.86 | -0.95 | 0.05 | -0.49 | 0.04 |
| | BV4-902-905 | 9.44 | -1.02 | 0.03 | -0.54 | 0.04 |
| | BV4-1005-1016a | 10.51 | -0.92 | 0.05 | -0.49 | 0.04 |
| | BV4-1108-1110 | 11.49 | -0.97 | 0.05 | -0.52 | 0.06 |
| | BV4-1202-1204 (A & B) | 12.43 | -0.98 | 0.05 | -0.50 | 0.06 |
| | BV4-1438-1440 (A & B) | 14.79 | -0.95 | 0.05 | -0.49 | 0.06 |
| | BV4-1598-1600 (A & B) | 16.39 | -0.89 | 0.05 | -0.49 | 0.06 |
| | BV4-1773-1776 (A & B) | 18.15 | -0.91 | 0.05 | -0.48 | 0.06 |
| | BV4-2096-2098 | 21.37 | -0.85 | 0.05 | -0.42 | 0.06 |
| | BV4-2253-2256 | 22.95 | -0.85 | 0.05 | -0.46 | 0.06 |
| | BV4-2502-2505 | 25.44 | -0.91 | 0.03 | -0.46 | 0.04 |
| | BV4-2830-2833 | 28.72 | -1.05 | 0.03 | -0.56 | 0.04 |
| | BV4-2990-2998 | 30.34 | -0.84 | 0.05 | -0.41 | 0.04 |
| | BV4-3007-3010 | 30.49 | -0.92 | 0.05 | -0.46 | 0.06 |
| | Dolerite 1 | surface | -0.23 | 0.06 | -0.13 | 0.05 |
| Bulk Rock | Dolerite 2 | 0.60 | -0.20 | 0.06 | -0.12 | 0.05 |
| | Dolerite 3 | 2.20 | -0.24 | 0.06 | -0.12 | 0.05 |
| | Beacon Valley Fresh Snow (1/5/11) | | -0.98 | 0.06 | -0.51 | 0.07 |
| Taylor Glacier/Snow | Taylor Glacier 1 | | -0.86 | 0.06 | -0.50 | 0.05 |
| | Taylor Glacier 2 | | -0.84 | 0.06 | -0.40 | 0.05 |
| | Taylor Glacier Nirvana | | -1.06 | 0.06 | -0.53 | 0.07 |

2SD of Mg isotopic values represents two standard deviation of the bracketing standard measurements during a full analytical session.

## 2.6 Discussion

In this section, we present evidence of chemical weathering in permafrost sediment and ice, discuss the controls over chemical weathering, and quantify the extent of weathering using Mg isotopic composition. We discovered that Antarctic permafrost provides a unique environment where leaching is limited and products from chemical weathering reactions tend to remain in the permafrost over time, providing a record of these reactions. As discussed below, this accumulation of weathering products coincides with changes in ionic content, pH values, and Mg isotopes of the thawed permafrost ice over the sampling depth.

### 2.6.1 Magnesium in the MDV

Magnesium in Beacon Valley permafrost is primarily sourced from two reservoirs: (1) marine aerosols, and (2) chemical weathering of Ferrar dolerite (Claridge and Campbell, 1977; Keys and Williams, 1981). The first source of Mg, marine aerosols, is deposited by dust, katabatic winds, and snowmelt events which may sublimate or melt during strong solar radiation in summer months thereby releasing any entrained salts (Liu et al., 2015). Due to the hyperarid conditions of the MDV, ions released by snowfall become enriched over time and sediment eventually becomes brine rich with a depressed freezing point (Anderson and Morgenstern, 1973; Hagedorn et al., 2010; Murrmann, 1973). These brine films, along with salts inherited during sediment deposition, persist throughout the depth of the permafrost.

Ferrar dolerite is the second major source of Mg in Beacon Valley and dolerite rock fragments are found throughout Beacon Valley. Ferrar dolerite is a medium to fine-grained mafic igneous rock with a bulk composition consisting mainly of calcium-rich plagioclase ($An_{89}Ab_{11}$) and magnesium-rich pyroxene ($Wo_4En_{81}Fs_{15}$), with accessory biotite, hornblende and iron oxides

(Campbell and Claridge, 1987; Elliot et al., 1995; Gunn, 1962). Three key reactions dictate the weathering products of Ferrar Dolerite:

$$(Ca_{0.4}, Mg_{0.8}, Fe_{0.15})SiO_{3_{(s)}}(enstatite) + H_2O + 2H^+ \rightarrow (Ca^{2+}_{0.4}, Mg^{2+}_{0.8}, Fe^{2+}_{0.15})_{(aq)} + H_4SiO_{4_{(aq)}}$$

$$CaAl_2Si_2O_{8_{(s)}}(anorthite) + H_2O + 2H^+ \rightarrow Ca^{2+}{}_{(aq)} + Al_2Si_2O_5(OH)_4$$

$$2NaAlSi_3O_{8_{(s)}}(albite) + 9H_2O + 2H^+ \rightarrow 2Na^{2+}{}_{(aq)} + Al_2Si_2O_5(OH)_4 + 4H_4SiO_{4_{(aq)}}$$

These weathering reactants and products will be used to trace the extent of chemical weathering that occurs in the permafrost.

## 2.6.2 Controls on Permafrost Chemistry

### *2.6.2.1 Evidence of Weathering in Permafrost Sediment*

Previous studies have shown the mineral weathering susceptibility sequence olivine > pyroxene > amphibole > plagioclase > K-feldspar (Colman, 1982; Craig and Loughnan, 1964; Eggleton et al., 1987; Stefánsson et al., 2001). Therefore, loss of Mg and Ca from pyroxene (and to a lesser extent, Ca and Na from plagioclase) should be evident in the major element composition of the bulk sediment. To look more closely at just dolerite in the permafrost sediment, we use evidence of a two-lithology system from a qualitative XRD analysis showing a system of quartz-rich sandstone and dolerite (shown as Mg-rich pyroxene and Ca-rich

plagioclase in an XRD analysis). Using a two-end member mixing equation, the percent dolerite and sandstone in each sample can be calculated using an immobile element, such as $Al_2O_3$ (Nesbitt and Wilson, 1992):

$$Al_2O_{3_{sandstone}} * (X) + Al_2O_{3_{dolerite}} * (1 - X) = Al_2O_{3_{sediment}} \quad (2.1)$$

where x represents the fraction of sandstone in each sample. The percent of dolerite in each sample can then be used to adjust the major element composition to account for only dolerite sediment in the samples (Figure ) to compare to unweathered dolerite values. MgO and CaO show a similar trend for the major element composition. The top four samples start off similar to the composition of unweathered dolerite and decrease in concentration moving down to 7.0 m. Below 7.0 m, they are constant and lower than the bulk dolerite composition. $K_2O$ and $Na_2O$ both remain constant throughout the core. $Na_2O$ in each sample has a similar composition to the unweathered dolerite, while $K_2O$ is higher, suggesting $K_2O$ may be coming from another source.

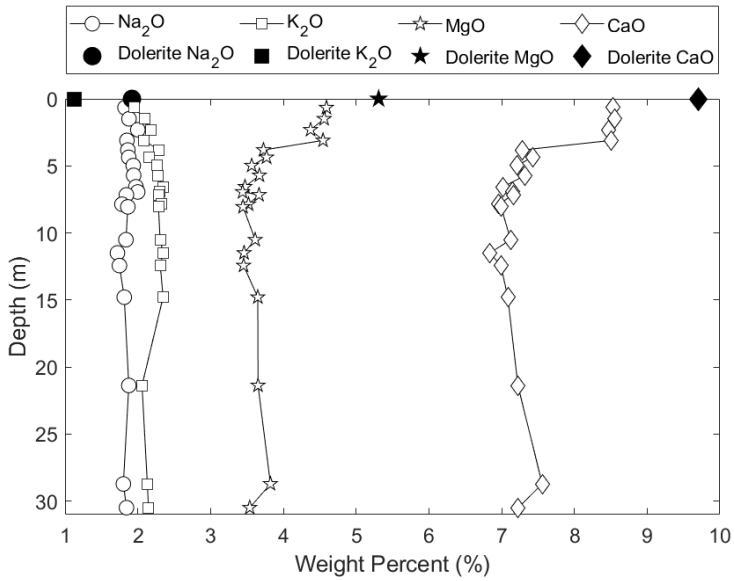


Figure 2.5: Major element composition of the < 2mm size fraction of CaO, $K_2O$, MgO, and $Na_2O$ (in weight %) normalized to the amount of dolerite in each sample, and unweathered dolerite. CaO and MgO both decrease with depth, while $K_2O$ and $Na_2O$ remain constant.

While there is no granitic bedrock source in Beacon Valley, alkali-feldspar rich granite erratics have been found on the Beacon Valley surface and may be an additional source of $K_2O$ in the sediment (Dickinson et al., 2017). Muscovite identified in XRD analysis supports this hypothesis. However, based on the low percentage of muscovite in samples (muscovite < 2%) and comparable low MgO concentration in granite erratics compared to dolerite ($MgO_{granite}$ = 0.39 wt%, $MgO_{dolerite}$ = 4.66 wt%), the granite erratics would not have much influence on the MgO composition of the sediment.

Overall, major element composition of the permafrost sediment alone does not show clear evidence for chemical weathering. However, when the major element composition of permafrost sediment is compared to the $\delta^{26}Mg$ of the thawed permafrost ice, a few trends become apparent (Figure 2.6). There is a clear negative correlation between the MgO content of the permafrost sediment and $\delta^{26}Mg$ values of thawed permafrost ice in the upper 7.0 meters ($R^2$ = -0.63). This negative correlation is explained by the loss of Mg from dolerite sediment during dissolution that is documented by the decreasing MgO concentration in the sediment, and an input of isotopically heavier Mg into the brine released from dolerite weathering, causing the Mg isotopic composition of thawed permafrost ice to become heavier. This trend suggests that the Mg isotopic composition of the thawed permafrost ice is controlled by mixing between the two Mg reservoirs rather than fractionation during dissolution. The MgO and $\delta^{26}Mg$ in the lower 7-30 meters do not show a clear correlation ($R^2$ = 0.03), and MgO remains constant.

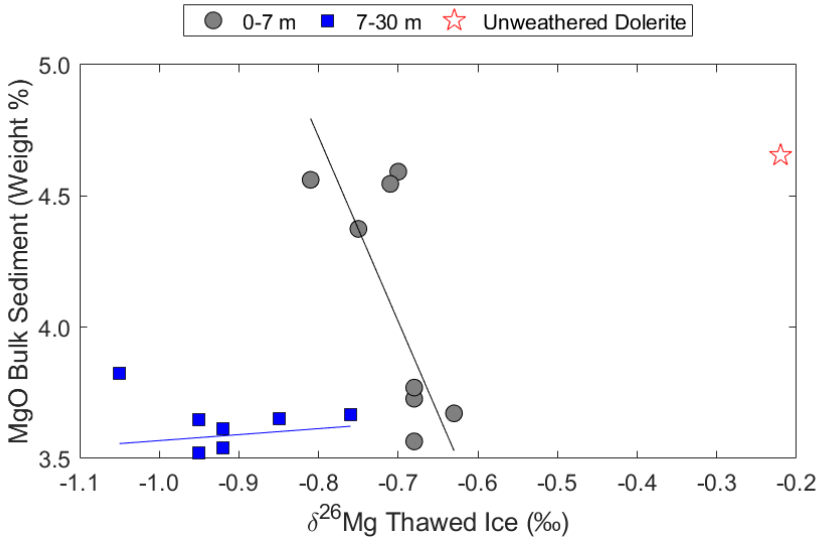


Figure 2.6: MgO of bulk sediment corrected for % dolerite (weight %) vs $\delta^{26}$Mg (‰) of thawed ice for the upper 0.0-7.0 meters, lower 7.0-30.0 meters of the core, and unweathered dolerite. The upper 7 meters shows a negative correlation where the $\delta^{26}$Mg in the thawed ice becomes enriched in the heavy isotope as the MgO content decreases in the bulk sediment. The lower 7-30 meters do not show any obvious correlation.

*2.6.2.2 Evidence of Chemical Weathering in Thawed Permafrost Ice*

Chemical weathering is most apparent in pH and Mg isotopic composition of the thawed permafrost ice. Chemical weathering of silicate minerals consumes protons during the dissolution of plagioclase and pyroxene which leads to an increase in pH values. pH values in the core have higher values in the upper 0.40 to 7.0 m (average = 7.29), lower values in the middle 7.0 to 18.0 m (average = 7.01), and higher values at 18.0 to 30.0 m (average = 7.30) (Figure 2.2c). While an increase in pH with chemical weathering is a known phenomenon (van Breemen et al., 1983), there are few natural examples of this processes due to leaching of weathering products by percolating water. However, it is apparent in the Beacon Valley core that the weathering products are retained in the ice-rich permafrost which leads to the trend observed in the thawed permafrost ice fraction of the sediment profile. The pH data are consistent with the

weathering trends revealed in the Mg isotopic composition. Magnesium is released as a weathering product during the hydrolysis of pyroxene. Because the weathering products remain in the ice and the two Beacon Valley Mg reservoirs have such distinct isotopic signatures, sections of the core that experience more chemical weathering have values intermediate between the two end members. This is seen in the upper 0.4-7.0 m, and to a lesser degree in the lower 18.0-30.0 m.

*2.6.2.3 Influence of Unfrozen Water*

The main control over chemical weathering is the amount of unfrozen water in the sediment profile, which is modeled as a function of ionic composition of the thawed permafrost ice and temperature. When compared with unfrozen water content, pH and Mg isotopic composition show a similar parabolic curve with a rapid increase in pH and Mg isotopic composition as unfrozen water reaches 1.5% of ice content and a near-constant value when the water content is above 1.5% of ice content (Figure 2.7).

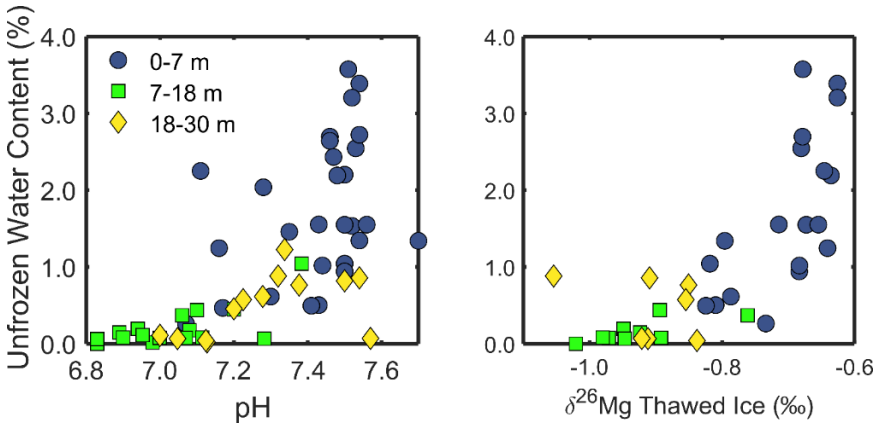


Figure 2.7: Modeled unfrozen water content (%) vs pH and $\delta^{26}$Mg of the thawed core samples divided into three sections: (1) 0-7 meters (blue dots), (2) 7-18 meters (green squares), and 18-30 meters, (yellow diamonds). Each section shows higher pH and $\delta^{26}$Mg in regions with higher modeled unfrozen water content.

Comparing this trend with sample depth indicates an increase in pH and Mg isotopic ratios in the 0.4-7.0 m and 18.0-30.0 m range. One hypothesis for the parabolic nature of these trends is that as fresh mineral surfaces are initially weathered, there is a rapid initial consumption of $H^+$ and release of Mg, followed by a retardation of these processes as the amount of fresh mineral surfaces is reduced (Gérard et al., 2003; White, 2003).

*2.6.2.4 Correcting for Mg Inputs from Marine Aerosols in Thawed Permafrost Ice*

By correcting for Mg inputs from marine aerosols, we can more closely examine the degree of dissolution and whether any reactions (i.e., secondary mineral precipitation or cation exchange) have changed the ionic or isotopic composition of the thawed permafrost ice samples. This can be done independently using either the Mg concentration or the Mg isotopic composition of the core samples. The Mg concentration in the thawed permafrost ice is corrected for the marine Mg input using a $Cl^-$ correction as a conservative ion tracer of marine input (Tipper et al., 2010; White et al., 2009). Because $Cl^-$ is sourced only from marine aerosols and not chemical weathering (Bao et al., 2008), the $Cl^-$ correction factor will return the Mg concentration in each sample that is derived only from chemical weathering:

$$Mg^*_{Cl^-} = Mg_{sample} - \left(\frac{Mg}{Cl}\right)_{TG} x\ Cl^-_{sample} \quad (2.2)$$

where $Mg^*_{Cl^-}$ is the Mg concentration corrected for marine aerosols, $Mg_{sample}$ is the measured Mg concentration of each sample (ppm), $\left(\frac{Mg}{Cl}\right)_{TG}$ is the ratio of Taylor Glacier/Beacon Snowfall values which represents marine aerosols, and $Cl^-_{sample}$ is the measured $Cl^-$ concentration from

each sample (ppm). The second constraint that can be used to correct for marine aerosol values is the Mg isotopic composition of the samples (Tipper et al., 2010):

$$Mg^{*}_{\delta^{26}Mg} = Mg_{sample}\left(\frac{\delta^{26}Mg_{sample} - \delta^{26}Mg_{TG}}{\delta^{26}Mg_{dolerite} - \delta^{26}Mg_{sample}}\right) \quad (2.3)$$

where $Mg^{*}_{\delta^{26}Mg}$ is the Mg concentration based on isotopic composition, $\delta^{26}Mg_{sample}$ is the isotopic composition of the samples, $\delta^{26}Mg_{TG}$ is the isotopic composition of Taylor Glacier/Beacon Snowfall, and $\delta^{26}Mg_{dolerite}$ is the isotopic composition of dolerite. These two calculations independently provide the Mg concentration in the permafrost profile sourced only from chemical weathering of dolerite. Both cases assume that Mg is only sourced from the two end members, Mg is a conservative element, and that Mg does not participate in any other reactions in the permafrost profile. Furthermore, the MDV are devoid of vegetation, so vegetation that influences Mg or $Cl^-$ values are not an issue in these samples. If these assumptions are correct, these two values should be equal and fall along a 1:1 slope (Figure 2.8).

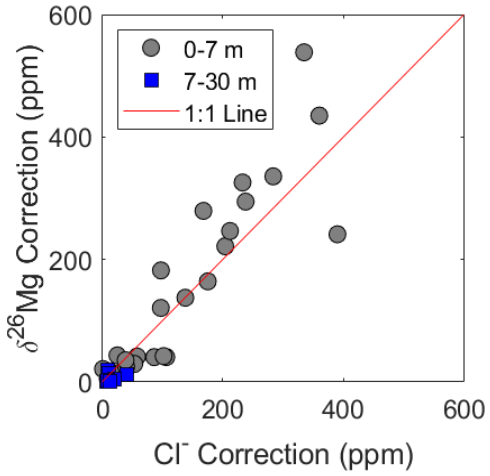


Figure 2.8: $\delta^{26}Mg$ correction vs $Cl^-$ correction for Mg isotopic and ionic values of the thawed ice. These corrections represent the Mg concentrations derived from chemical weathering and should fall along a 1:1 line if no other processes influence Mg or $Cl^-$ values.

The calculated values fall nearly along the 1:1 line, with most values in the upper 7.0 m of the core falling slightly above and a few below the 1:1 line. Many of the values below 7.0 m returned negative values (and are not plotted), suggesting loss of Mg to secondary minerals (clays or secondary salts) (Tipper et al., 2010). Similarly, the effect of losing Mg from the system on samples that did not return negative values would result in values plotting above the 1:1 line, where $Mg^{*}_{Cl^-}$ would decrease more rapidly than $Mg^{*}_{\delta^{26}Mg}$ (Tipper et al., 2010).

*2.6.2.5 Influence of Secondary Minerals*

These results suggest that secondary Mg clays or salts present in the sediment core may have an influence on the Mg isotopic composition of the thawed permafrost ice samples. XRD analysis shows the presence of kaolinite and saponite in the sediment profile, with saponite as the dominant alteration phase. Saponite is a trioctahedral smectite formed from weathering of mafic rocks with high amounts of structural Mg (as opposed to Mg in interlayer and exchangeable sites) (Borchardt, 1989). Structural Mg that is incorporated into clay mineral octahedral lattice sites prefer the heavy isotope (Wimpenny et al., 2014), which can lead to the thawed permafrost having a lighter isotopic composition. Secondary salt precipitation may influence the Mg isotopic composition in a similar way. XRD analysis also reveals small amounts of gypsum ($CaSO_4 \cdot 2H_2O$) in two core samples. Coprecipitation of Mg with gypsum has been shown to occur in laboratory experiments, but the amount that coprecipitates with gypsum is small compared to the amount of Mg in solution due to the small partition coefficient between $0.1 \times 10^{-5}$ and $4.3 \times 10^{-5}$ (Kushnir, 1980). Another possibility is the formation of epsomite ($MgSO_4 \cdot 7H_2O$) and meridianiite ($MgSO_4 \cdot 11H_2O$) that may form in trace amounts in MDV sediment. While neither mineral is detected by XRD in the Beacon Core samples, their presence in trace

amounts may affect the Mg isotopes in the thawed permafrost ice significantly given their high Mg concentrations. When either epsomite or meridianiite form, heavy isotopes are preferentially removed from solution and incorporated into the mineral structure of that secondary salt (Li et al., 2011; Schauble, 2011). The average experimental fractionation factor between epsomite and $MgSO_4$ solution is 0.6‰ (Li et al., 2011), and the theoretical fractionation factor between meridianiite and $MgSO_4$ solution is between 0.3 to 2.2‰ (Rustad et al., 2010; Schauble, 2011). Both fractionation factors are temperature dependent and have not been calibrated explicitly at subfreezing temperatures. Formation of secondary clays and salts along the depth of the core would make the Mg composition of the thawed permafrost ice dependent not just on the two end members, but also on the magnitude of fractionation that occurs during mineral formation. These processes may also explain the two lighter-than-Taylor Glacier Mg isotopic values in the lower 7.0-30.0 meters of the core. While further work is needed to explore the role of secondary minerals and their influence on the Mg isotopic composition at subfreezing temperatures, the tendency of secondary Mg salts precipitating can be modeled using the ionic composition and temperature of the permafrost.

*2.6.2.6 Ionic Ratios and Secondary Salts*

Secondary salt precipitation can be identified in two ways: (1) using ionic ratios to determine the source of salts to Beacon Valley and trace weathering reactions down the sediment profile; and (2) using PHREEQC modeling to determine the saturation index (where saturation index > 0 predicts the salt will precipitate) of each sample based on the soluble salt concentration and temperature. When evaluating ionic ratios, $Cl^-$ can be a useful provenance indicator because it is a most conservative anion and is sourced only from atmospheric inputs (Bao et al., 2008). For most ionic ratios in the core, there is a shift at 7.0 m, suggesting a possible change in source or salt precipitation (Figure 2.9).

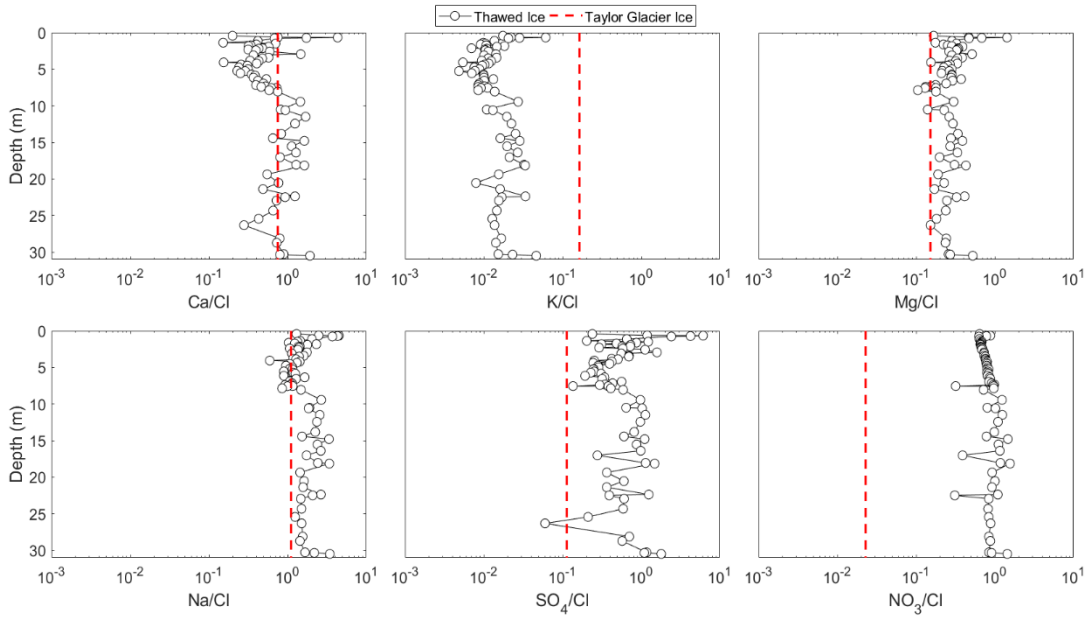


Figure 2.9: Ionic ratios of Ca, K, Mg, Na, $SO_4$, and $NO_3$ with respect to $Cl^-$ of thawed ice from the Beacon Valley core (black) and Taylor Glacier ice (dashed line).

The Ca/Cl ratio and the Na/Cl ratio follow a similar trend, where both are lower in the upper 7.0 m and higher in the lower 7.0-30.0 m. This trend is also seen in the $SO_4$/Cl ratio, suggesting the formation of calcium and sodium sulfates. When modeled in PHREEQC, precipitation of gypsum ($CaSO_4 \cdot 2H_2O$) and mirabilite ($Na_2SO_4 \cdot 10H_2O$) occurs throughout the core, with the

highest saturation index occurring in the upper 7.0 m (Figure 2.10). The Mg/Cl ratios follow an opposite trend as Ca/Cl and Na/Cl. The Mg/Cl ratio in the upper section of the core is greater than that in the lower section of the core. One possible explanation for the shift in the Mg/Cl ratio is a greater amount of Mg is released from dissolution, and a smaller amount of Mg is consumed by precipitation reactions compared to Ca or Na. Evidence from Mg isotopes and pH supports a greater amount of dissolution in the upper 7.0 m. Furthermore, Mg salts are more soluble than Ca and Na salts (Kushnir, 1980), and there will be a smaller amount of sulfate available to precipitate with Mg in the brine after it is consumed by gypsum and mirabilite precipitation. Nonetheless, chemical models show small amounts of magnesium sulfates precipitating in the form of meridianiite ($MgSO_4 \cdot 11H_2O$) and epsomite ($MgSO_4 \cdot 7H_2O$). PHREEQC modeling results of secondary Mg salts precipitating may explain why samples fall above the 1:1 line when correcting Mg ions and Mg isotopes for marine aerosols (Figure 2.8). Overall, secondary salts, including gypsum ($CaSO_4 \cdot 2H_2O$), mirabilite ($Na_2SO_4 \cdot 10H_2O$), epsomite ($MgSO_4 \cdot 7H_2O$), meridianiite ($MgSO_4 \cdot 11H_2O$), and hydrohalite ($NaCl \cdot 2H_2O$) all are modeled to form within the core. The low-temperature database for PHREEQC does not contain nitrate and those species were not modeled.

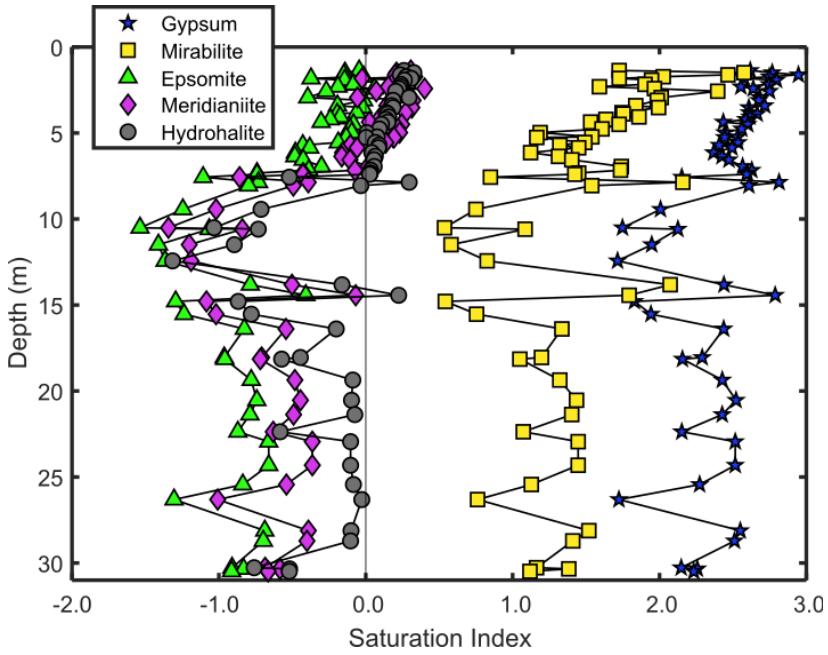


Figure 2.10: Modeled solubility index in the 30-meter core of gypsum, mirabilite, epsomite, meridianiite, and hydrohalite based on temperature and soluble salt concentration. Models show all five salts can precipitate in the core.

### 2.6.3 Degree of Chemical Weathering

The degree of weathering based on the Mg isotopic composition in the thawed ice can be calculated using a mass balance equation of the two-end member system:

$$\%\, Weathering = \frac{\delta^{26}Mg_{sample} - \delta^{26}Mg_{TG}}{\delta^{26}Mg_{dolerite} - \delta^{26}Mg_{TG}} \quad (2.4)$$

Figure 2.11 plotted the calculated degree of weathering of Beacon Valley core using Eq. (2.4). Since these values do not consider potential fractionation from secondary mineral formation, they provide a conservative estimate of chemical weathering. In the upper 7.0 m, two distinct trends are seen. The highest degree of weathering occurs from 0.40-1.5 m, where up to 60% of Mg sourced from weathering. At 1.6 m, weathering contributes approximately 20% of Mg, and increases to near 42% at 7.0 m.

The amount of Mg derived from dolerite weathering increases rapidly from 1.6 m to 4.0 m, and then remains constant at around 40% from 4.0 to 7.0 m. In the lower 7.0-30 m, weathering contributes a range of 0-20% of Mg to the permafrost and increases with depth in the core.

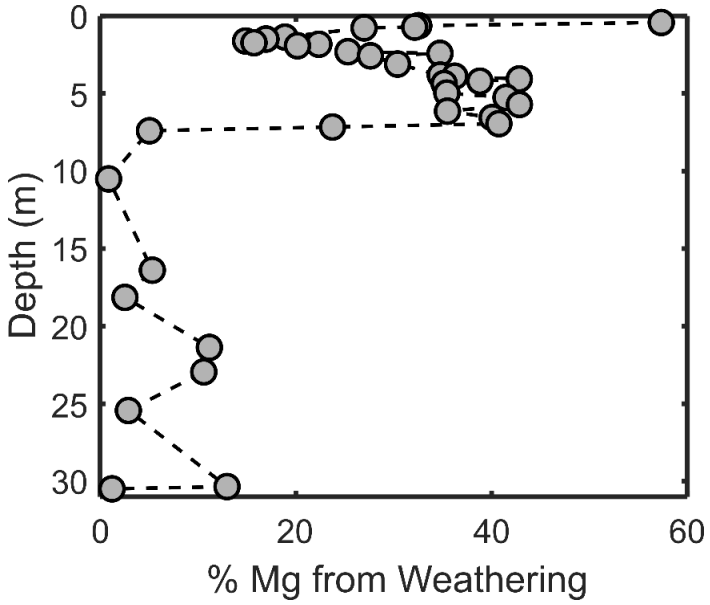


Figure 2.11: The percentage of Mg derived from dissolution of dolerite in the Beacon Valley core for a Taylor Glacier end member. More dissolution occurs in the upper section of the core compared to the lower section of the core.

## 2.6.4. Implications

Chemical weathering of silicate rocks is one of the primary sinks of carbon dioxide from the atmosphere over long time scales (Berner, 1992). To understand and quantify chemical weathering on a continental and global scale, weathering must be studied under a variety of climatic conditions and geologic settings, including cold and dry permafrost-dominated regions. These data provide important steps towards understanding and quantifying silicate weathering over time in permafrost dominated regions. Our study of chemical weathering in the ice-cemented permafrost profile demonstrates that even in the cold and dry environment of the

MDV, in-situ rock-water interactions lead to significant weathering. Since permafrost dominated soils occur in over 20% of the ice-free surfaces on Earth, weathering here cannot be discounted.

Furthermore, our results indicate the extent of chemical weathering in cold and dry permafrost environments depends on the ionic content and the temperature. An important finding of our study supports the concept of a "eutectic layer active zone", where unfrozen water (and chemical weathering) is present to the depth at which the maximum temperature exceeds the eutectic point of the dominant salt. In this study, the dominant salt is NaCl with a eutectic temperature of -21°C, which is the maximum temperature below 7.0 meters where there is limited to no chemical weathering in the sediment core. The findings here have implications for studies of areas such as Don Juan Pond, which is dominated by $CaCl_2$ salts with a eutectic point of -50.4°C (Marion, 1997), and the martian environment, where perchlorates lower the eutectic point to as low as -74.6°C (Marion et al., 2010). Regions with such low eutectic points may experience chemical weathering and see a higher content of unfrozen water extending to deeper depths than previously thought.

## 2.7 Conclusions

This study provides direct evidence of chemical weathering in ice-rich permafrost in the McMurdo Dry Valleys. The continuously frozen permafrost allows weathering products to accumulate in the ice-rich sediments, thereby, uniquely documenting in-situ chemical weathering in permafrost over long timescales. The evidence of chemical weathering is recorded in the elemental composition of the permafrost sediment, the Mg isotopic composition, pH, and ionic ratios of the thawed permafrost ice, and is strongly correlated to the percent of unfrozen water

content. This work provides important conclusions about the history of chemical weathering processes in cold and dry environments:

(1) Evidence for chemical weathering based on salts, pH, and Mg isotopes shows weathering occurred in the upper 7.0 meters of ice-cemented permafrost, where up to 60% of Mg is derived from dolerite. In the lower 7.0-30 meters, less weathering occurs with an average of 5% of Mg sourced from dolerite weathering.

(2) The unfrozen water, as modeled using ground temperature and soluble salt concentration, is the major control on the degree of weathering. The evidence supporting weathering includes a heavier Mg isotopic composition due to dolerite dissolution and higher pH due to proton consumption; both are more pronounced where there is a higher percentage of unfrozen water. The temperatures at which we see unfrozen water suggests that chemical weathering occurs when ground temperatures exceed the eutectic point of the dominant salt and unfrozen water is present even deep within the permafrost core at subzero temperatures.

(3) Secondary minerals may have a small influence on Mg isotopic composition in Beacon Valley. Fractionation caused by clay formation and secondary salt precipitation may explain why $Mg^{*}_{Cl^-}$ and $Mg^{*}_{\delta^{26}Mg}$ correction values do not fall along a 1:1 line, and the Mg values that are lighter than Taylor Glacier in the lower 7.0-3.0 meters. Further work is needed to constrain secondary minerals and the temperature dependence of fractionation factors in permafrost conditions.

**Acknowledgements:** Financial and logistic support is provided by Grant Nos. OPP-1341680 and OPP-0636998 from the National Science Foundation, and Grant 80NSSC17K0715 from NASA. Funding was also provided by the GSA Graduate Student Research Grant and the Vance Fellowship in Geology Science. Drilling support and equipment was contracted from Webster

Drilling and Exploration Limited, Wellington, New Zealand. Special thanks to the XRD analysis and interpretation provided by Doug Ming and Valerie Tu at the NASA Johnson Space Center. We are also grateful for the insightful reviews by C. McKay, who suggested using the term "Eutectic layer active zone," W. Dickinson, an anonymous reviewer, and Guest Editor Xiao-Ming Liu.

## Deciphering magnesium isotope fractionation in permafrost weathering: implications for global Mg cycling

Nicolas Cuozzo, Ronald S. Sletten, Yan Hu, Fang-Zhen Teng, and Lu Liu

## 3.1 Abstract

Weathering in Antarctic permafrost provides an opportunity to study equilibrium Mg isotope fractionation during chemical weathering processes because unfrozen brines remain in contact with the weathering products and are not flushed away. A comprehensive analysis of Mg isotopes in a 30-meter ice-rich permafrost core collected from Beacon Valley, Antarctica, demonstrates significant fractionation during the formation of secondary minerals at subzero temperatures. Mg in unfrozen brines is distributed between the permafrost ice, secondary salts, clay fractions, and exchange sites. Both secondary salts and clays that form in Beacon Valley accumulate heavy Mg isotopes. The predominant Mg-bearing secondary salts predicted by geochemical modeling are epsomite and meridianiite. They are isotopically heavier ($\delta^{26}$Mg = -0.30 to -0.77‰) than the thawed permafrost ice ($\delta^{26}$Mg = -0.52 to -1.05‰), showing an increase in fractionation with decreasing temperature. The isotopic composition of exchangeable Mg ($\delta^{26}$Mg = -0.65 to -0.95‰) reflects the exchanging reservoir (i.e., thawed permafrost ice) with a slight preference for the heavy isotope. The dominant Mg-bearing clay in Beacon Valley soils, predicted by geochemical modeling and measured by XRD, is saponite and an analysis of the Mg isotopic composition of the clay-sized fraction of the sediment ($\delta^{26}$Mg = -0.10 to 0.03‰) display a preference for heavy isotopes, with an average fractionation factor between the saponite and thawed ice of 0.83‰. This value can also be used to provide constraints on the global ocean Mg budget because saponite is the major Mg-bearing mineral that forms during low-temperature alteration of oceanic crust and is a major Mg sink. Using this fractionation factor, we estimate

the low-temperature alteration Mg flux of 0.16 x $10^{12}$ mol/yr, which is significantly lower than previous estimates of the low-temperature alteration flux.

## 3.2 Introduction

Substantial weathering occurs in ice-cemented permafrost at temperatures as low as -21°C, revealed from our previous study of a permafrost core from Antarctica (Cuozzo et al., 2020). The primary control on weathering is unfrozen water due to ions being excluded from the ice and freezing point depression of the accumulated brine (Cuozzo et al., 2020). Because the permafrost core is continuously frozen, the weathering products remain in contact with the primary minerals that are weathering. Using the same 30-meter ice-rich core collected from Beacon Valley as previously reported (Cuozzo et al., 2020), this study focuses on secondary mineral formation, including precipitation of salts and formation of in-situ clays. It provides a unique opportunity to study equilibrium isotopic fractionation and isotopic mixing of weathering products in natural samples.

Studies of chemical weathering often are focused on humid, tropical regions, where weathering rates are enhanced due to abundant rainfall and warmer climate. In contrast, in dry and cold environments, such as polar regions, chemical weathering is believed to be less significant. However, our recent study of the Beacon Valley core reveals that chemical weathering occurs actively in hyper-arid subfreezing conditions in the presence of unfrozen brine formed due to salt-depressed freezing points (Cuozzo et al., 2020). Water extracted from thawed ice-rich permafrost in a 30.0-m core shows contrasting Mg isotopic compositions above and below 7.0 meters, reflecting a change in dominant Mg source from Ferrar dolerite (-0.22 ± 0.07‰) to meltwater from Taylor glacier (-0.93 ± 0.06‰): chemical dissolution of dolerite

contributes to over 60% of soluble Mg in the upper 7 m core, elevating its $\delta^{26}$Mg to between -0.82 and -0.64%, whereas dolerite-sourced Mg decreased to < 5% total Mg budget in the deeper section of the core where $\delta^{26}$Mg (-1.05 to -0.76‰) reflects Taylor Glacier composition (Cuozzo et al., 2020) primarily. Furthermore, an interesting observation is that the thawed permafrost ice deeper in the core is on average lighter than the Taylor Glacier end-member, suggesting other processes may be influencing the Mg isotopic composition.

Secondary mineral formation (salt precipitates and clays) is the most likely process to account for the lighter-than-Taylor Glacier $\delta^{26}$Mg values in the Beacon Valley core thawed ice. The secondary Mg-bearing minerals are dominantly saponite with less abundant epsomite and meridianiite. The fractionation between Mg-bearing salts and fluids has been constrained by experimental studies or chemical modeling; both found that Mg-salt preferentially incorporates the heavy Mg isotope in their structure (Li et al., 2011; Rustad et al., 2010; Schauble, 2011). Precipitation of these salts could thus deplete the heavy Mg isotopes in the permafrost ice. On the other hand, the direction of Mg isotope fractionation during saponite formation remains uncertain. A recent experimental study concludes that light Mg is preferentially incorporated into structural sites of saponite (Hindshaw et al., 2020), which is opposite to the finding that altered saponites in oceanic crust samples prefer heavy Mg isotopes (Huang et al., 2018). Fractionation factors determined experimentally will vary with experimental parameters and the state of reaction equilibrium; however, this study provides an in-situ analysis of saponite that remains in contact with the fluid phase and can provide independent constraints on the mineral-fluid equilibrium fractionation factor.

To quantify how Mg-salts and saponite formation affect the Mg isotopic compositions of the Beacon Valley permafrost ice and determine their equilibrium fractionation factors, we

separated all components of Mg involved in weathering reactions. We analyzed their Mg isotopes, including the thawed permafrost ice, salt precipitates, exchange sites, and structural clay sites. Our results provide one of the most complete weathering studies in a permafrost environment and reveal that secondary mineral formation occurs even at subzero temperatures and explains the lighter-than-Taylor Glacier $\delta^{26}$Mg values in the thawed ice in the lower sections of the Beacon Valley core. Furthermore, the equilibrium fractionation factors determined in this study can also be applied to answer questions about the global ocean Mg cycle. This work provides comprehensive results on fractionation between saponite and the fluid phase, which can be used to represent the fractionation that may occur during low-temperature alteration of oceanic crust that weathers basalt to saponite, one of the major Mg sinks in the global ocean Mg budget.

## 3.2 Study Site

### 3.2.1 Beacon Valley, Antarctica

The MDV are a hyperarid, polar desert that remain free of ice-cover as a result of the high elevation threshold of the Transantarctic Mountains, which divert ice from the East Antarctic Ice Sheet (EAIS) away from McMurdo Sound, and the Wilson Piedmont Glacier, which isolate the MDV from the Ross Sea and blocks snowfall from them (Chinn, 1990; Hall and Denton, 2002). Beacon Valley is one of the southern-most valleys, trending northeast-southwest and covering an area approximately 3 km wide and 12 km long (Figure 3.1). Average annual temperatures are around -22.9°C (Liu et al., 2015), with less than 100 mm/year of precipitation in the form of snowfall (Fountain et al., 2010). The lower valley on its northeast end is bounded by Taylor Glacier, an EAIS outlet glacier. Bedrock in Beacon Valley consists of

Devonian to Jurassic Beacon Group sandstones, siltstones, and shales, with sills and dikes of tholeiitic Jurassic Ferrar Dolerite (McElroy and Rose, 1987).

The ice-cemented permafrost core analyzed in this study was collected in lower Beacon Valley (77°48'11.4" S, 160°42'49.8" E). The surface of Beacon Valley is covered by patterned ground with polygonal diameters of 10 to 20 m, and the core was collected in the center of a polygon, which is considered the most stable region (Linkletter et al., 1973; Sletten et al., 2003). Sediment in the Beacon valley core comprises mostly sand-sized grains of quartz and dolerite cemented by an ice-rich matrix. The sediment is believed to be sourced from glacial deposits and aeolian processes, and based on modeled sublimation rates, the sediment age is estimated to be at least 1 Ma (Liu et al., 2015).

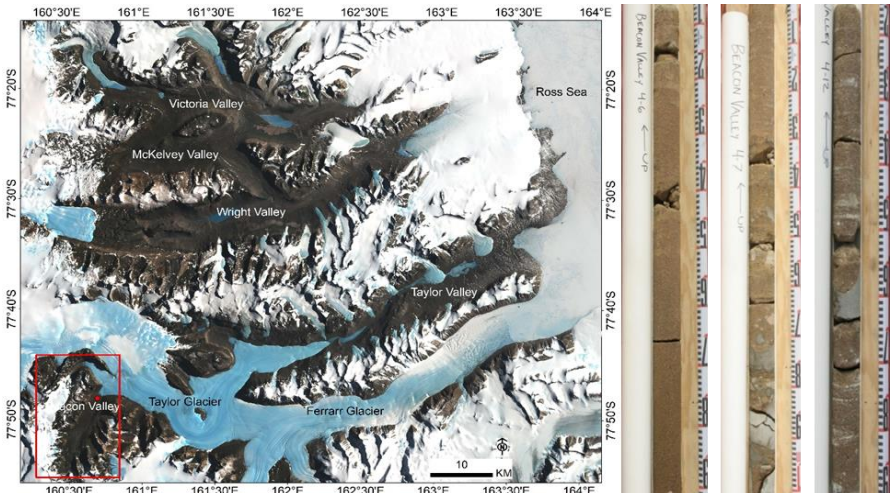


Figure 3.1: Landsat Image of Mosaic of the MDV (available at http://lima.usgs.gov/), with the location of the site (red dot) where the 30-meter ice-cemented permafrost core was collected. Meter sections of the ice-cemented permafrost core are included (6 m, 7 m, and 12 m from left to right).

## 3.3 Methods

### 3.3.1 Sample Collection

A 30.0-m ice-cemented permafrost core was collected in lower Beacon Valley in 2008 and stored in a -30.0°C freezer at the University of Washington, Seattle. Drilling began 0.4 m below dry permafrost at the top of the ice-cemented permafrost layer. The dry permafrost layer was sampled separately. The permafrost core was cut into subsamples at 0.1 to 0.3 m intervals along its depth using a carbide-tipped band saw. The frozen sediment samples were then thawed overnight in a refrigerator in sealed polyethylene bags. The meltwater was extracted from the thawed sediment by centrifuging in a double-bottom centrifuge cup (a perforated cup fitted with a 0.45 μm Nucleopore filter followed by a closed cup). The total ice content of each sample was determined gravimetrically. Two large dolerite clasts were sampled from the core at 0.6 and 2.2 m, and multiple surface dolerite samples were collected in Beacon Valley. Taylor Glacier ice from an archived core collected near the glacier terminus in Taylor Valley by Pettit et al. (2014), and fresh Beacon Valley snowfall was thawed as well.

### 3.3.2 Mg concentrations and isotope measurements

#### *3.3.2.1 Extraction Procedures and Composition*

To isolate and analyze different Mg components, 5 g of the < 2 mm fraction of permafrost sediment isolated from the 30.0-m core underwent three sequential procedures (Figure 3.2).

Secondary salt precipitates were redissolved into solution using a 1:25 soil-water extraction (SWE) following the procedure outlined in Toner et al. (2013) where 5 grams of sediment are mixed with 125 mL of water, and samples are shaken for 1 hour. The supernatant is then carefully decanting using a vacuum siphon to avoid removing any clay-sized particles, and the procedure is repeated three times. Following the SWE, exchangeable cations were removed by adding 25 mL of 1 M $NH_4$-Acetate to the same 5 g of sediment that underwent the SWE, shaking the samples for 1 hour, and vacuum siphoning the supernatant. This procedure was repeated three times to ensure the removal of all exchangeable cations (Bolou-Bi et al., 2012; Jackson, 2005; Opfergelt et al., 2014; Wimpenny et al., 2014). The supernatants from both the SWE and cation-exchange extraction were then filtered using 0.22 µm Millipore filters. After

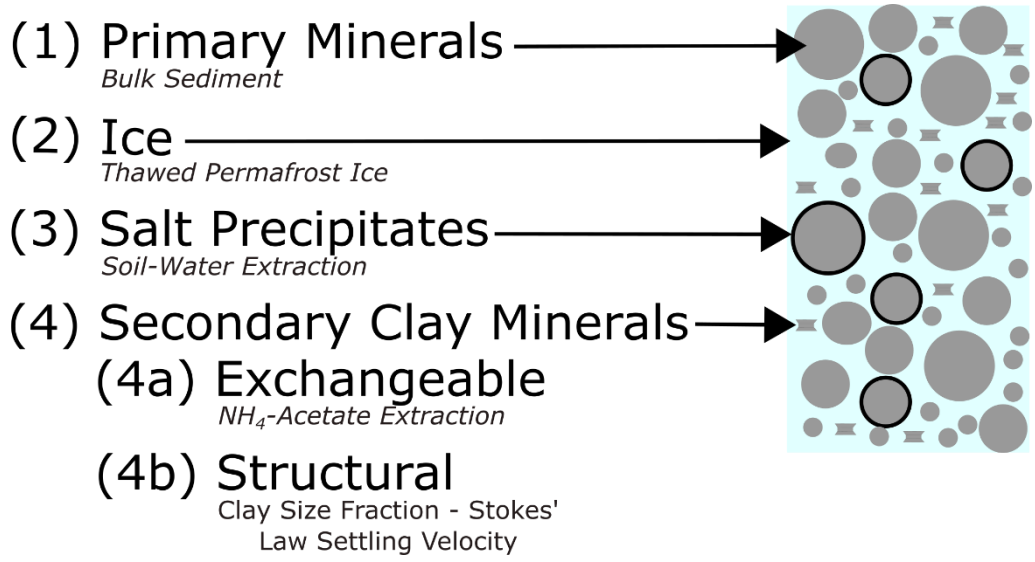


Figure 3.2: Extraction procedure in sequential order of processing. Primary minerals and permafrost ice were isolated using centrifugation after thawing permafrost samples. Following separation of sediment and ice, three successive procedures were performed on permafrost sediment to isolate different Mg reservoirs: soil-water extraction (isolates salt precipitates), $NH_4$-Acetate extraction (isolates exchangeable cations), and Stokes' Law Settling Velocity experiments (to isolate the clay size fraction). Each reservoir was then analyzed for ionic composition and Mg isotopic composition.

both SWE and cation exchange extractions, the clay-sized fraction of the remaining sediment was isolated using Stokes' Law settling velocity separations (Jackson, 2005). The SWE, cation-exchange extraction, and digested clay-sized fractions were analyzed for major cations ($Ca^{2+}$, $Mg^{2+}$, $Na^{+}$, and $K^{+}$) using Inductively Coupled Plasma Optical Emission Spectroscopy (ICP-OES) (Perkin Elmer Optima 8300).

The elemental composition of the < 2mm fraction of the permafrost sediment and bulk rock samples were determined using a ThermoARK X-ray Fluorescence Spectrometer (XRF) at the GeoAnalytical Lab at Washington State University. Mineralogy was determined using a Rigaku MiniFlex 600 benchtop X-ray diffractometer (XRD) at NASA Johnson Space Center. Particle size was determined using a Beckman Coulter LS 12-320 at the University of Washington. These procedures and results are reported in Cuozzo et al. (2020).

*3.3.3.2 Magnesium Isotope Analysis*

Magnesium isotopes were analyzed for SWE, exchangeable cations, clay-sized fraction, bulk sediment, and thawed Taylor Glacier samples. Rock digestion, chemical separation, and isotopic analysis were performed at the Isotope Laboratory at the University of Washington, following the methods detailed in Teng et al. (2007) and Yang et al. (2009). The clay and bulk sediment samples were dissolved sequentially using Optima-grade concentrated HF-$HNO_3$, $HNO_3$-HCl, and $HNO_3$. The water samples (SWE, exchangeable cations, and glacier samples) were evaporated to contain 20 µg Mg. Samples with a Ca:Mg ratio > 10 were run through Ca removal columns before Mg columns. Separation of Mg was achieved by loading 100 µL of sample dissolved in 1 N $HNO_3$ on a cation exchange chromatography column containing pre-

cleaned Bio-Rad AG50W-X8 resin (200-400 mesh) and was eluted using sequential additions of 1 N $HNO_3$. This procedure is repeated twice for each sample to ensure purification.

Magnesium isotopic ratios were measured on a Nu Plasma II Multi-Collector-ICP-MS using standard-sample bracketing (alternating measurements of samples and standards) to correct instrumental fractionation (Teng and Yang, 2014). Magnesium isotopic data are reported in delta (δ) notation, which represents parts per thousand (‰) deviations of the ratio between the sample and standard, where X refers to mass 25 or 26:

$$\delta^{x}Mg\ (‰) = 10^{3}\ x\ \left\{\frac{(^{X}Mg/^{24}Mg)_{\text{sample}}}{(^{X}Mg/^{24}Mg)_{\text{DSM3}}} - 1\right\}$$

The accuracy of the analysis was assessed using two in-house standards (Hawaiian Seawater and San Carlos Olivine) and two USGS rock standards (BHVO Basalt and MAG-1 Marine Mud). The results of these standards (Table 3.1) agree with recommended values (Hu et al., 2016; Teng et al., 2015).

Table 3.1: Magnesium isotope composition of Mg standards.

| Standard | n | $\delta^{26}$Mg | 2SD | $\delta^{25}$Mg | 2SD |
|---|---|---|---|---|---|
| Hawaii Seawater (in-house) | | -0.87 | 0.06 | -0.37 | 0.07 |
| | | -0.89 | 0.06 | -0.39 | 0.07 |
| | | -0.82 | 0.06 | -0.41 | 0.07 |
| | | -0.81 | 0.06 | -0.41 | 0.07 |
| | | -0.83 | 0.08 | -0.44 | 0.07 |
| | | -0.83 | 0.05 | -0.40 | 0.06 |
| **Average** | **6** | **-0.84** | **0.06** | **-0.40** | **0.07** |
| *Ling et al. (2011)* | *90* | *-0.83* | *0.05* | *-0.46* | *0.05* |

| | | | | | |
|---|---|---|---|---|---|
| San Carlo Olivine | | -0.23 | 0.06 | -0.14 | 0.04 |
| | | -0.26 | 0.06 | -0.12 | 0.07 |
| | | -0.26 | 0.06 | -0.15 | 0.07 |
| **Average** | **3** | **-0.25** | **0.06** | **-0.14** | **0.06** |
| *Hu et al. (2016)* | *28* | *-0.24* | *0.03* | *-0.12* | *0.02* |
| BHVO (USGS) | | -0.17 | 0.06 | -0.15 | 0.07 |
| Basalt, Hawaii Volcanic Observatory | | -0.17 | 0.06 | -0.12 | 0.07 |
| | | -0.18 | 0.06 | -0.13 | 0.06 |
| **Average** | **3** | **-0.17** | **0.06** | **-0.13** | **0.07** |
| *Teng et al. (2015)* | | *-0.21* | *0.04* | *-0.12* | *0.03* |
| MAG-1 (USGS) | | -0.23 | 0.06 | -0.12 | 0.07 |
| Marine Mud, Guld of Maine | | -0.22 | 0.06 | -0.18 | 0.07 |
| | | -0.22 | 0.08 | -0.17 | 0.07 |
| **Average** | **3** | **-0.22** | **0.07** | **-0.16** | **0.07** |
| *Teng et al. (2015)* | | *-0.25* | *0.05* | *-0.11* | *0.04* |

Results of Mg standards (n = number of analysis) run between the samples. Bolded values represent the average values of the standards in all runs and italicized represent the literature values. 2SD of Mg isotopic values represent two standard deviations of the bracketing-standard measurement during an entire analytical session.

### 3.3.3 Geochemical Modeling

Potential weathering transfers of minerals along the Beacon Valley core can be examined via equilibrium thermodynamic models using the computer-based geochemical reaction model PHREEQCi. This calculation is achieved by defining the hydro-chemical and mineralogical data collected from the Beacon Valley core. PHREEQCi utilizes the mass balance approach but allows multiple alternative weathering scenarios to be tested simultaneously. It also easily allows mineral-specific weathering processes to be modeled and alternative estimates to be made of the consumption and/or production of important species under differing weathering scenarios. Specifically in this simulation, the PHREEQCi model initially estimates the speciation based on the measured solutes in the input and output solutions at different depths, checks that the solutions are charge-balanced, and then calculates different weathering scenarios that can

account for the changes in solution chemistry using a suite of simultaneous mole-balance equations constrained by the minerals available in the Beacon Valley core; kinetic parameters are not included. Speciation and saturation-state calculations assume thermodynamic equilibrium.

## 3.4 Results

### 3.4.1 Ionic composition of thawed ice, SWE, exchangeable sites, and clay size fraction

The ionic composition was measured in the thawed permafrost ice, SWE, exchangeable cation reservoirs of the sediment, and clay size fraction (after SWE and exchangeable cation

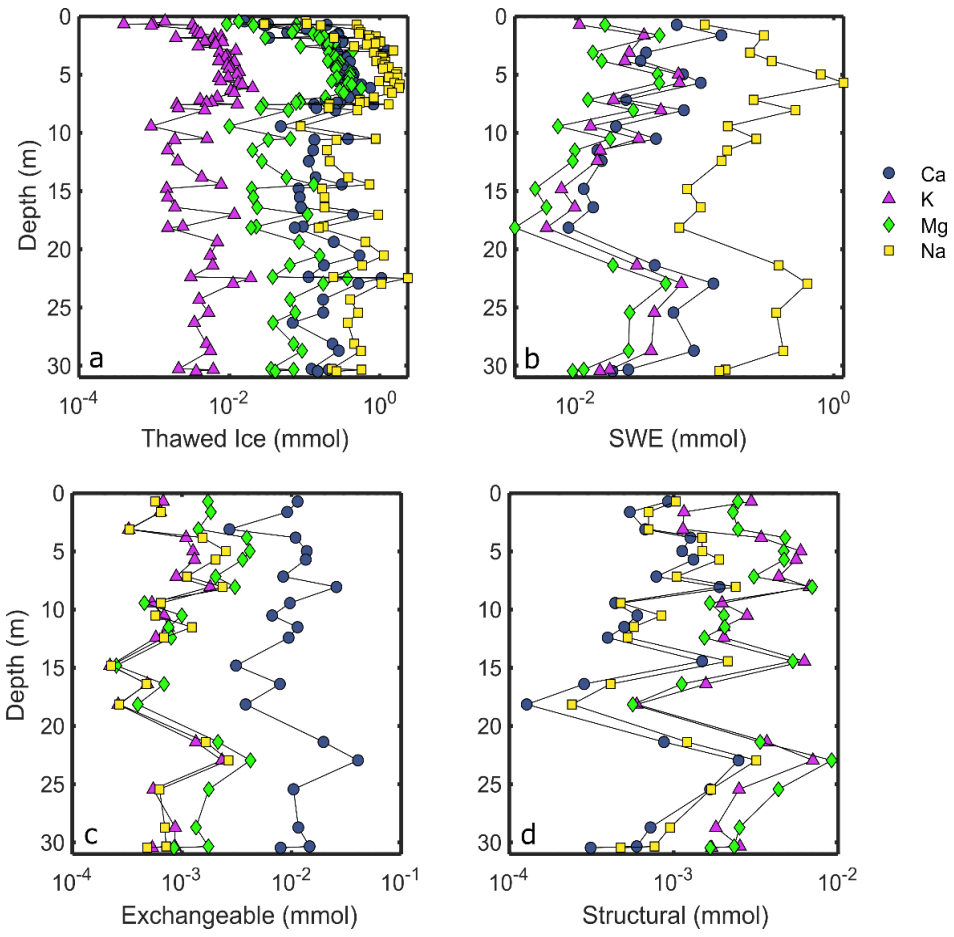


Figure 3.3: Cation ($Ca^{2+}$, $K^{+}$, $Mg^{2+}$, and $Na^{+}$) concentrations in mmol for each Mg component: (a) thawed permafrost ice, (b) Soil-water extractions (SWE), (c) Exchange sites, and (d) structural Mg (clay sized fraction).

extraction procedure) (Figure 3.3). Concentrations were converted to mmol to compare the total amount of Mg in each component and ultimately create a mass balance of Mg in the whole system. The composition of the thawed ice changes at 7.0 m. Above 7.0 m, $[Na]_{thawed\text{-}ice} >> [Ca]_{thawed\text{-}ice} = [Mg]_{thawed\text{-}ice} > [K]_{thawed\text{-}ice}$, while below 7.0 m $[Na]_{thawed\text{-}ice} > [Ca]_{thawed\text{-}ice} > [Mg]_{thawed\text{-}ice} > [K]_{thawed\text{-}ice}$. The SWE composition is dominated by Na and is consistent along the length of the core with $[Na]_{swe} >> [Ca]_{swe} \geq [K]_{swe} \geq [Mg]_{swe}$.

While Ca is the dominant cation in the exchangeable sites along the entirety of the core, there is a shift in composition at 7.0 m. Above 7.0 m, $[Ca]_{exch} > [Mg]_{exch} > [Na]_{exch} = [K]_{exch}$, while below 7.0 m, , $[Ca]_{exch} >> [Mg]_{exch} \geq [Na]_{exch} = [K]_{exch}$. The CEC (meq $kg^{-1}$) and equivalent fractions of exchange sites is represented in Figure 3.4.

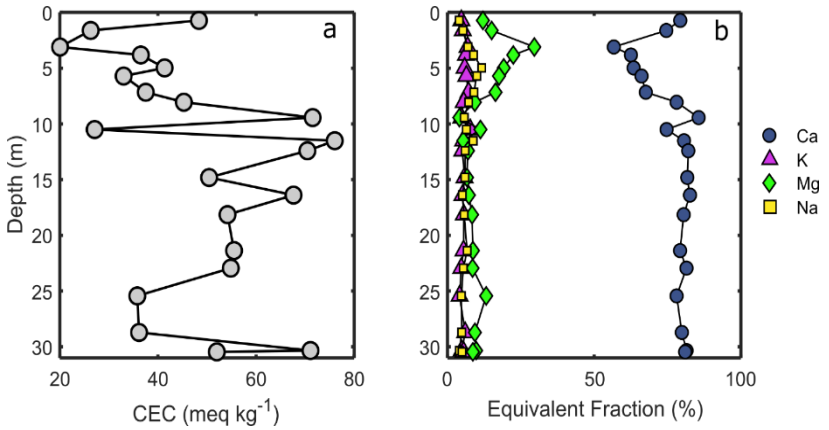


Figure 3.4: (a) Cation exchange capacity (CEC) in meq $kg^{-1}$ and (b) equivalent fraction (%) of exchangeable $Ca^{2+}$, $K^{+}$, $Mg^{2+}$, $Na^{+}$

The shift in the composition of the exchange sites is more apparent in equivalent fractions. Ca and Mg vary inversely and appear to be the controlling cations on exchange sites. The Mg fraction in the upper 7.0 m averages ~ 20%, while the Ca fraction averages ~ 67%. Below 7.0 m, the Mg fraction decreases (average = 9%), and the Ca fraction increases (average = 80%). There

is also a shift in the CEC of the sediment. The CEC is lower in the upper 7.0 m of the core (avg = 34.25 meq $kg^{-1}$; std = 9.32) and increases below 7.0 m (avg = 53.70 meq $kg^{-1}$, std = 14.79) and displays more variation. The CEC range of these soils is similar to the CEC of soils from a 2.0 m borehole in Taylor Valley (Toner and Sletten, 2013). The clay size fraction (analyzed after SWE and exchangeable cation extraction) is consistent throughout the core, with $[Mg]_{clay} = [K]_{clay} > [Na]_{clay} = [Ca]_{clay}$. The distribution of Mg is divided among the thawed ice, secondary salt precipitates, clay size fractions (structural Mg) (< 2 µm), and exchange sites (Figure 3.5). In the upper 7.0 m, $[Mg]_{thawed\ ice} >> [Mg]_{SWE} > [Mg]_{structural} \geq [Mg]_{exchangeable}$. The distribution changes below 7.0 m where $[Mg]_{thawed\ ice} > [Mg]_{SWE} > [Mg]_{structural} > [Mg]_{exchangeable}$. The Mg concentration in mmol for each component is provided in the Supplemental Material.

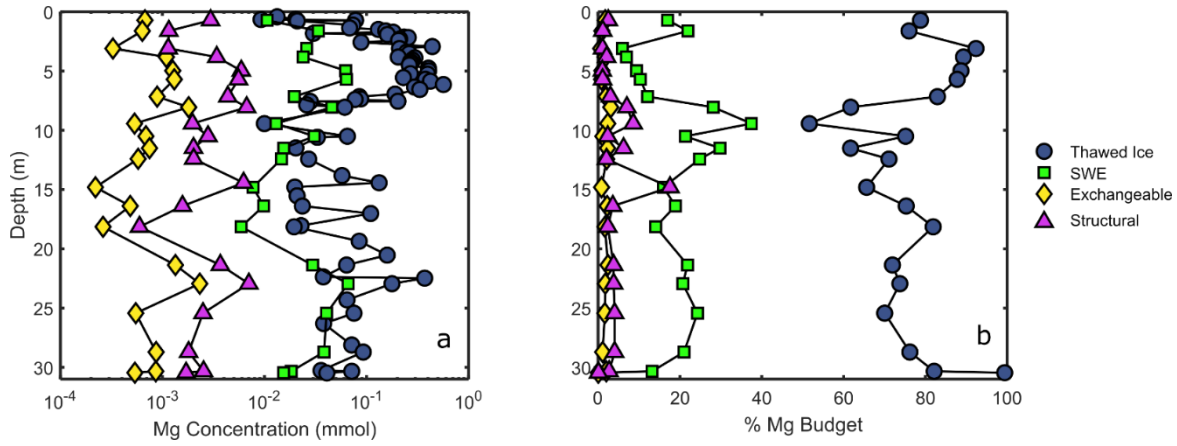


Figure 3.5: (a) Mg concentration (mmol) of each component and (b) corresponding Mg budget. Thawed permafrost ice is the largest Mg component followed by SWE, structural Mg, and exchangeable Mg.

### 3.4.2 Clay Content, Mineralogy, and Model Results

The clay-sized fraction of sediment in the Beacon Valley core profile ranges from 0.43 to 2.83% (Figure 3.6). There is a slight shift in composition at 7.0 m. Above 7.0 m, the clay fraction

is lower and more variable, with an average value of 1.29% and a standard deviation of 0.65%. Below 7.0 m, the average clay fraction is more consistent with an average value of 1.63% and a standard deviation of 0.32%

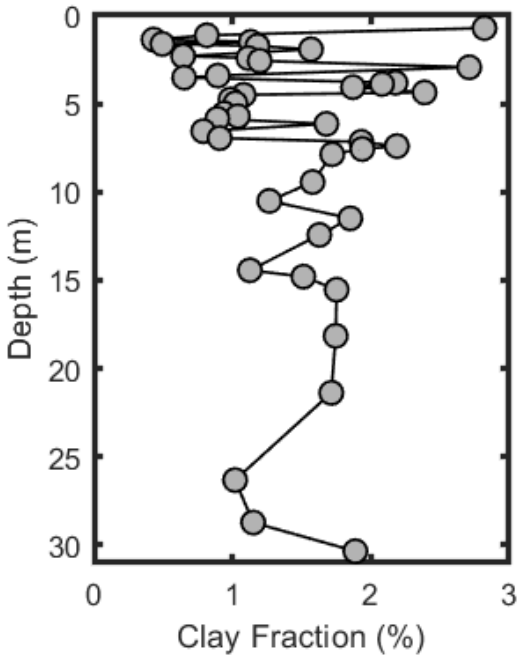


Figure 3.6: Clay sized fraction (%) along the core's depth. The clay size fraction ranges from 0.43% to 2.82%.

XRD analysis of the core sediment (reported in Cuozzo et al. (2020)) indicates that clay mineral abundance ranges 4.0-7.4% and identified saponite, kaolinite, and montmorillonite as the dominant clay minerals. Saponite is the most abundant clay and the most Mg-rich clay found in the core (Ross and Hendricks, 1945). Furthermore, the geochemical weathering scenarios generated from PHREEQCi suggest that silicate weathering is likely to be dominated by orthopyroxene weathering to saponite; however, the extent of this weathering reaction needs further investigation. CEC and the clay-sized fraction display a positive correlation with the

percentage of secondary clays, with $R^2$ values of 0.82 and 0.89, respectively (Figure 3.7). This correlation is expected as most cation exchange sites are found in clay minerals, and most clay minerals fall within the clay-sized range. We exclude one outlier (sample BV4-105-113), which has a high % secondary clay, but a consistently low CEC and low clay-sized fraction.

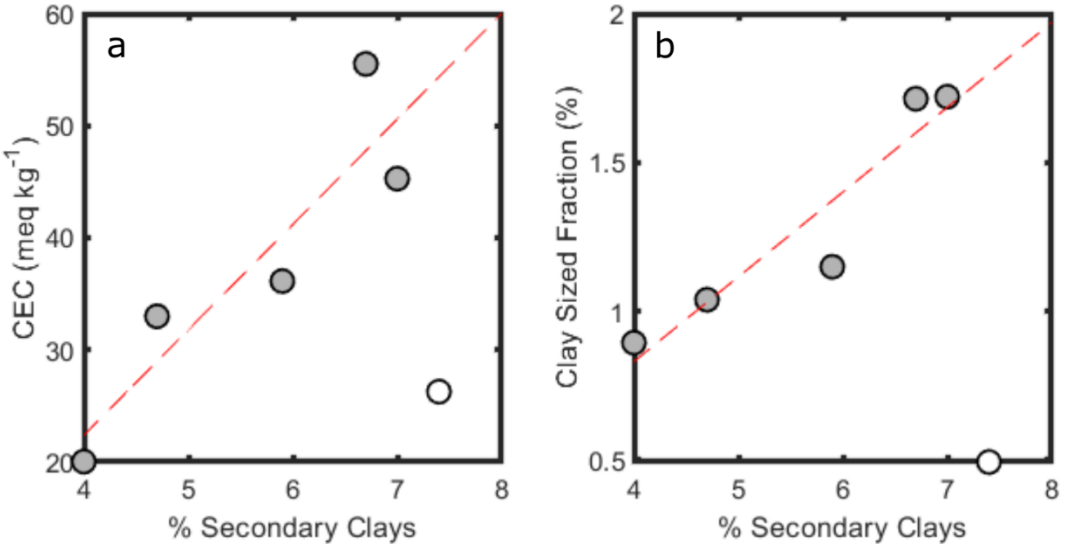


Figure 3.7: (a) Comparison of CEC vs % secondary clays measured by XRD analysis and (b) Clay sized fraction (%) vs % secondary clays measured by XRD analysis. Both figures show positive correlations.

### 3.4.3 Mg Isotopic Composition

Mg isotopes were analyzed at similar depths for bulk soils, clay fractions, exchangeable Mg, SWE, and thawed permafrost ice (Figure 3.8, Table 3.2). The two Mg isotopic endmembers are dolerite ($\delta^{26}$Mg = -0.22 ± 0.07‰, n =3) and Taylor Glacier Ice ($\delta^{26}$Mg = -0.93 ± 0.06‰, n = 6). The thawed permafrost ice is most enriched in the light isotopes relative to other components, with a range of -1.05 to -0.52‰, and there is a clear shift in composition at 7.0 m. In the upper 7.0 m, the Mg isotopic values are intermediate (average $\delta^{26}$Mg = -0.70 ± 0.05‰) between the two end members, and below 7.0 m, the Mg isotopic values are lighter (average $\delta^{26}$Mg = -0.90 ± 0.05‰) and are similar to the Taylor Glacier end-member. Some thawed permafrost ice samples

below 7.0 m have Mg isotopic values lighter than the Taylor Glacier end-member. SWE Mg isotopic composition is more enriched in the heavy isotope than the thawed ice, with a range of -0.77 to -0.39‰. There appears to be a larger difference between the thawed permafrost ice and SWE below 7.0 m. The Mg isotopic composition of clays consists of two distinct reservoirs: exchangeable Mg and structural Mg (clay-sized fraction). Exchangeable Mg isotopic composition is within error of the thawed ice in most cases and has a range of 0.95 to -0.65‰. There are a few exceptions where the Mg isotopic composition of the exchangeable Mg is slightly heavier than the thawed permafrost ice composition. In comparison, structural Mg, or Mg incorporated during the formation of clay minerals, is isotopically heavier than all other reservoirs (including dolerite rock and bulk sediment), suggesting preferential incorporation of the heavy isotope. The Mg isotopic composition of structural Mg is consistent along the length of the core, with a range of -0.10 to + 0.03‰.

Table 3.2: Mg isotopic composition of Beacon Valley bulk sediment, thawed permafrost ice, soil-water extraction, exchangeable, structural, rock, and Taylor Glacier ice.

| Sample Type | Sample Name | Midpoint Depth (m) | $\delta^{26}$Mg | 2SD | $\delta^{25}$Mg | 2SD |
|---|---|---|---|---|---|---|
| Bulk Sediment | BV4-105-113 | 1.49 | -0.26 | 0.06 | -0.14 | 0.05 |
| | BV4-529-532 | 5.71 | -0.22 | 0.06 | -0.12 | 0.05 |
| | BV4-675-677 | 7.16 | -0.22 | 0.06 | -0.10 | 0.05 |
| | BV4-744-748 | 7.86 | -0.17 | 0.06 | -0.08 | 0.05 |
| | BV4-902-905 | 9.44 | -0.23 | 0.06 | -0.10 | 0.05 |
| | BV4-1005-1016 | 10.51 | -0.19 | 0.06 | -0.07 | 0.05 |
| | BV4-1108-1110 | 11.49 | -0.17 | 0.06 | -0.08 | 0.05 |
| | BV4-1202-1204 | 12.43 | -0.13 | 0.06 | -0.07 | 0.05 |
| | BV4-1438-1440 | 14.79 | -0.18 | 0.06 | -0.10 | 0.05 |
| | BV4-2096-2098 | 21.37 | -0.21 | 0.06 | -0.07 | 0.05 |
| | BV4-2830-2833 | 28.72 | -0.21 | 0.06 | -0.10 | 0.05 |
| Thawed Permafrost Ice* | BV4-0-4.5 | 0.42 | -0.52 | 0.05 | -0.23 | 0.05 |
| | BV4-22-24 | 0.63 | -0.70 | 0.05 | -0.34 | 0.05 |
| | BV4-28-35 | 0.72 | -0.70 | 0.05 | -0.39 | 0.05 |
| | BV4-34.5-39.5 | 0.77 | -0.74 | 0.05 | -0.38 | 0.05 |

| | | | | | | |
|---|---|---|---|---|---|---|
| | BV4-93-100 | 1.37 | -0.80 | 0.05 | -0.42 | 0.05 |
| | BV4-105-113 | 1.49 | -0.81 | 0.05 | -0.44 | 0.05 |
| | BV4-120-123 | 1.62 | -0.82 | 0.05 | -0.42 | 0.05 |
| | BV4-130-135 | 1.73 | -0.82 | 0.05 | -0.44 | 0.05 |
| | BV4-142-143 | 1.83 | -0.77 | 0.05 | -0.41 | 0.05 |
| | BV4-150-154 | 1.92 | -0.79 | 0.05 | -0.42 | 0.05 |
| | BV4-189-192 | 2.31 | -0.75 | 0.05 | -0.40 | 0.05 |
| | BV4-200-203 | 2.42 | -0.68 | 0.05 | -0.34 | 0.05 |
| | BV4-215-219 | 2.57 | -0.73 | 0.05 | -0.37 | 0.05 |
| | BV4-269-271 | 3.10 | -0.71 | 0.05 | -0.39 | 0.05 |
| | BV4-340-343 | 3.82 | -0.68 | 0.05 | -0.38 | 0.05 |
| | BV4-347-350 | 3.89 | -0.67 | 0.05 | -0.35 | 0.05 |
| | BV4-364-368 | 4.06 | -0.63 | 0.05 | -0.33 | 0.05 |
| | BV4-379-382 | 4.21 | -0.65 | 0.05 | -0.34 | 0.05 |
| | BV4-395-397 | 4.36 | -0.68 | 0.05 | -0.36 | 0.04 |
| | BV4-455-460 | 4.98 | -0.68 | 0.05 | -0.37 | 0.04 |
| | BV4-483-488 | 5.26 | -0.64 | 0.05 | -0.34 | 0.04 |
| | BV4-529-532 | 5.71 | -0.63 | 0.05 | -0.32 | 0.04 |
| | BV4-573-575 | 6.14 | -0.68 | 0.05 | -0.35 | 0.04 |
| | BV4-613-618 | 6.56 | -0.65 | 0.05 | -0.35 | 0.04 |
| | BV4-653-656 | 6.95 | -0.64 | 0.05 | -0.34 | 0.04 |
| | BV4-675-677 | 7.16 | -0.76 | 0.05 | -0.41 | 0.04 |
| | BV4-698-702 | 7.40 | -0.89 | 0.05 | -0.45 | 0.04 |
| | BV4-744-748 | 7.86 | -0.95 | 0.05 | -0.49 | 0.04 |
| | BV4-902-905 | 9.44 | -1.02 | 0.03 | -0.54 | 0.04 |
| | BV4-1005-1016 | 10.51 | -0.92 | 0.05 | -0.49 | 0.04 |
| | BV4-1108-1110 | 11.49 | -0.97 | 0.05 | -0.52 | 0.06 |
| | BV4-1202-1204 | 12.43 | -0.98 | 0.05 | -0.50 | 0.06 |
| | BV4-1438-1440 | 14.79 | -0.95 | 0.05 | -0.49 | 0.06 |
| | BV4-1598-1600 | 16.39 | -0.89 | 0.05 | -0.49 | 0.06 |
| | BV4-1773-1776 | 18.15 | -0.91 | 0.05 | -0.48 | 0.06 |
| | BV4-2096-2098 | 21.37 | -0.85 | 0.05 | -0.42 | 0.06 |
| | BV4-2253-2256 | 22.95 | -0.85 | 0.05 | -0.46 | 0.06 |
| | BV4-2502-2505 | 25.44 | -0.91 | 0.03 | -0.46 | 0.04 |
| | BV4-2830-2833 | 28.72 | -1.05 | 0.03 | -0.56 | 0.04 |
| | BV4-2990-2998 | 30.34 | -0.84 | 0.05 | -0.41 | 0.04 |
| | BV4-3007-3010 | 30.49 | -0.92 | 0.05 | -0.46 | 0.06 |
| SWE | BV4-28-35 | 0.72 | -0.71 | 0.06 | -0.35 | 0.04 |
| | BV4-105-113 | 1.49 | -0.77 | 0.06 | -0.41 | 0.06 |
| | BV4-340-343 | 3.82 | -0.42 | 0.06 | -0.26 | 0.04 |
| | BV4-529-532 | 5.71 | -0.50 | 0.06 | -0.26 | 0.06 |
| | BV4-675-677 | 7.16 | -0.46 | 0.06 | -0.26 | 0.06 |

| | | | | | | |
|---|---|---|---|---|---|---|
| | BV4-744-748 | 7.86 | -0.74 | 0.06 | -0.39 | 0.06 |
| | BV4-902-905 | 9.44 | -0.69 | 0.06 | -0.36 | 0.06 |
| | BV4-1005-1016 | 10.51 | -0.54 | 0.06 | -0.29 | 0.06 |
| | BV4-1108-1110 | 11.49 | -0.51 | 0.06 | -0.28 | 0.06 |
| | BV4-1202-1204 | 12.43 | -0.64 | 0.06 | -0.32 | 0.06 |
| | BV4-1438-1440 | 14.79 | -0.51 | 0.06 | -0.24 | 0.06 |
| | BV4-1598-1600 | 16.39 | -0.46 | 0.06 | -0.28 | 0.09 |
| | BV4-1773-1776 | 18.15 | -0.54 | 0.06 | -0.30 | 0.04 |
| | BV4-2096-2098 | 21.37 | -0.53 | 0.06 | -0.27 | 0.06 |
| | BV4-2253-2256 | 22.95 | -0.58 | 0.06 | -0.29 | 0.04 |
| | BV4-2830-2833 | 28.72 | -0.74 | 0.06 | -0.37 | 0.06 |
| | BV4-2990-2998 | 30.34 | -0.39 | 0.06 | -0.30 | 0.04 |
| Exchangeable | BV4-28-35 | 0.72 | -0.85 | 0.08 | -0.42 | 0.07 |
| | BV4-120-123 | 1.62 | -0.89 | 0.08 | -0.46 | 0.07 |
| | BV4-340-343 | 3.82 | -0.72 | 0.08 | -0.38 | 0.07 |
| | BV4-455-460 | 4.98 | -0.74 | 0.08 | -0.40 | 0.07 |
| | BV4-529-532 | 5.71 | -0.65 | 0.06 | -0.49 | 0.09 |
| | BV4-675-677 | 7.16 | -0.75 | 0.08 | -0.38 | 0.07 |
| | BV4-763-768 | 8.06 | -0.95 | 0.08 | -0.51 | 0.07 |
| | BV4-902-905 | 9.44 | -0.79 | 0.08 | -0.40 | 0.07 |
| | BV4-1005-1016 | 10.51 | -0.93 | 0.08 | -0.44 | 0.07 |
| | BV4-1110-1112 | 11.51 | -0.73 | 0.08 | -0.42 | 0.07 |
| | BV4-1200-1202 | 12.41 | -0.81 | 0.06 | -0.48 | 0.09 |
| | BV4-1440-1442 | 14.81 | -0.79 | 0.06 | -0.44 | 0.09 |
| | BV4-1598-1600 | 16.39 | -0.89 | 0.08 | -0.49 | 0.07 |
| | BV4-1773-1776 | 18.15 | -0.88 | 0.08 | -0.50 | 0.07 |
| | BV4-2096-2098 | 21.37 | -0.88 | 0.08 | -0.48 | 0.07 |
| | BV4-2253-2256 | 22.95 | -0.89 | 0.08 | -0.48 | 0.07 |
| | BV4-2502-2505 | 25.44 | -0.78 | 0.08 | -0.49 | 0.07 |
| | BV4-2830-2833 | 28.72 | -0.85 | 0.06 | -0.52 | 0.09 |
| | BV4-2990-2998 | 30.34 | -0.80 | 0.06 | -0.51 | 0.06 |
| Structural | BV4-28-35 | 0.72 | -0.10 | 0.05 | -0.02 | 0.06 |
| | BV4-120-123 | 1.62 | 0.02 | 0.06 | -0.05 | 0.09 |
| | BV4-269-271 | 3.10 | -0.05 | 0.05 | -0.05 | 0.06 |
| | BV4-340-343 | 3.82 | -0.03 | 0.05 | -0.07 | 0.06 |
| | BV4-455-460 | 4.98 | 0.02 | 0.06 | -0.10 | 0.09 |
| | BV4-529-532 | 5.71 | -0.03 | 0.06 | -0.01 | 0.06 |
| | BV4-675-677 | 7.16 | -0.04 | 0.06 | -0.07 | 0.06 |
| | BV4-763-768 | 8.06 | -0.06 | 0.06 | -0.01 | 0.06 |
| | BV4-902-905 | 9.44 | -0.04 | 0.06 | -0.11 | 0.09 |
| | BV4-1005-1016 | 10.51 | -0.06 | 0.06 | -0.06 | 0.06 |
| | BV4-1108-1110 | 11.49 | -0.03 | 0.06 | -0.13 | 0.09 |

| | | | | | | |
|---|---|---|---|---|---|---|
| | BV4-1200-1202 | 12.41 | -0.05 | 0.06 | -0.07 | 0.06 |
| | BV4-1440-1442 | 14.81 | -0.08 | 0.06 | -0.02 | 0.06 |
| | BV4-1598-1600 | 16.39 | -0.06 | 0.06 | -0.09 | 0.06 |
| | BV4-1773-1776 | 18.15 | -0.08 | 0.06 | -0.07 | 0.06 |
| | BV4-2096-2098 | 21.37 | -0.01 | 0.06 | -0.08 | 0.09 |
| | BV4-2253-2256 | 22.95 | 0.03 | 0.06 | -0.12 | 0.09 |
| | BV4-2502-2505 | 25.44 | -0.03 | 0.06 | -0.02 | 0.06 |
| | BV4-2830-2833 | 28.72 | -0.06 | 0.06 | -0.02 | 0.06 |
| | BV4-2990-2998 | 30.34 | -0.06 | 0.06 | -0.01 | 0.06 |
| | BV4-3005-3007 | 30.46 | -0.05 | 0.06 | -0.06 | 0.06 |
| Rock* | Dolerite 1 | surface | -0.23 | 0.06 | -0.13 | 0.05 |
| | Dolerite 2 (from core) | 0.60 | -0.20 | 0.06 | -0.12 | 0.05 |
| | Dolerite 3 (from core) | 2.20 | -0.24 | 0.06 | -0.12 | 0.05 |
| Taylor Glacier/Snow | Beacon Valley Fresh Snow* | surface | -0.98 | 0.06 | -0.51 | 0.07 |
| | Taylor Glacier 1* | calved | -0.86 | 0.06 | -0.50 | 0.05 |
| | Taylor Glacier 2* | calved | -0.84 | 0.06 | -0.40 | 0.05 |
| | Taylor Glacier Nirvana A* | surface | -1.06 | 0.06 | -0.53 | 0.07 |
| | Taylor Glacier Nirvana Core A1 | 0.52 | -1.03 | 0.06 | -0.49 | 0.04 |
| | Taylor Glacier Nirvana Core 6 | 2.87 | -0.94 | 0.06 | -0.55 | 0.09 |
| | Taylor Glacier Nirvana Core 9 | 5.60 | -1.02 | 0.06 | -0.54 | 0.04 |
| | Taylor Glacier Nirvana Core 14 | 9.24 | -0.80 | 0.06 | -0.46 | 0.04 |
| | Taylor Glacier Nirvana Core 17 | 11.86 | -0.87 | 0.06 | -0.51 | 0.04 |
| | Taylor Glacier Nirvana Core 22 | 16.02 | -0.87 | 0.06 | -0.53 | 0.09 |

2SD of Mg isotopic values represent two standard deviations of the bracketing standard measurement during an entire analytical session.

* Data from Cuozzo et al. (2020)

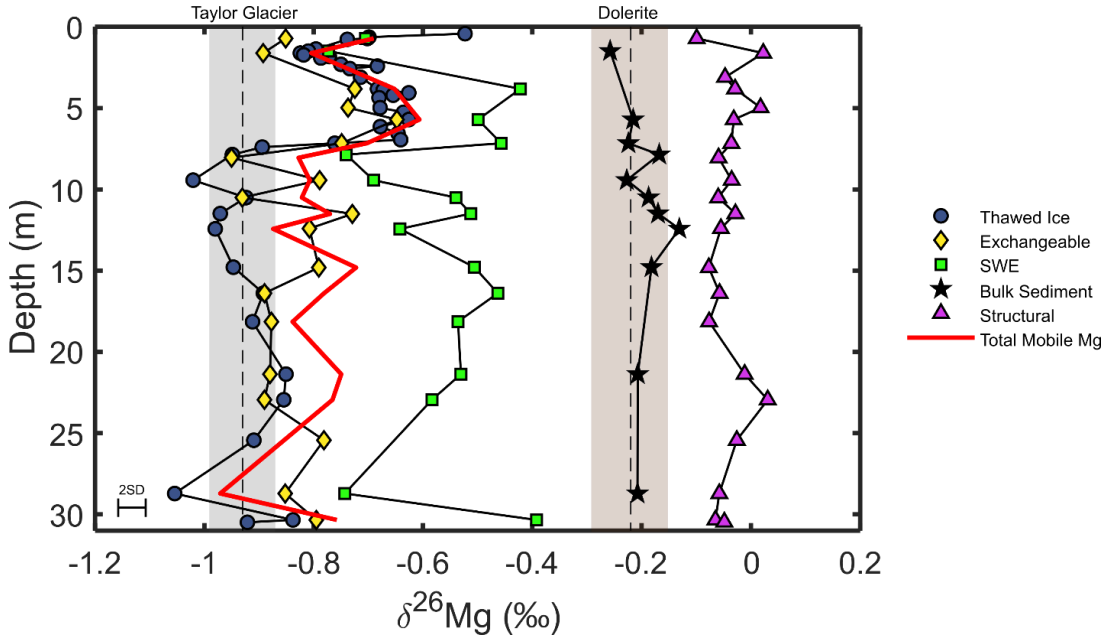


Figure 3.8: Mg isotopic analysis of the thawed permafrost ice samples, soil-water extractions, exchangeable Mg, structural Mg (clay-sized fraction), averaged dolerite rocks, and averaged Taylor Glacier/Beacon snowfall values. The Mg sources in the Antarctica Dry Valleys are shown in the shaded regions. Taylor Glacier/Beacon snowfall (gray) has an Mg isotopic composition of -0.93 ± 0.06‰ and dolerite (brown) has an average value of -0.22 ± 0.07‰. Thawed permafrost ice values are plotted with blue circles. From 0-7 meters, the Mg isotopic composition is intermediate between Taylor Glacier/Beacon snowfall and dolerite, and from 7-30 meters, the isotopic composition is near or within the range of Taylor Glacier/Beacon snowfall. The exchangeable Mg (yellow diamonds) has a similar composition to the thawed permafrost ice, with a slight preference for the heavy isotope. Soil-water extractions (green squares), representing secondary salt precipitates, preferentially incorporate heavy isotopes into their structure compared to the thawed permafrost ice. The structural Mg in the clay sized fraction (pink triangles) is the heaviest Mg component and is consistent along the depth of the core with a preference for the heavy isotope. The bolded red line represents the corrected thawed permafrost ice corrections when considering the influence of all Mg components in the Beacon Valley core.

## 3.5 Discussion

Magnesium in Beacon Valley permafrost is primarily sourced from two reservoirs: marine aerosols (represented by Taylor Glacier ice), deposited by dust, katabatic winds, and snowmelt events during warmer summer months, and chemical weathering of Ferrar Dolerite. In Cuozzo et al. (2020), we explored the extent of chemical weathering of dolerite in the Beacon Valley core using the Mg isotopic composition of the thawed permafrost ice. In this study, we

expand on this analysis and use Mg isotopes to further trace rock-water interactions, including evaluating the influence of secondary salt precipitation, cation exchange, and clay mineral formation, and provide an updated analysis of the controls on rock-water interactions in the MDV. Because weathering products remain locked in place, we also calculate fractionation factors between the fluid phase and each Mg component and show how these equilibrium fractionation factors can be applied to other systems that help constrain the global Mg budget.

### 3.5.1 Secondary Salt Precipitation

Salts are commonly found in the MDV and typically consist of Mg, Ca, or Na sulfates. Evidence for precipitation of secondary salts in Beacon Valley soils is revealed in the XRD analysis, primarily in the form of gypsum. While Mg-bearing salts were not identified in XRD analysis, there is potential for Mg to coprecipitate with gypsum. Furthermore, extractable Mg was still released during the SWE, suggesting Mg-bearing salts exist in the sediment. Chemical models of secondary salt precipitation in the Beacon Valley core (Cuozzo et al., 2020) suggest that Mg-sulfates, epsomite and meridianiite, may form in the soil profile. It is noted that the effects of ion exclusion during freezing was not included in the chemical model presented in Cuozzo et al. (2020), which may lead to underestimation of accumulated Mg salts. When water-rich sediment freezes, mobile ions are expelled from the ice and accumulate on the interface between the growing ice lens and the mineral layer (Hallet, 1978; Ostroumov et al., 2001). This process creates zones of high solute concentrations, and ultimately, zones of secondary mineral precipitation. This phenomenon may explain why regions in the lower 7.0 – 30.0 m of the core have adjacent sections of very high ice content (up to 80%) and low ice content (< 20%).

*3.5.1.1 Fractionation factor of Mg-Salt Precipitation*

There are two main hypotheses for Mg secondary minerals precipitation: (1) coprecipitation of Mg with gypsum, and (2) precipitation of epsomite ($MgSO_4 \cdot 7H_2O$) and/or meridianiite ($MgSO_4 \cdot 11H_2O$). Coprecipitation of Mg with gypsum has been shown to occur in laboratory experiments, but the amount that coprecipitates with gypsum is small compared to the amount of Mg in solution and has a small partition coefficient between $0.1 \times 10^{-5}$ and $4.3 \times 10^{-5}$ (Kushnir, 1980). However, these experiments were performed at temperatures higher than those experienced in Beacon Valley and under laboratory conditions. Few other studies have looked at Mg isotopic fractionation from coprecipitation of Mg with gypsum, especially at subfreezing temperatures.

The second, and more likely scenario, is the precipitation of magnesium sulfates, epsomite, and meridianiite. When epsomite or meridianiite forms, heavy isotopes are preferentially removed from the solution and incorporated into the mineral structure (Li et al., 2011). The average experimental fractionation factor between epsomite and $MgSO_4$ in solution is 0.6‰ (Li et al., 2011). The theoretical fractionation factor between meridianiite and the solution has been determined to be 0.3 and 2.2‰, with a large difference between the two values resulting from different model scenarios. (Rustad et al., 2010; Schauble, 2011).

The fractionation factor between the soil-water extraction and thawed permafrost ice in the Beacon Core sediment can be calculated using the following equation:

$$\Delta^{26}Mg_{min-soln} = \delta^{26}Mg_{min} - \delta^{26}Mg_{soln} \quad (3.1)$$

Where $\delta^{26}Mg_{min}$ is the Mg isotopic composition of the SWE and $\delta^{26}Mg_{soln}$ is the Mg isotopic composition of the thawed ice. The average fractionation factor is 0.3‰ and is consistent with

the theoretical fractionation factor of meridianiite determined from (Schauble, 2011) (Figure 3.9, Table 3.3) with a similar best-fit equation for a $\Delta^{26}$Mg-1/T$^2$ diagram:

$$\Delta^{26}Mg_{min-soln} = 0.0192 \times 10^6/T^2 \quad (3.2)$$

Temperature for the Beacon Valley core is reported in Cuozzo et al. (2020) and was determined based on hourly temperature recorded at depths of 1.25, 2.5, 5.0, 10.0, 20.0, and 30.0 m and interpolated to each sample depth. The fractionation factor between the thawed ice and SWE displays a temperature dependence and is greatest at the coldest temperature in the core. This is consistent with equilibrium isotopic fractionation generally decreasing with increasing temperature in proportion to 1/T$^2$ (Bigeleisen and Mayer, 1947; O'Neil, 1986). Above 7.0 m, where temperatures are warmer, the average fractionation factor is 0.11‰, while below 7.0 m,

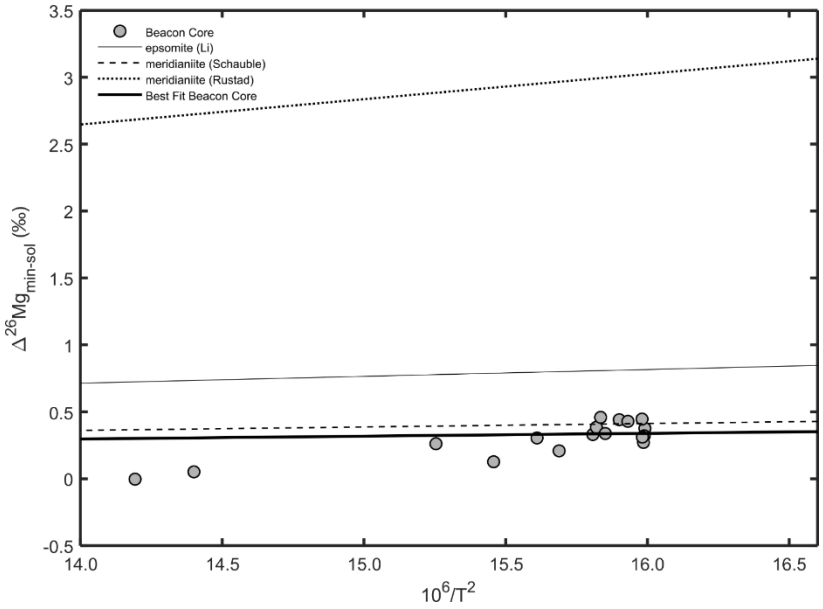


Figure 3.9: Plot of Mg isotopic fractionation factor between the thawed permafrost ice and secondary salt precipitates isolated using a soil-water extraction as a function of 10$^6$/T$^2$. The dark bolded lines represent the best fit equation for the fractionation factor forced through the origin. The two dashed lines represent previously determine fractionation factors for meridianiite calculated by Schauble (2011) and (Rustad et al., 2010), and the thin solid line represents the experimental fractionation factor for epsomite determined by (Li et al., 2011). While meridianiite was not discovered during XRD analysis of these samples, the fractionation factors is consistent with the theoretical fractionation factor determined by Schauble (2011).

where temperatures are colder, the average fractionation factor is 0.35‰. This difference may help explain the Mg isotopic composition of the thawed permafrost ice that was lighter than Taylor Glacier values seen below 7.0 m.

Table 3.3: Core temperature and fractionation factor between thawed permafrost ice and secondary salt precipitates

| Sample ID | Temperature (°C) | Temperature (K) | $10^6/T^2$ | Fractionation |
|---|---|---|---|---|
| BV4-28-35 | -7.71 | 265.44 | 14.19 | 0.00 |
| BV4-120-123 | -9.63 | 263.52 | 14.40 | 0.05 |
| BV4-340-343 | -17.11 | 256.04 | 15.25 | 0.26 |
| BV4-529-532 | -18.80 | 254.35 | 15.46 | 0.13 |
| BV4-675-677 | -20.05 | 253.10 | 15.61 | 0.30 |
| BV4-763-768 | -20.68 | 252.47 | 15.69 | 0.21 |
| BV4-902-905b | -21.63 | 251.52 | 15.81 | 0.33 |
| BV4-1005-1016 | -21.73 | 251.42 | 15.82 | 0.38 |
| BV4-1110-1112 | -21.85 | 251.30 | 15.83 | 0.46 |
| BV4-1200-1202 | -21.98 | 251.17 | 15.85 | 0.34 |
| BV4-1440-1442 | -22.37 | 250.78 | 15.90 | 0.44 |
| BV4-1598-1600 | -22.61 | 250.54 | 15.93 | 0.43 |
| BV4-1773-1776 | -23.08 | 250.07 | 15.99 | 0.38 |
| BV4-2096-2098 | -23.06 | 250.09 | 15.99 | 0.32 |
| BV4-2253-2256 | -23.04 | 250.11 | 15.99 | 0.27 |
| BV4-2830-2833 | -23.01 | 250.14 | 15.98 | 0.31 |
| BV4-2990-2998 | -23.00 | 250.15 | 15.98 | 0.45 |

### 3.5.2 Secondary Clay Minerals

In clay minerals, there are two sites where Mg is held: (1) adsorbed on exchange sites, and (2) structurally bound in octahedral sites. Mg held on each of these may exhibit different fractionation properties. Clay minerals in the Beacon Valley core consist primarily of saponite, a trioctahedral smectite that forms from weathering of mafic rocks with high amounts of structural Mg. Smectites are 2:1 phyllosilicates that have layers of octahedra ($Mg^{2+}$ or $Al^{3+}$ bonded to an O

or OH) between two tetrahedra layers ($Si^{4+}$ surrounded by oxygen atoms). Because of the large amounts of Mg incorporated into the structure of these clay minerals, most of the Mg is found in structural sites rather than exchange sites, which is reflected in Beacon Valley sediment. In the upper 7.0 m, exchangeable and structural Mg consists of approximately 42% and 58% of Mg in clay minerals, respectively. In the lower 7.0-30.0 m, exchangeable and structural Mg consists of roughly 34% and 66%, respectively (Figure 3.10).

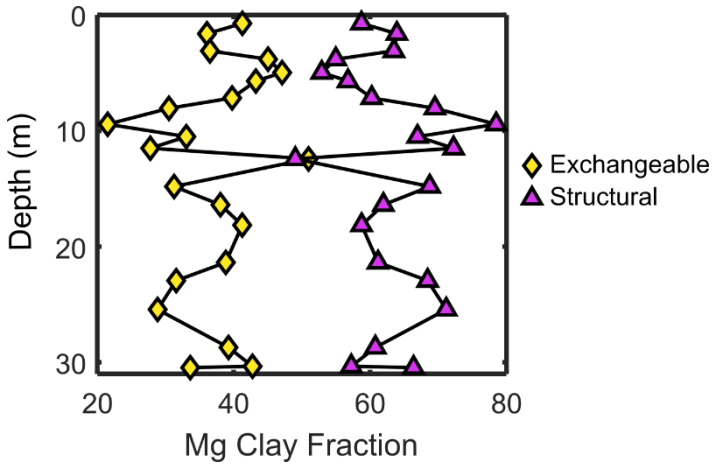


Figure 3.10: Distribution (%) of Mg in the clay sized fraction. Structural Mg is the dominant component along the core's depth.

This difference can be explained by the higher concentration of aqueous Mg in the upper 7.0 m of the thawed permafrost ice, creating a larger Mg pool to react with the exchange sites. While Ca is the dominant cation on the exchange sites, the Ca/Mg ratio in the upper 7.0 m of the core is approximately 1.0, while below 7.0 m, the Ca/Mg ratio is greater than 1.0. The smaller Ca/Mg ratio allows Mg to occupy more exchange sites, as seen in the concentration of exchangeable Mg (Figure 3.11). This change in composition with depth suggests that structural Mg may impart a greater influence on the Mg isotopic composition in the lower sections of this core. In comparison, exchangeable Mg has a greater influence on upper sections of the core.

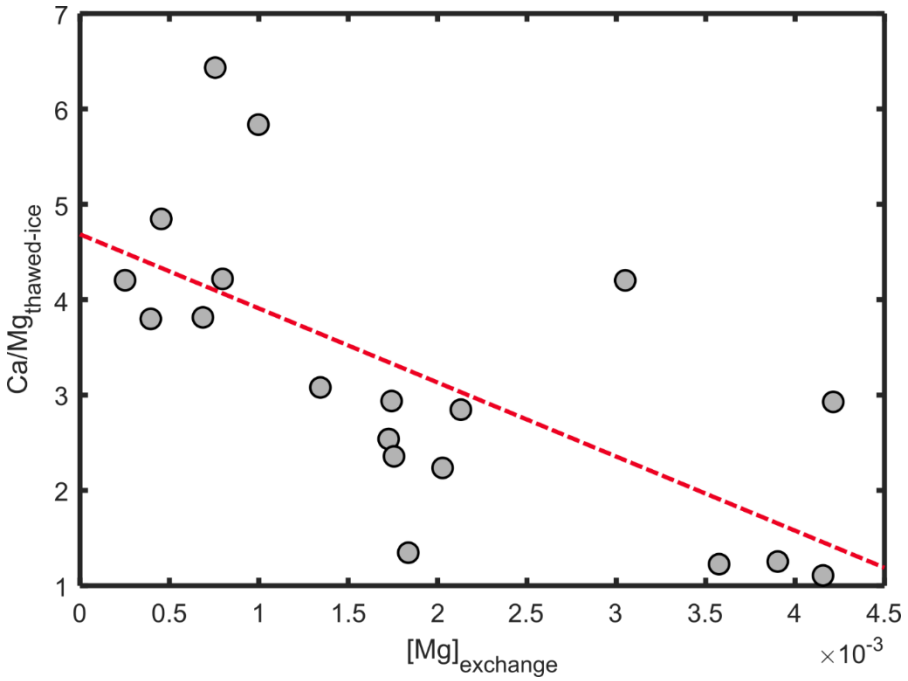


Figure 3.11: Plot of Ca/Mg ratio in the thawed ice and $[Mg]_{exchangeable}$. There data exhibits a negative correlation where the Ca/Mg ratio decreases, the amount of exchangeable Mg increases.

*3.5.2.1 Exchangeable Mg Fractionation*

Previous studies have explored the effects of exchange reactions on Mg isotopic composition of soils and have shown that the exchangeable composition is typically dependent on two factors: (1) fractionation and (2) composition of the pool of exchangeable cations (Hindshaw et al., 2020; Huang et al., 2012; Opfergelt et al., 2014; Opfergelt et al., 2012; Teng et al., 2010; Wimpenny et al., 2014). Hindshaw et al. (2020), using experimental data, found that saponite exchange sites preferentially retain the light Mg isotope. In contrast, in Beacon Valley soils, the control on the Mg isotopic composition of exchangeable Mg appears to be the isotopic composition of the thawed permafrost ice, which is the source of Mg to the exchange sites. When $\delta^{26}Mg_{exchangeable}$ is plotted against $\delta^{26}Mg_{thawed\text{-}ice}$, the values cluster around a 1:1 ratio line (Figure 3.12). Those values that plot away from a 1:1 ratio all fall within the lower 7.0 – 30.0 meters of

the core and are above the 1:1 ratio line, indicating that these samples preferentially incorporate the heavy isotope onto the exchange sites. A potential control on the apparent fractionation between some samples may be due to the concentration of Mg on the exchange sites (Figure 3.12). Those samples that fall away from the 1:1 line all have low $[Mg]_{exchangeable}$ compared to those that fall along the 1:1 line. One possible explanation is that soils with $[Mg]_{exchangeable}$ may be more strongly influenced by any residual salts remaining on the sediment during the extraction. While the SWE should have removed the majority of extractable salts that remained on the sediment (Toner et al., 2013), there is still potential that not all extractable salts were removed. While this may not have had a strong influence on those samples with higher $[Mg]_{exchangeable}$, it may influence those with lower concentrations. The heavier Mg isotopic composition of these samples is consistent with the SWE having a heavier Mg isotopic composition than the exchangeable Mg. Nonetheless, the largest influence on the Mg isotopic composition of the exchange sites appears to be the Mg isotopic composition of the thawed ice reservoir that is in contact with the exchange sites, with a slight prefer for the heavy isotope.

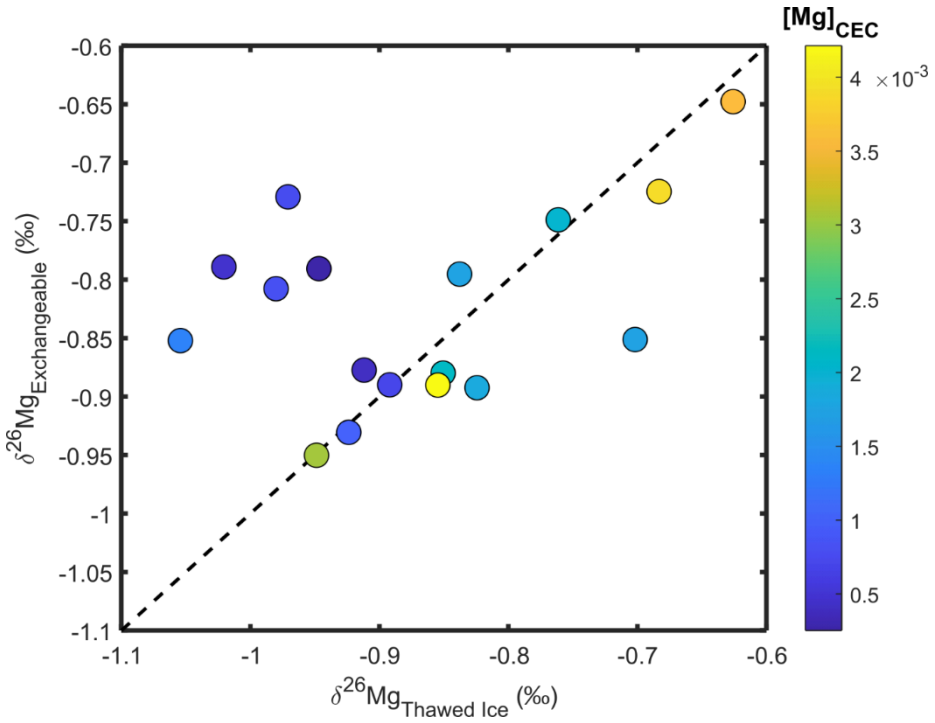


Figure 3.12: Comparison of the $\delta^{26}Mg_{exchangeable}$ and $\delta^{26}Mg_{thawed\ ice}$ plotted with a 1:1 line. The Mg isotopic composition of exchangeable Mg is consistent with the Mg isotopic composition of the thawed ice, suggesting little to no fractionation. Those values that do not fall along the 1:1 line have a low $[Mg]_{CEC}$ suggesting a potential influence from secondary salts remaining on sediment.

*3.5.2.2 Structural Mg Fractionation - Saponite*

While clay mineral formation is minimal in the MDV, clays have been discovered in the MDVs with varying climate conditions; amorphous and incomplete clay formation suggests that these clays have formed in-situ (Quinn et al., 2020). Saponite forms in environments with mafic parent rock materials, consistent with the sediment in Beacon Valley. Furthermore, chemical modeling, based on the mineralogical and ionic composition of the Beacon Valley core, supports the in-situ formation of saponites due to weathering of orthopyroxene. The Mg isotopic composition of the clay-sized fraction is the heaviest Mg component in the core showing little change with depth (Figure 3.8). The heavy Mg isotopic composition of the clay-sized fraction

indicates that the structural clay sites preferentially incorporate the heavy isotope into its structure. Using Equation 3.1 to calculate the fractionation factor between saponite and the thawed permafrost ice gives a value of 0.83‰. This value is identical to the average value found by Huang et al. (2018) and significantly smaller than the value determined by Shalev et al. (2019) of ~ 1.6‰. The fractionation factor from this study also shows fractionation between fluid and saponite occurs in the opposite direction as determined by Hindshaw et al. (2020).

*3.5.2.3 Saponite Fractionation and the Global Mg Budget*

There has been recent controversy over the direction of Mg fractionation during saponite formation. Hindshaw et al. (2020) provided experimental data on the Mg isotopic fractionation of saponite, and found that saponite preferentially retains the light isotope, while other field studies have found saponite to prefer the heavy isotope (Huang et al., 2018). Prior studies suggest that fractionation is dependent on the type of clay and the difference in bond strength between the reactants (aqueous Mg complex) and products (clays). Stronger bonds prefer the heavy isotope and weaker bonds prefer the lighter isotope (Hindshaw et al., 2020; Li et al., 2014; Ryu et al., 2016; Wimpenny et al., 2010). Some studies have proposed a relationship between bond-length of Mg-O complexes to the direction of fractionation (Hindshaw et al., 2020; Liu et al., 2014), and a complete summary of this work can be seen in Hindshaw et al. (2020). However, the differences in bond length between the octahedrally coordinated Mg in clay and Mg in aqua complex is extremely small, and depending on the cited study, it often shows conflicting results. Similarly, there is no data on bond-length specifically for Mg in saponite or bond-lengths of octahedrally coordinated sites at subzero temperatures. Furthermore, experimental data on clay mineral formation has not always been consistent and is potentially

dependent on how the clays were synthesized or if they reached equilibrium. For example, two independent studies using lab-synthesized brucite showed fractionation occurred in opposite directions (Li et al., 2014; Wimpenny et al., 2010). Therefore, more field studies of in-situ formation of saponite are needed to resolve this issue.

The direction and size of saponite fractionation are critical because of its contribution to the global Mg ocean budget. The homogenous Mg isotopic composition of seawater, -0.83 ± 0.09‰ (Ling et al., 2011), is controlled by its source and sinks. The primary sources of Mg to seawater is riverine and groundwater inputs (Arvidson et al., 2006; Berner, 2004; Holland, 2005; Mayfield et al., 2021), which have $\delta^{26}$Mg values of -1.09‰ (Tipper et al., 2006) and ~ -1.40‰ (Mayfield et al., 2021), respectively, and are significantly lighter than the homogenous seawater Mg isotopic composition. The lighter Mg sources must be balanced by Mg sinks, mainly through removal and fractionation of Mg through high-temperature hydrothermal circulation, carbonate deposition (dolomite), and low-temperature alteration of oceanic crust (Arvidson et al., 2011; Arvidson et al., 2006; Elderfield and Schultz, 1996; Holland, 2005; Morse and Mackenzie, 1990). Currently, the flux of Mg sinks, specifically the flux of low-temperature alteration of oceanic crust, are poorly constrained. This study can help address this uncertainty since one of the major Mg-bearing minerals that form during low-temperature alteration of oceanic crust is saponite (Alt, 1995; Bowers and Taylor Jr, 1985; Huang et al., 2018).

If saponite formation incorporates heavy Mg isotope during low-temperature alteration of oceanic crust, more dolomite precipitation (which prefers the light Mg isotope) is needed to drive seawater to its homogeneous value. The opposite will be true if saponite formation incorporates the light isotope. Our result on the fractionation of saponite formation supports the result of Huang et al. (2018), where saponite prefers the heavy isotope. Further work by Shalev et al.

(2019) supports preferential incorporation of heavy isotopes in oceanic crust during low-temperature alteration. However, this study did not identify the secondary minerals that form during this process and found a significantly higher fractionation value. The results in this study are more consistent with measurements of altered oceanic crust that contain abundant saponites (Huang et al., 2018), as well as field studies that have analyzed the Mg isotopic composition of other clay minerals and have found preferential incorporation of the heavy isotope (Opfergelt et al., 2012; Ryu et al., 2016; Ryu et al., 2021; Teng et al., 2010), supporting the mechanism proposed by Huang et al. (2018) and (Shalev et al., 2019).

Using the fractionation factor between saponite and the fluid phase from this study to represent fractionation during low-temperature alteration of oceanic crust, we can calculate the total oceanic Mg flux of low-temperature alteration. While there are some key differences between the environment of the MDV (lower temperature and higher salt content) and the environment of low-temperature alteration of oceanic crust, our results provide the first field estimates of the equilibrium fractionation factor of saponite and the fluid phase in a natural setting. We create a simple mass balance using oceanic Mg inputs (riverine and groundwater) and outputs (high-temperature hydrothermal circulation, dolomitization, and low-temperature alteration of oceanic crust):

$$(\delta^{26}Mg_{riv} - \delta^{26}Mg_{sw})\,F_{riv} + (\delta^{26}Mg_{gw} - \delta^{26}Mg_{sw})\,F_{gw} = (\delta^{26}Mg_{hyd} - \delta^{26}Mg_{sw})\,F_{hyd} + (\delta^{26}Mg_{dol} - \delta^{26}Mg_{sw})\,F_{dol} + (\Delta^{26}Mg_{min-soln})\,F_{AOC} \quad (3.3)$$

Where $\delta^{26}Mg_{riv,}$ $\delta^{26}Mg_{gw}$ , $\delta^{26}Mg_{hyd,}$ $\delta^{26}Mg_{dol,}$ $\delta^{26}Mg_{sw}$, and $\Delta^{26}Mg_{min\text{-}soln}$ is the Mg isotopic composition of riverine input, $\delta^{26}Mg$ = -1.09‰ (Tipper et al., 2006)), groundwater, $\delta^{26}Mg$ = -

1.40‰ (Mayfield et al., 2021), high-temperature hydrothermal fluid, $\delta^{26}Mg \sim$ seawater composition (Tipper et al., 2006)), dolomite formation, $\delta^{26}Mg$ = -2.0‰ (Higgins and Schrag, 2010)) and the fractionation factor between saponite and the fluid phase, 0.83‰ (this study), respectively, and $F_{riv}$, $F_{gw,}$ $F_{hyd,}$ $F_{dol,}$ and $F_{AOC}$ are the flux for riverine input, 5.5 x $10^{12}$ mol/yr (Tipper et al., 2006), average groundwater, 0.75 x $10^{12}$ mol/yr (Luijendijk et al., 2020; Mayfield et al., 2021; Zhou et al., 2019), high-temperature hydrothermal fluid, 1.5-2.2 x $10^{12}$ mol/yr (Elderfield and Schultz, 1996; Nielsen et al., 2006), dolomite formation, 1.7 x $10^{12}$ mol/yr (Holland, 2005), and altered oceanic crust, which is unknown, respectively. Using this mass balance to solve for the flux of Mg into altered oceanic crust, we determine a flux of 0.16 x $10^{12}$ mol/yr. This value is significantly lower than previous values of 0.67 x $10^{12}$ mol/yr (Huang et al., 2012) and 1.0-1.7 x $10^{12}$ mol/yr (Shalev et al., 2019) and is the first to include the influence of groundwater input. The incorporation of groundwater flux appears to have a substantial impact on this value since groundwater is isotopically lighter than the riverine input. This lower value for the low-temperature hydrothermal flux suggests a lower dolomite flux than proposed in previous studies.

### 3.5.3 Lighter than Taylor Glacier Mg Isotopic Composition in Beacon Core

To correct for the influence of all of Mg weathering components on the Mg isotopic composition and test our hypothesis if salt precipitation and clay minerals can explain the lighter-than-Taylor-Glacier Mg isotopic composition, we use a simple mass balance equation:

$$\delta^{26}Mg_{corrected} = (F_{thawed\ ice} * \delta^{26}Mg_{thawed\ ice}) + (F_{SWE} * \delta^{26}Mg_{SWE}) + (F_{exchangeable} * \delta^{26}Mg_{exchangeable}) + (F_{structural} * \delta^{26}Mg_{structural}) \quad (3.4)$$

Where F is the fraction of Mg within each component (Figure 3.5). This mass balance is used to correct the Mg isotopic composition of the thawed ice and shifts towards a heavier composition, with the biggest change in the lower 7.0-30.0 m, which is consistent with a greater contribution from secondary minerals (Figure 3.8). In the upper 7.0 m, the average change between the thawed ice and corrected thawed ice is approximately 0.02‰, while below 7.0 m, the average change is approximately 0.12‰. Below 7.0 m, the corrected value is heavier than Taylor Glacier and falls within the range of seawater, with most values suggesting greater chemical weathering than previously estimated. To determine the extent of chemical weathering, we use a two end-member mass balance equation:

$$\%\ weathering = \frac{\delta^{26}Mg_{corrected} - \delta^{26}Mg_{TG}}{\delta^{26}Mg_{dolerite} - \delta^{26}Mg_{TG}} \quad (3.5)$$

Figure 3.13 shows the percent Mg derived from chemical weathering when correcting for all Mg components compared to when not accounting for all potential components. When corrected for all potential reservoirs, weathering is greater in all core sections with changes ranging from a difference of 1.0 to 30.0%. If these reservoirs are not accounted for, the amount of Mg derived from chemical weathering is significantly underestimated. Furthermore, there is clear evidence of other rock-water interactions, such as the formation of clays, exchange processes, and precipitation of salts at subfreezing temperatures.

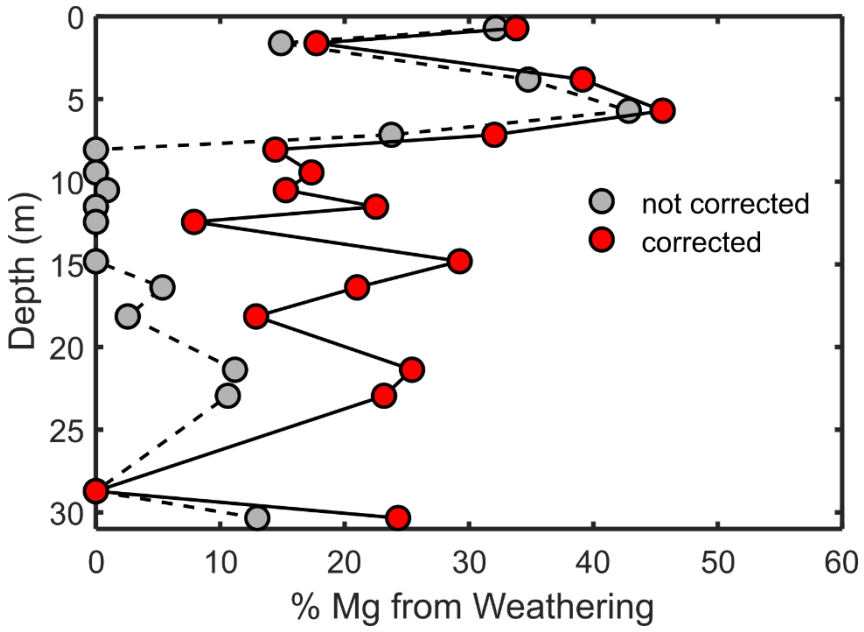


Figure 3.13: Mass balance correction on % Mg from chemical weathering considered the influence of all Mg components in the system: thawed permafrost ice, secondary salts, exchangeable Mg, and structural clay Mg. In the upper 7.0 m, there is a little to no change in the amount of weathering, while below 7.0 m, % Mg from weathering increased significantly.

## 3.6 Conclusion

This study builds upon previous work completed on a 30.0-meter ice-rich core in Beacon Valley that found significant chemical weathering occurs even at subzero temperatures and is controlled by the amount of unfrozen brine that persists within the core (Cuozzo et al., 2020). Here, the same 30.0-meter ice-rich core traces the influence and extent of secondary mineral formation, including salt precipitation and clay formation, along the core's length. We present a comprehensive analysis of rock-water interactions and Mg isotope systematics using $\delta^{26}$Mg measurements in thawed permafrost ice, secondary salts, secondary clays (exchange and structural sites), and bulk sediment of an ice-cemented permafrost core from Beacon Valley, Antarctica. The main conclusions from this study are:

(1) Accounting for all components of the Mg budget is essential to account for all rock-water interactions in a soil profile. This is the first study to look at all Mg components and trace these interactions in a permafrost environment. Using a mass balance to quantify all processes, the results show that chemical weathering is underestimated by up to 30% when not accounting for all components of the Mg budget. Furthermore, the fractionation associated with these processes explains the anomalous lighter-than-Taylor Glacier values found in the thawed permafrost ice below 7.0 m.

(2) Magnesium isotopes fractionate during secondary salt precipitation and prefer the heavy isotope. Isotopic fractionation followed an equilibrium temperature dependence and was greatest at the lowest temperatures with an average $\Delta Mg_{min\text{-}sol} = 0.30‰$. While XRD analysis did not identify evidence of any Mg-salts, chemical modeling suggests epsomite and meridianiite are the dominant Mg-salts, and the fractionation factor is consistent with the modeled fractionation factor of meridianiite determined by Schauble (2011).

(3) $\delta^{26}Mg_{exchangeable}$ is controlled by the isotopic composition of the exchanging fluid, i.e., $\delta^{26}Mg_{thawed\ ice}$. Little to no fractionation occurred between the thawed ice and exchange sites, except for a few samples where the exchange sites preferred the heavy isotope.

(4) Saponite is the dominant clay mineral and is found at all depths in the core. Based on chemical modeling, saponite forms in-situ as a weathering product of orthopyroxene. Most Mg in the clay fraction occurs within structural sites rather than exchange sites. $\delta^{26}Mg_{structural}$ is the heaviest isotopic component in the system (heavier than the bulk sediment) and preferentially

incorporated the heavy isotope, which contrasts what was observed in laboratory studies of the same clay mineral. The average fraction factor between saponite and the fluid phase is 0.83‰.

(5) Using the fractionation factor between saponite and the fluid phase in the Beacon Valley core to represent the fractionation that occurs during low-temperature alteration of ocean crust, the Mg flux sink is calculated to be 0.16 x $10^{12}$ mol/yr based on a simple mass balance calculation. The flux calculated in this study is lower than the previously calculated fluxes of 0.67 x $10^{12}$ mol/yr and 1.0-1.7 x $10^{12}$ mol/yr. This calculation is also the first mass balance calculation to include the influence of groundwater in the global Mg budget, which has a strong influence on the flux due to its lighter Mg isotopic composition. This lower flux also implies a lower dolomite flux is needed to balance the Mg budget.

**Acknowledgments**: Financial and logistic support is provided by Grant Nos. OPP-1341680 and OPP-0636998 from the National Science Foundation, and Grant 80NSSC17K0715 from NASA. Funding was also provided by the Howard Coombs Teaching Award from the University of Washington. Drilling support and equipment were contracted from Webster Drilling and Exploration Limited, Wellington, New Zealand. Special thanks to Zezhou Wang and Tianyi Huang for their assistance in analyzing samples on the MC-ICP-MS at the University of Washington.

## 3.7 Supplementary Material

Table S3. 1: Mg composition (mmol) of each component in the Beacon Valley core

| Sample ID | Depth (m) | Mg Concentration | | | |
|---|---|---|---|---|---|
| | | Thawed Ice mmol | SWE mmol | CEC mmol | Clay mmol |
| BV4-28-35 | 0.7 | 0.08 | 0.017 | 0.0017 | 0.002 |
| BV4-120-123 | 1.6 | 0.15 | 0.044 | 0.0018 | 0.002 |
| BV4-340-343 | 3.8 | 0.20 | 0.016 | 0.0039 | 0.005 |
| BV4-529-532 | 5.7 | 0.38 | 0.044 | 0.0036 | 0.005 |
| BV4-675-677 | 7.2 | 0.08 | 0.012 | 0.0020 | 0.003 |
| BV4-763-768 | 8.1 | 0.06 | 0.028 | 0.0030 | 0.007 |
| BV4-902-905b | 9.4 | 0.01 | 0.007 | 0.0005 | 0.002 |
| BV4-1005-1016 | 10.5 | 0.06 | 0.018 | 0.0010 | 0.002 |
| BV4-1110-1112 | 11.5 | 0.02 | 0.010 | 0.0008 | 0.002 |
| BV4-1200-1202 | 12.4 | 0.03 | 0.009 | 0.0008 | 0.001 |
| BV4-1440-1442 | 14.8 | 0.02 | 0.005 | 0.0003 | 0.005 |
| BV4-1598-1600 | 16.4 | 0.02 | 0.006 | 0.0007 | 0.001 |
| BV4-1773-1776 | 18.1 | 0.02 | 0.003 | 0.0004 | 0.001 |
| BV4-2096-2098 | 21.4 | 0.06 | 0.019 | 0.0021 | 0.003 |
| BV4-2253-2256 | 22.9 | 0.18 | 0.050 | 0.0042 | 0.009 |
| BV4-2830-2833 | 28.7 | 0.09 | 0.026 | 0.0013 | 0.002 |
| BV4-2990-2998 | 30.3 | 0.07 | 0.011 | 0.0017 | 0.002 |

# Dating glacial deposits using cosmogenic isotopes in a permafrost core reveals wet-based glacial advance in Victoria Valley during the Plio-Pleistocene

Nicolas Cuozzo[a], Ronald S. Sletten[a], Benjamin Mishkin[b], John Stone[a], Michael L. Prentice[c]

## 4.1 Abstract

The study presents a novel approach to interpret and date glacial deposits in the McMurdo Dry Valleys, Antarctica using a 15-meter core collected in Upper Victoria Valley and provides evidence of a wet-based glacial event during the early Pleistocene/late Pliocene in Victoria Valley. Using sedimentological and geochemical evidence, we identified the depositional environment of three distinct glaciogenic deposits in the core. A multi-isotope ($^{26}$Al and $^{10}$Be) cosmogenic nuclide approach was then used to test burial and exposure scenarios to provide age constraints on the depositional units and glacial events. The deepest unit, Unit 1, is interpreted as a subglacial till formed during the advance of a wet-based Victoria Upper Glacier. This unit experienced at least 3.9 Ma of glacial cover and at least 0.65 Ma of surface exposure before its deposition at the core location approximately 0.7 Ma ago, suggesting a Plio-Pleistocene wet-based glacial event. This is consistent with other studies that have provided constraints on wet-based glaciation in connecting valleys. Unit 2, deposited 0.66 Ma ago, is interpreted as reworked proglacial sand deposited during the retreat of Victoria Upper Glacier. The youngest deposit in the core, Unit 3, is a typical cold-based glacial deposit, suggesting a return to cold-based glacial regimes after the late Pliocene. These records provide evidence suggesting a valley-wide wet-based depositional event during the Plio-Pleistocene and provide the first evidence of wet-based glaciation in Victoria Valley.

## 4.2 Introduction

The McMurdo Dry Valleys (MDV) contain some of the most well-preserved geologic records of Antarctic glaciation and are frequently used to understand past dynamics of the East Antarctic Ice Sheet (EAIS) (Armstrong, 1978; Armstrong et al., 1968; Bockheim and McLeod, 2008; Bockheim and McLeod, 2013; Brook et al., 1993; Brown et al., 1991; Denton et al., 1971; Denton et al., 1984; Denton et al., 1993; Hall et al., 1993; Hall et al., 2002; Higgins et al., 2000; Prentice et al., 1998a; Schäfer et al., 2000; Staiger et al., 2006a; Swanger et al., 2019; Swanger et al., 2017; Swanger et al., 2011b). Located along the Transantarctic Mountains (TAM), the MDV contains EAIS outlet glaciers whose deposits may constrain the extent and timing of EAIS advance and retreat. Dating these deposits may help address long-standing questions about the stability of the EAIS during warmer and wetter climates (Austermann et al., 2015; Cook et al., 2013; Dutton et al., 2015).

Specifically, the stability of the EAIS during the Plio-Pleistocene has been debated (Denton et al., 1993; Webb et al., 1984). During the Late Pliocene, a period characterized by $CO_2$ values that are comparable to today's values (Bartoli et al., 2011; Pagani et al., 2010; Seki et al., 2010) and global mean temperatures similar to those predicted for the end of the century (Austermann et al., 2015; Dowsett et al., 2012), the marine record suggests a total collapse of the West Antarctic and Greenland Ice Sheet (Lunt et al., 2008; Naish et al., 2009; Pollard et al., 2015) and potential partial collapse of subglacial basins of the EAIS (Cook et al., 2013; Dolan et al., 2011; Patterson et al., 2014). However, there is still uncertainty about the behavior of interior EAIS and EAIS outlet glaciers that terminate on land and whether they underwent dynamic changes. There is further uncertainty about the stability of the EAIS during Pleistocene glacial-interglacial cycles. Variations in sediment provenance identified in the offshore ANDRILL

AND-1B core suggest a dynamic EAIS during the Pleistocene and a shift from warm/polythermal to cold-based glaciation during the Mid-Pleistocene Transition (MPT) (Naish et al., 2007; Talarico et al., 2012). Geochemical evidence from within the Wilkes Basin supports a dynamic EAIS during exceptionally warm Pleistocene interglacial periods, such as MIS 11 ( ~ 400 Kya) (Blackburn et al., 2020).

Here, we examine the stability of the EAIS during the Plio-Pleistocene by identifying and dating buried glacial deposits in Victoria Valley. Sediment deposits in Victoria Valley result from the dual nature of cold-based glaciers to both preserve and modify the landscape (Atkins, 2013). Thin, patchy glacial deposits, most often identified as depositional features of cold-based glaciers, blanket the Victoria Valley surface. These deposits in the MDV can be several meters thick (Atkins, 2013) and are deposited over well-preserved relict deposits from prior advances of Victoria Upper Glacier. Evidence of buried soils, preserved desert pavements, surface oxidation units, and patterned ground in the relict deposits throughout the MDV suggests these post-depositional features are preserved over potentially multiple glaciations (Bockheim, 2002; Bockheim, 2010; Hall et al., 1993; Staiger et al., 2006a). Based on the stratigraphic and geochemical interpretation of a 15-meter ice cemented permafrost core collected in Upper Victoria Valley at ~4.8 km below the current Victoria Upper Glacier (VUG), three distinct glaciogenic deposits were identified within the core. Based on this interpretation, cosmogenic nuclides, $^{26}$Al and $^{10}$Be, were used to create a forward model to constrain the timing of glacial deposition and periods of glacial cover in Victoria Valley. These findings support growing evidence of wet-based glaciation in the MDV during the Pliocene.

## 4.3 Study Area

### 4.3.1 Victoria Valley and Core Location

The MDV are a hyperarid, polar desert that remains free of ice-cover as a result of the high threshold of the TAM, which diverts ice from the EAIS away from McMurdo Sound, and the Wilson Piedmont Glacier, which isolates the valleys from the Ross Sea (Chinn, 1990). Victoria Valley is the northernmost valley in the MDV system (Figure 4.1) bound by the Clare and St Johns Range on the north, with a present-day mean annual temperature of -27.4°C (Doran et al., 2002) and yearly average precipitation, measured ~15 km away at the nearest weather station, of < 10 mm (water equivalent) (Riordan, 1973; Thompson, 1973). Two large glacier tongues flow into Victoria Valley: Victoria Lower Glacier on the east, fed by the Wilson Piedmont Glacier, and Victoria Upper Glacier on the northwest, fed by the EAIS and local neve fields. Victoria Upper Glacier covers approximately 80 $km^2$, two-thirds occupied by neve fields (Calkin, 1964). At the terminus of Victoria Upper Glacier is permanently ice-covered proglacial Victoria Upper Lake and two smaller adjacent lakes that extend southeast approximately 5 km. The 15-meter core used in this study was collected in upper Victoria Valley (-77.33095, 161.601) about 4.80 km south-southeast of Victoria Upper Glacier and approximately 0.35 km west of the smaller adjacent proglacial frozen lakes (Figure 4.1a). The core was drilled into an alluvial fan with lateral moraines a few km to the west of the drill site. The surface of this region of Victoria Valley is covered by polygonal patterned ground, with polygons approximately 10-20 m in diameter. The core was collected in the center of a polygon, which is believed to be the most stable region (Linkletter et al., 1973; Sletten et al., 2003).

The bedrock geology of Victoria Upper Valley consists of multiple different formations (Turnbull et al., 1994):

(1) Salmon Marble Formation – coarse white, rusty-weathering marble and gneiss. Ages are debated but believed to be Proterozoic. Outcrops are seen along the flow path of Victoria Upper Glacier and in Mt. Insel in Victoria Upper Valley.

(2) Granite Harbor Intrusive – St. John's Pluton (often called Vida granite) is a member of the Granite Harbor Intrusive found in Victoria Upper Valley that forms the western two-thirds of the St. Johns Range. Vida Granite is homogenous, medium-grained, poor in mafic minerals, and often contains alkali feldspars megacrysts.

(3) Beacon Supergroup - Devonian to Jurassic sandstones, siltstones, and shales. Occurs in the St. Johns Range as small sections resting unconformably ion basement rock or overlain by Ferrar dolerite.

(4) Ferrar Supergroup – Jurassic igneous rocks that occur throughout the St. Johns range, Olympus Range, and Clare Range. Dolerites are dark reddish brown to black and fine to medium grained.

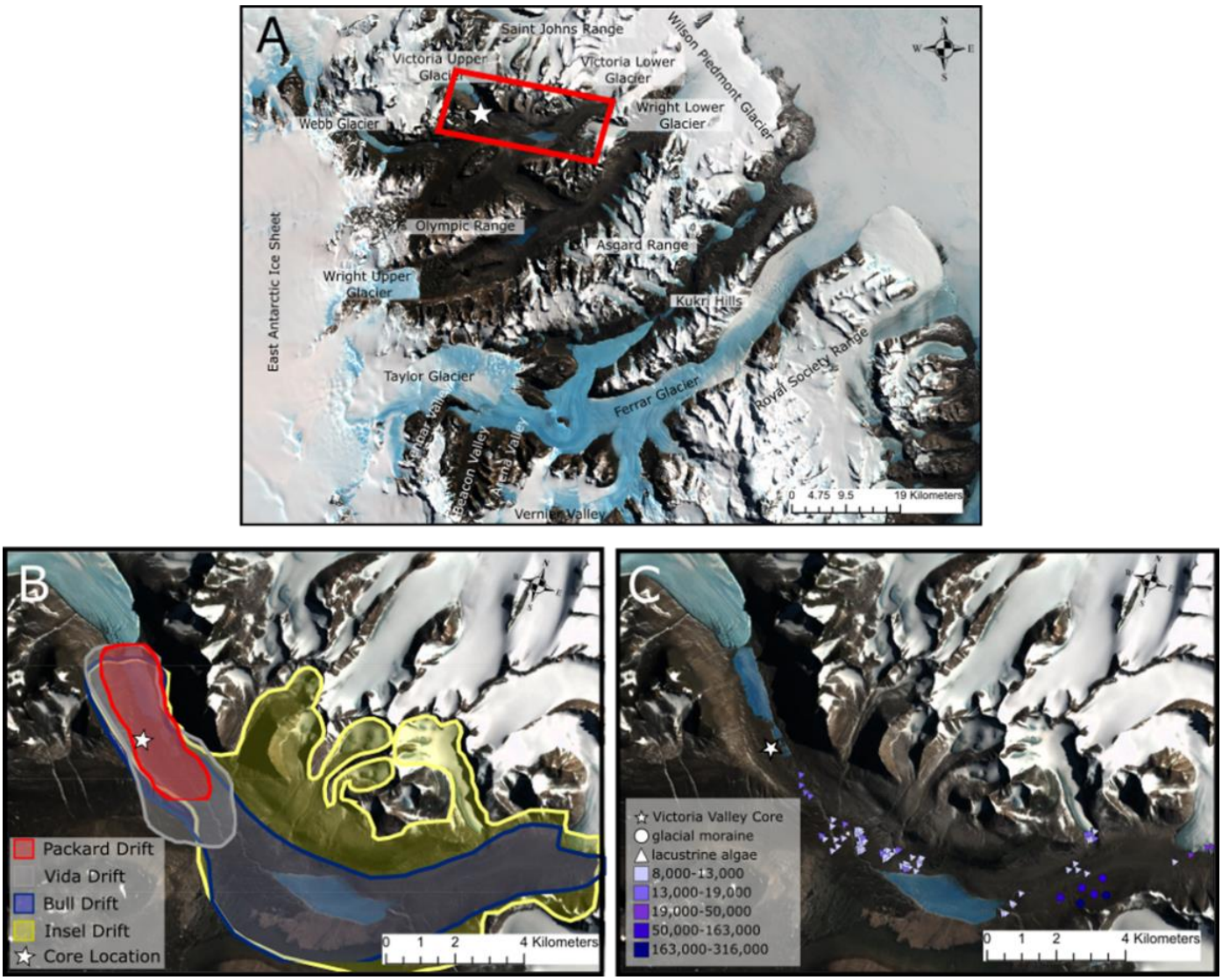


Figure 4.1: (A) Landsat Image of a mosaic of the MDV (available at http://lima.usgs.gov/). This map provides the location of the site where the 15-meter ice-cemented permafrost core was collected (☆), with a red box around Victoria Valley; (B) The extent of glacial drift in Victoria Valley. The yellow shaded area represents Insel drift, blue represents the Bull drift, grey represents the Vida drift, and red represents the Packard drift. All four drifts fall within the region where the core was collected (Bockheim and McLeod, 2013; Bull, 1962; Calkin, 1964; Prentice et al., 1998a); (C) Location and ages of material dated in Victoria valley prior to this study. Dated material include lacustrine algae (Hall et al., 2002) (Δ) and glacial moraines (○) (McGowan et al., 2014)

### 4.3.2 Upper Victoria Valley Glacial History

Victoria Upper Glacier (VUG) is fed by local snowfields and, during periods of growth, by the EAIS. Presently, Victoria Upper Glacier is believed to be a cold-based glacier, defined as a glacier whose basal ice is below the pressure melting point and lacks free-flowing basal meltwater. While erosion is minimal compared to wet-based glaciation, cold-based glaciers modify the landscape through deposition (Atkins, 2013; Fitzsimons et al., 2008; Hambrey and Fitzsimons, 2010). Cold-based glaciers entrain sediment in multiple ways: (1) supraglacial material derived from rock-falls from surrounding rockfaces and aeolian sand, (2) large basal debris loads that form when advancing glaciers override and incorporate the frontal apron composed of ice, debris from calving, and supraglacial melt, and (3) by overriding proglacial lakes and freezing-on lake sediment, often called pro-glacial lake-ice conveyers (Hendy et al., 2000; SHAW, 1977). When cold-based glaciers begin to retreat, deposition is dominated by sublimation of ice, and bulk deposition of basal and englacial debris is limited to a few meters (Hambrey and Glasser, 2012). While cold-based glaciers dominate the MDV today, that may not have always been the case. Evidence for wet-based glaciation in the MDV has been proposed by multiple studies, suggesting a very different climate in the MDV. (Bockheim and McLeod, 2008; Bockheim and McLeod, 2013; Krusic et al., 2009; Prentice et al., 1998b). However, the timing of a potential wet-based glaciation in the MDV is not well constrained.

VUG is believed to have advanced into Victoria Valley on multiple occasions, depositing widespread glacial drifts composed of unconsolidated boulder debris with clasts of sand and gravel, and several meter-high drop moraines, composed of a loose collection of clast-supported boulders and cobbles with some sand and gravel (Atkins, 2013). The evidence for multiple advances of the VUG into lower elevation valleys in the MDV was first documented by

pioneering work done by Péwé (1960), Bull (1962), and Calkin (1964), who provided surficial and geomorphic evidence of at least four valley-wide glaciations, each less expansive than the previous (Figure 4.1b). Further work was completed by Prentice et al. (1998a), who provides a summary of the early evidence of multiple glaciations in the MDV. In Victoria Valley, the drifts associated with these glacial events were named, from oldest to youngest, the Insel Drift, the Bull Drift, the Vida Drift, and the Packard Drift. Recent mapping of these drifts by Bockheim and McLeod (2013) suggests that all four drifts fall within the location of the core site (Figure 4.1b). Presently, none of the deposits in upper Victoria Valley are dated.

While there are no direct dates of glacial deposits in upper Victoria Valley, a few studies provide estimates of surface age (Figure 4.1c). Based on radiocarbon dates from lacustrine algae preserved in deltaic and glaciolacustrine deposits, it is suggested that a valley-wide lake, Glacial Lake Victoria, existed in Victoria Valley between 20,000 and 8,600 yr BP from the melting of the Wilson Piedmont Glacier, Victoria Lower Glacier, Victoria Upper Glacier, and small alpine glaciers (Hall et al., 2002). Hall proposes that lacustrine sediment from this event is widespread on the surface of Victoria Valley, suggesting a relatively young surface age in Victoria Valley. Sletten et al. (2003) propose a similar surface age, approximately 12,000 yrs, in Victoria Upper Valley based on the formation rate of sand wedges in the polygonal patterned ground. While this work does not confirm the presence of Glacial Lake Victoria, it provides similar surface age estimates. Atkins and Dickinson (2007) interpret the large, disordered spread of ages found by Hall and Denton (2002) to be a result of multiple deposits of meltwater channels from Packard Glacier rather than a large lake. Furthermore, the only study to date that has used cosmogenic dating to provide age constraints on Victoria Valley deposits calls into question the existence of the proposed Glacial Lake Victoria while providing potential constraints on the valley's glacial

history (McGowan et al., 2014). Six samples from a sequence of three recessional moraines from Packard Drift in Lower Victoria Valley, and glacial erratics from inferred paleo-shorelines identified by Hall et al. (2002) were dated using $^{10}$Be. The six samples from the recessional moraine showed a sequential decrease in age of the three moraines towards Packard Glacier's terminus, with exposure ages of 163 ± 11.2 ka, 112 ± 8.4 ka, and 63 ± 4.4 ka. Dates of granite glacial erratics on the benches of the features interpreted as paleo-shorelines have ages of 316.1 ± 23.2 ka and 293.8 ± 21.9, and 138.5± 9.8 ka. The glacial erratics dates suggest that the proposed paleo-shorelines did not form during Marine Isotope Stages 2 and 3 when Glacial Lake Victoria is believed to have existed and the topography suggests they are remnants of slope mass movement deposits. However, this work did not consider cosmogenic scatter, inheritance, or explore more complicated burial histories commonly found in glacier erratics in the MDV.

## 4.4 Victoria Valley Permafrost Core

### 4.4.1 Core Collection, Description, and Analytical Methods

A 15-m ice-cemented permafrost core was collected in upper Victoria Valley in 2008 and stored in a -30°C freezer at the University of Washington, Seattle. Drilling began 0.33 m below the dry, unconsolidated sands and gravels at the top of the ice-cemented permafrost boundary. Based on oxidized layers, carbonate coatings, salt content, and stable isotopes of the thawed permafrost ice, the core has been divided into three depositional units (with 0 m representing the top of the core): 14.60-6.60 m (Unit 1), 6.60-1.30 m (Unit 2), 1.30-0.0 m (Unit 3) (Figure 4.2). The permafrost core was subsampled near the top, middle, and bottom of each identified glacial deposit using a carbide-tipped band saw. The frozen sediment samples were then thawed overnight in a refrigerator in sealed polyethylene bags. The meltwater was extracted from the

thawed sediment by centrifuging in a double-bottom centrifuge cup (a perforated cup fitted with a 0.45 µm Nucleopore filter followed by a closed cup).

Oxidized layers were identified in the soil stratigraphy based on extractable iron using citrate-dithionite-bicarbonate solution (Mehra and Jackson, 1960). This extraction procedure was repeated three times to ensure all extractable iron was removed. Oxygen isotopes were analyzed in the thawed permafrost ice at the University of Washington IsoLab using a Picarro L2140i cavity ring-down spectrometer. The soluble salts in the thawed permafrost ice were analyzed for major cations ($Ca^{2+}$, $Mg^{2+}$, $Na^{+}$, and $K^{+}$) using Inductively Coupled Plasma Optical Emission Spectroscopy (ICP-OES) (Perkin Elmer Optima 3300 DV) and major anions ($Cl^{-}$, $F^{-}$, $SO_4^{-2}$, and $NO_3^{-}$) using Ion Chromatography (IC) (Dionex ICS 2500). Particle Size analysis was performed on ~ 1 g of the < 2 mm size fraction of permafrost sediment samples. Samples were split using a sample splitter to avoid sampling bias and analyzed using a laser diffraction particle size analyzer (Beckman Coulter LS 13-320). Samples were dispersed using an ultrasonic probe with the addition of 5 mL of 0.05% sodium bicarbonate sodium hexametaphosphate to keep samples in suspension.

Cosmogenic nuclides sample processing was completed at the University of Washington Cosmogenic Nuclide Laboratory. In preparation for the $^{10}Be$ and $^{26}Al$ analysis, each sample was sieved to the 250 – 500 µm range, iron oxides were removed using HCl, quartz was separated using a heavy liquid density separation, and the remaining sediment was etched using dilute HF (Kohl and Nishiizumi, 1992). $^{10}Be$ and $^{26}$ Al were extracted from quartz using the methods described in Stone (2004). Isotopic ratios were measured at the Lawrence Livermore National Laboratory Center for Accelerator Mass Spectrometry (LLNL-CAMS) and Purdue Rare Isotope Measurement Laboratory (PRIME Lab).

### 4.4.2 Stratigraphy

The stratigraphy of the three glacial deposits is described in Table 4.1 and shown in Figure 4.2.

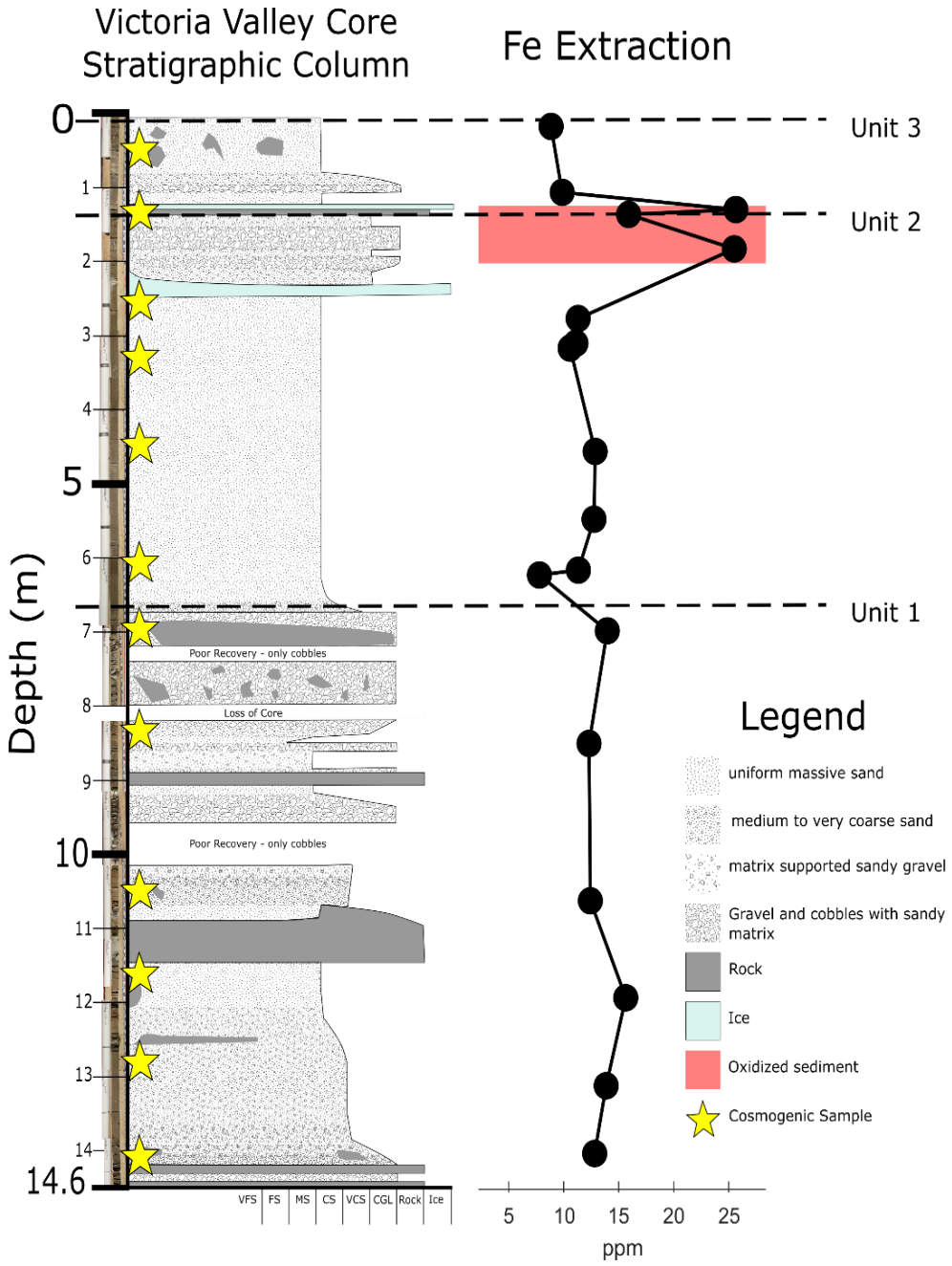


Figure 4.2: Photos, stratigraphic column, and Fe extraction of the 15-meter core collected in Victoria Valley. Units 1 (14.6-6.6 m), 2 (6.6-1.3 mm), and 3 (1.3-0.0 m) are divided by the black dotted lines with an oxidized paleosurface highlighted in red. Yellow stars represent the location of the cosmogenic nuclide samples.

Table 4.1: Core Description

| Unit | Core Depth (m) | Description | Depositional Interpretation |
|---|---|---|---|
| Unit 3 | 0.00 – 1.0 | Ice-cemented, medium-to-coarse grey-brown sand with alternating layers of subangular gravels and cobbles | Cold-based glacial deposition |
| | 1.3 – 1.0 | Upwards coarsening well-sorted medium sand and silt | |
| Unit 2 | 1.3 – 2.3 | 12 cm layer of segregated ice with inclined margins. 100% medium-to-coarse grained sand, coarsening upwards into an oxidized buried desert pavement with gravel clasts | Water-reworked proglacial sands |
| | 2.3 – 6.8 | Ice-cemented, upward coarsening medium-to-coarse grey-brown sand with no visible bedding or sedimentary structures. Rare cobbles and gravel up to 3-4 mm at approximately 6.0 m. | |
| Unit 1 | 6.8-7.0 | Weathering zone with ~ 5 cm desert pavement. Gravel clasts have carbonate coatings | Wet-Based glacial till |
| | 7.0 – 10.0 | Alternating layers of poorly sorted subangular to rounded/abraded cobbles to gravels with carbonate coatings | |
| | 10.0 – 10.9 | Poorly sorted mixture of gravel and medium-to-coarse sand with subangular clasts. Gravel clasts have carbonate coatings on exterior | |
| | 10.9 – 11.6 | Single large dolerite boulder | |
| | 11.6 – 12.6 | Medium-coarse brown sand with subangular gravels with carbonate coating on exterior | |
| | 12.6 – 13.8 | Upward fining, transitions from gravel-medium coarse sand to medium sand with rare, subangular gravels with carbonate coating on exterior. Top of section has large ~20 cm rock with small pockets of medium sand | |
| | 13.8 – 14.6 | Subangular to angular gravels and cobbles with a medium-coarse sand matrix. Gravels and cobbles have strongly developed carbonate coatings. Cobble clasts are greater than 12 cm in length. | |

Based on the sedimentological attributes, particularly lack of bedding, sorting, texture, the presence of large clasts and their morphology, these three units are interpreted as glaciogenic deposits. Unit 1 is the thickest depositional unit in the core (~ 8 m) and appears to be thicker than typical cold-based glacial deposits (Hambrey and Glasser, 2012; Staiger et al., 2006b). Furthermore, the core only records a minimum thickness of the deposit because the unit may extend further beneath the depth drilled. Unit 1 also shows the widest range of lithofacies within the core, with most sections have < 5% gravel sized clasts. Particle size analysis shows the majority of the < 2 mm size fraction is composed of sand-sized sediment (< 96%) with minor contributions from clay and silt-sized particles (Supplemental Material 4.A). This unit can potentially be described as a diamict. Flint et al. (1960a) and Flint et al. (1960b) define a diamict as " a non-sorted or poorly sorted terrigenous sediment that contains a wide range of particle sizes." A more specific textural definition of diamict is provided by Moncrieff (1989) and is based on the gravel, sand, and mud (clay + silt) sized fractions. The sediment falls with the classification of diamict based on the first definition, with an exception between 12.6 and 13.8 m, where there are large sections (< 1 m) with close to 100% sand-sized particles with only dispersed clasts > 2 mm (< 1%). Based on the small amount of clay and silt-sized particles (< 10%), the sediment in Unit 1 does not fit the Moncrieff (1989) definition of a diamict, and would be classified as a gravelly sandstone.

An analysis of 85 gravel-sized clasts (Supplemental Material 4.B) selected randomly throughout Unit 1 show that gravel in Unit 1 is composed of approximately 78% dolerite, 20% Vida Granite, and 1% Limestone. This is consistent with bedrock geology of Victoria Upper Valley, where Ferrar dolerite and Vida Granite dominate the region (Turnbull et al., 1994). Ventifacted clasts were identified based on having one to three smooth, well-developed, and

broadly convex surfaces. Approximately 25% of dolerite clasts showed evidence of ventifaction with no clear trends along the length of the unit. Ventifacts form on the surface of the MDV, and the proportion of ventifacted clasts on the surface typically range from 20-35%, depending on the duration of surface exposure (Bockheim, 2010). Similarly, 67% of all gravel sized clasts analyzed show evidence of carbonate crust on the exterior or sides of the gravels (Figure 4.3, Supplemental Material 4.B). Carbonate crusts are typically found on the bottoms of rocks located near the surface of the MDV (Claridge and Campbell, 1977). Extractable Fe is also uniformly elevated along the entirety of Unit 1, with no peak at the top of the unit. We interpret the presence of ventifacts and carbonate crusts throughout the unit at random orientations, and uniformly elevated extractable Fe as evidence that this unit is composed of sediment that was previously spread horizontally on the surface and reworked and redeposited by glaciation. While carbonate coatings are also found in lake deposits, we rule out this scenario because the carbonate coatings are mostly found on a single side of each clasts, rather than around all sides, as would be expected for lake carbonate coatings. There is no visible evidence of abrasion on gravel sized clasts, and most clasts are classified as subangular (45%) or subangular to rounded (34%), with a smaller amount of rounded (16%) clasts, with clear examples seen from 9.8-10.0 m (Figure 4.3 and Supplemental Material 4.C). Ultimately, based on the unit thickness and evidence of large-scale entrainment of a paleosurface, we propose that this unit is consistent with glacial sediment that formed as a basal till under a potentially wet-based glacier, and remained buried beneath the glacier until it was deposited at the surface during glacial retreat (Hambrey and Glasser, 2012; Krusic et al., 2009). We propose a potentially wet-based glaciation based on the texture of the unit, description of gravel-sized clasts, and the fact that large-scale entrainment

of sediment during cold-based glaciation on the scale observed in this unit is not typical in the MDV.

Unit 1 is capped by a thin desert pavement approximately 5 cm thick with clasts up to 7 cm, suggesting it was exposed at the surface after the glacier retreated. The desert pavement consists of approximately 40-50% clasts > 2.0 mm (compared to ~5-10% > 2.0 mm clasts directly below), which is lower than previous MDV desert pavement clasts analysis ranging from 63-92% > 2 mm (Bockheim, 2010). This may result from including finer sediment from just below the desert pavement in the analysis or may suggest that it is a poorly developed pavement

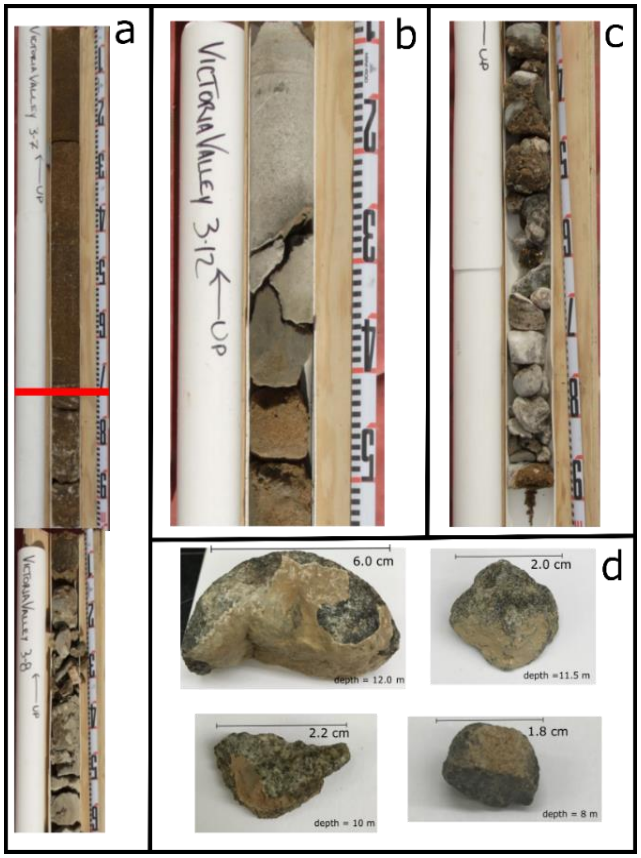


Figure 4.3: (a) boundary between Unit 1 and Unit 2. Unit 1 is capped by a 5 cm desert pavement; (b) large 37.5 cm boulder at 11.3 m depth; (c) rounded and glacially abraded cobbles at 9.8 m; (d) examples of carbonate coating on gravel clasts along entirety of Unit 1

that had a short duration of surface exposure. A short surface exposure is supported by the Fe extraction showing the surface is not strongly oxidized compared to the rest of the unit.

This deposit most closely resembles the description of the Bull or Insel drift as described by Calkin (1964). However, the published reports of these deposits focus on their surface characteristics, especially long-term weathering features, which cannot be directly compared with the buried sediment in the Victoria Valley core. The only other core drilled in Victoria Valley is the DVDP Core 6 at the west end of Lake Vida and in this core, 10.5 m of sediment was drilled before reaching bedrock (Kurasawa and MG JR, 1974). The deepest unit in the DVDP core is similar to Unit 1 from this study. Kurasawa and MG JR (1974) describe this unit as a 6.2 m thick glacial deposit consisting of medium to coarse sand with rounded to subangular cobbles and boulders up to 35 cm in size.

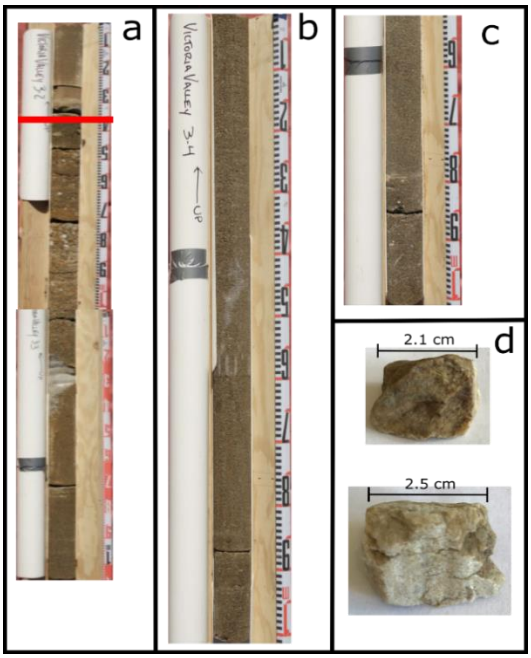


Figure 4.4: (a) boundary between Unit 2 and 3. Unit 2 is topped by a desert pavement with a strongly stained oxidized layer; (b) well-sorted uniform sands with little to no clasts > 2mm; (c) well sorted sands with few gravel clasts; (d) gravel sized clasts collected from the desert pavement.

Unit 2 is 5.5 m thick and is texturally more uniform than Unit 1. Unit 2 is composed of 98-100% < 2 mm sized particles, with a small section of < 1% gravel at ~ 6.0 m and a gravelly layer (up to 5%) at the top of the unit, which is interpreted as a desert pavement (Figure 4.4). Sand-sized particles make up over 98% of the < 2 mm sediment size fraction. Gravel-sized clasts collected from the desert pavement were analyzed in detail. These clasts consist of limestone (57%), dolerite (29%), and sandstone (14%), which is distinct from the dolerite and granite dominant clasts in Unit 1. No clasts were larger than 3 cm. This unit has no visible sedimentary structures with massive bedding. The well-sorted, sand-rich lithofacies suggest this unit was deposited by glaciofluvial processes during glacial retreat, and that sediment has been reworked and deposited by water. The coarse sand suggests this was not deposited by eolian processes. This unit is topped by a ~ 10 cm desert pavement, with deep staining from oxidation that extends ~ 50 cm, suggesting this unit has been exposed at the surface with minimal accumulation after deposition. Most clasts sampled from within the desert pavement have a light desert varnish; dolerite clasts were ventifacted.

Unit 3 is approximately 1.3 m thick with alternating layers of subangular gravels and cobbles with a medium to coarse sand matrix. Gravel-sized clasts consist of granite (71%) and dolerite (29%) with small sections (< 2 mm) near the surface covered with carbonate coating (Figure 4.5). This unit is consistent with small, poorly sorted deposits from cold-based glaciation typically seen on the surface of the MDV.

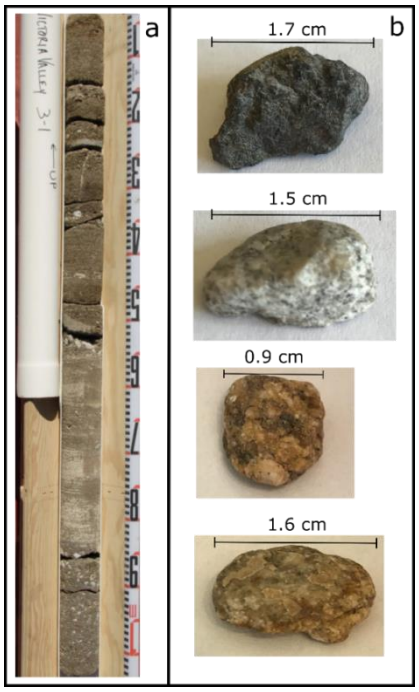


Figure 4.5: (a) meter length section of Unit 3; (b) gravel sized clasts found throughout Unit 3 consisting of dolerite and granite.

### 4.4.3 Ionic Composition

The ionic composition of the thawed permafrost ice was analyzed along the core's depth (Figure 4.6). Ionic concentration is highest in Unit 1, with an average total cation concentration of ~ 1800 ppm and average anion concentration of 3500 ppm. Large accumulations of $Ca^{2+}$ are consistent with abundant carbonate coatings, and accumulations of $NO_3^-$ suggest a long-term surface accumulation of salts that have not been flushed away by reworking by water. Nitrates in the MDV have isotopic signatures consistent with an exclusively atmospheric origin (Michalski et al., 2005). Previous studies have used atmospherically derived salts, particularly nitrate, to understand the exposure history and age of MDV sediment (Diaz et al., 2020; Graly et al., 2018; Lyons et al., 2016). Accumulations of nitrate in MDV sediment imply long exposure at the

surface with little moisture input to flush out the salts (Lyons et al., 2016). The high concentration of nitrate in Unit 1 strongly implies that this material existed as soil before erosion and redeposition at the core location. Unit 2 has a lower total concentration than Unit 1 (average cation and anion concentration is 1300 and 2000 ppm, respectively) and the low nitrate concentration in Unit 2 is consistent with an interpretation of reworking and flushing of salts by glaciofluvial processes. The extremely low concentration at approximately 2.5 m represents a large ice lens in Unit 2, most likely sourced from glacial ice. Unit 3 has the lowest concentrations of all units (average cation and anion concentration is 800 and 1450 ppm, respectively).

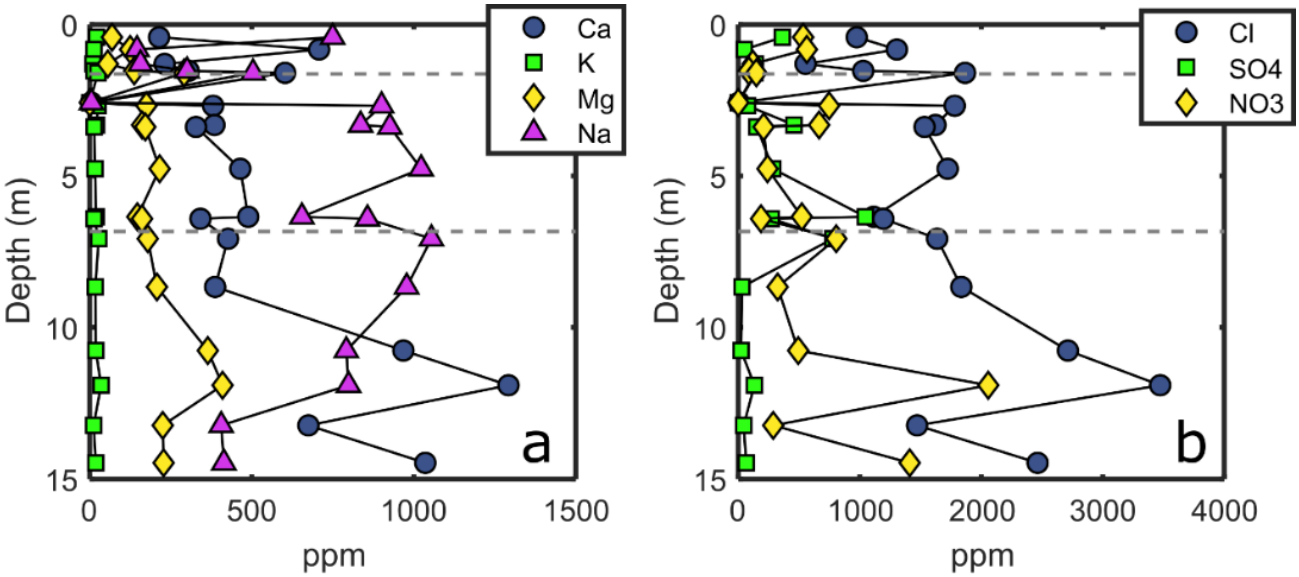


Figure 4.6: Ionic composition of the thawed permafrost ice. Boundary lines between depositional units are marked as grey dashed lines. Both cationic (a) and anionic (b) composition is greatest in Unit 1 with abundant $Ca^{2+}$ and $NO_3^-$ concentrations in Unit 1.

4.4.4 Stable Isotope Composition (δD, δ18O) in ice cement

Oxygen and deuterium isotopes were analyzed along the core's depth in the thawed permafrost ice (Table 4.2).

Table 4.2: δD (‰) and $\delta^{18}O$ (‰) measured in the thawed permafrost ice in the Victoria Valley core.

| Sample ID | Depth (m) | δD (‰) | $\delta^{18}O$ (‰) |
|---|---|---|---|
| VV3-8-10 | 0.42 | -190.09 | -16.75 |
| VV3-48-51 | 0.83 | -270.39 | -32.04 |
| VV3-96-98 | 1.30 | -277.84 | -33.65 |
| VV3-117-123 | 1.53 | -273.05 | -32.56 |
| VV3-123-130 | 1.59 | -271.62 | -32.18 |
| VV3-223-226 | 2.58 | -265.31 | -30.39 |
| VV3-232-238 | 2.68 | -258.13 | -29.33 |
| VV3-297-300 | 3.32 | -255.38 | -28.24 |
| VV3-300-310 | 3.38 | -253.77 | -27.74 |
| VV3-438-448 | 4.76 | -255.75 | -27.92 |
| VV3-600-603 | 6.35 | -245.81 | -26.34 |
| VV3-603-613 | 6.41 | -238.14 | -25.02 |
| VV3-672-676 | 7.07 | -236.62 | -24.13 |
| VV3-829-837 | 8.66 | -231.31 | -24.75 |
| VV3-1039-1047 | 10.76 | -226.72 | -26.26 |
| VV3-1154-1161 | 11.91 | -217.49 | -25.10 |
| VV3-1285-1295 | 13.23 | -228.90 | -27.64 |
| VV3-1407-1420 | 14.46 | -226.52 | -27.62 |

These data are combined with data from a shallow core in Victoria Valley from Hagedorn et al. (2010) (Figure 4.7) and are described starting from the bottom of the core. Oxygen isotopes roughly follow trends that coincide with divisions in the stratigraphic record. Moving up the core, Unit 1 (14.6-6.6 m) displays a shift towards heavy isotopes. Isotopic values start near MDV glacial values at -27.63‰ and increase to -24.13‰. Unit 2 (6.6-1.3 m) exhibits the opposite trend and shifts from heavy to light isotopes moving up-core, from -25.02‰ to 30.39‰. Unit 3 (1.3-0 m) has a similar trend as Unit 1, with a much more dramatic shift towards heavy isotopes, changing from -32.18‰ to 16.75‰. This trend is consistent with $\delta^{18}O$ data collected by Hagedorn et al. (2010). Stable isotope depth profiles in the MDV thawed permafrost ice have been analyzed previously by Hagedorn et al. (2010) in a shallow core collected near our study site in Victoria Valley and by Lacelle et al. (2011) in a buried ice body in University Valley. In both studies, stable isotope depth profiles displayed a concave upward profile, with a heavy

isotopic composition near the surface. This trend results from highly evaporated (potentially up to 95%) snowmelt that, as a result of losing light isotopes during evaporation, has become enriched in the heavy isotopes and proceeds to percolate down into the ice cement. The observed isotopic profiles reflect a mix between the original ground ice composition, which is presumed to be glacial in origin, and the isotopically heavy meltwater. This observation can be used to help delineate different stratigraphic units within the 15-meter permafrost core. If each unit was exposed at the surface under similar climate conditions that support snowmelt percolating into the soil profile and with a similar depositional history, there should be multiple concave upward trends in the sediment profile.

The isotopes in Unit 1 display a weakly concave upward trend that is more apparent in the oxygen isotopes than deuterium and potentially represents a shorter surface exposure time. Deuterium is less sensitive to kinetic effects than oxygen, which may explain the stronger trend in the oxygen isotope profile (Dansgaard, 1964). D-excess (d-excess = $\delta D - 8\ \delta^{18}O$) values become more negative towards the paleosurface, supporting greater kinetic fractionation towards the upper section of the unit due to infiltrating partially-evaporated meltwater (Dansgaard, 1964; Hagedorn et al., 2010). The surface unit, Unit 3 displays a strong upward concave trend and is very similar to that seen in Hagedorn et al. (2010), providing a clear geochemical boundary between Units 3 and 2. Unit 3 also shows a similar d-excess trend as Unit 1. Unit 2 does not show a concave upward trend but displays an upwards enrichment in the light isotope. This trend suggests that the ice in Unit 2 may have been formed under different conditions than Units 3 and 1. Unit 2 sediment is also distinct from Units 1 and 3 and is much more uniform with mostly

sand-sized particles. This is consistent with the interpretation is that the sediment ice is sourced primarily from glaciofluvial processes.

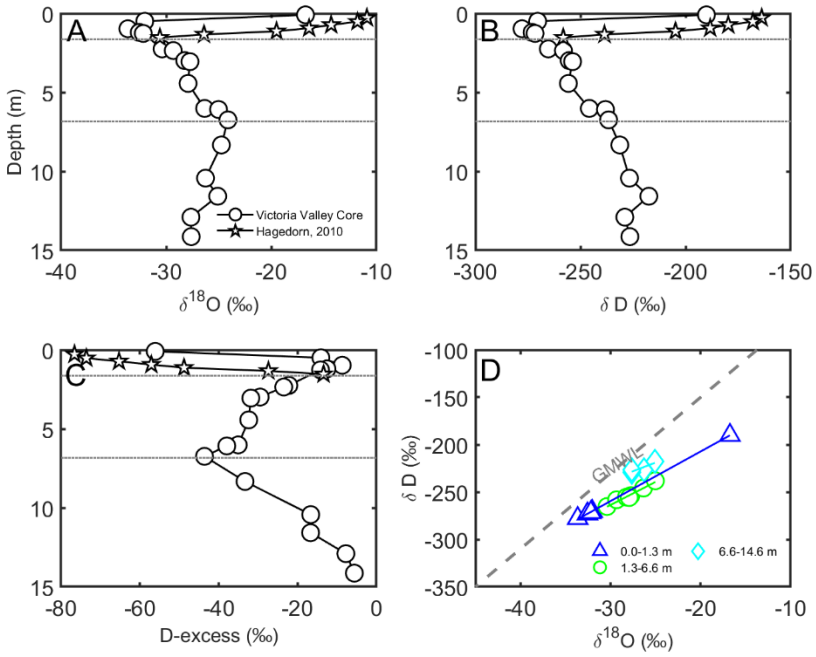


Figure 4.7: (A, B, and C) $\delta^{18}O$, $\delta D$, and d-excess isotopic values (‰) of the thawed permafrost ice along the depth profile of the Victoria Valley Core. Dotted lines represent the boundary between different glacial deposits. (D) $\delta D$ vs $\delta^{18}O$ values of the thawed permafrost ice. The deviations from the global meteoric water line (GMWL) and unique slopes for each glacial deposit suggests that the ice underwent kinetic fractionation.

When isolated, each group has an $R^2$ values > 0.98. The slope for Unit 3, 2, and 1, respectively, are 5.2, 4.9, 3.6. We remove two outliers on Unit 1 that are sampled near the paleosurface of that unit. Compared to the global meteoric water line ($\delta D = 10 + 8 * \delta^{18}O$), which has a slope of 8, these lower and varied slopes of from the Victoria Core data suggest a deviation from equilibrium processes due to evaporation or sublimation (Meyer et al., 2002)

### 4.4.5 Cosmogenic Nuclides

$^{10}$Be and $^{26}$Al measured values are shown in Table 4.3, and the $^{26}$Al/$^{10}$Be depth profiles with dividing lines for the three depositional units shown in Figure 4.8, which will be described starting from the bottom of the core. The cosmogenic nuclide profile generally increases towards the surface, except for the lowest sample in Unit 2 and all of Unit 3. Unit 3 has higher concentrations than those in Unit 2. Based on the young surface ages determined by Hall et al. (2002) and Sletten et al. (2003), we suggest Unit 3 samples are mostly comprised of inherited

Table 4.3: $^{10}$Be and $^{26}$Al measured in the sediment of Victoria Valley core.

| Sample ID | Depth (cm) | $^{10}$Be[a] ($10^5$ atoms $g^{-1}$) | 26-Al[a] ($10^5$ atoms $g^{-1}$) | Al/Be ratio |
|---|---|---|---|---|
| VV3-48-51 | 82.50 | 35.55 ± 0.538 | 147.66 ± 0.701 | 4.15 |
| VV3-117-123 | 153.00 | 35.22 ± 0.311 | 140.69 ± 0.311 | |
| VV3-232-238 | 257.50 | 46.04 ± 0.733 | 197.91 ± 1.77 | 4.30 |
| VV3-300-310 | 338.00 | 43.85 ± 0.409 | 179.23 ± 0.569 | 4.09 |
| VV3-438-448 | 476.00 | 41.14 ± 0.418 | 161.11 ± 0.946 | 3.92 |
| VV3-603-613 | 634.50 | 17.45 ± 0.213 | 40.66 ± 0.152 | 2.33 |
| VV3-672-676 | 707.00 | 10.21 ± 0.146 | 31.55 ± 0.242 | 3.08 |
| VV3-829-837 | 866.00 | 4.84 ± 0.092 | 8.13 ± 0.057 | 1.68 |
| VV3-1039-1047 | 1076.00 | 4.66 ± 0.092 | 4.15 ± 0.031 | 0.89 |
| VV3-1154-1161 | 1190.50 | 4.36 ± 0.085 | 3.83 ± 0.043 | 0.88 |
| VV3-1285-1295 | 1323.00 | 4.09 ± 0.079 | 3.11 ± 0.019 | 0.76 |
| VV3-1407-1420 | 1446.50 | 3.69 ± 0.073 | 2.86 ± 0.017 | 0.78 |

nuclides because they have only been exposed at the surface for a short time and would not accumulate such high concentrations in ~10,000 years. $^{26}$Al/$^{10}$Be ratios show a similar trend of increasing ratios moving up the core, with the same exceptions as the concentrations.

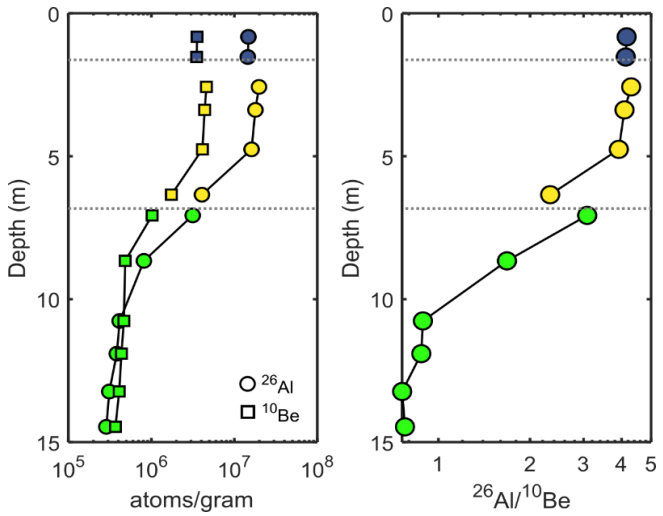


Figure 4.8: $^{10}$Be and $^{26}$Al concentration and $^{26}$Al/$^{10}$Be ratio in the permafrost sediment along the depth of the core. The dotted lines represent the boundaries between glacial deposit. Samples are colored in green, yellow, and blue for Units 1, 2, and 3, respectively.

A preliminary minimum burial age can be determined using a two-isotope diagram that compares the $^{26}$Al-$^{10}$Be ratio of the samples to their $^{10}$Be concentration. (Figure 4.9). A sample that has experienced continuous exposure will fall within the steady-state erosion island (shown by the bold grey lines), while samples that fall below the island suggest a more complicated history of both exposure and burial. The burial time is mainly determined by the $^{26}$Al/$^{10}$Be ratio (with 95% uncertainty ellipses propagating measurement error) and is shown with isochrons of expected burial time. Samples are shown grouped by depositional unit on the two-isotope diagram. Unit 1 (green circles) has a large range of $^{26}$Al/$^{10}$Be ratios ranging from 0.76 – 3.08. These ratios are significantly below the production ratio and indicate these samples have had a more complicated burial-exposure history on million-year timescales. Based on the two-isotope diagram, these samples have a burial age of 1.3 – 3.9 Ma. Unit 2 samples (yellow circles), have a much smaller range of expected values and have a more consistent $^{26}$Al/$^{10}$Be ratio. Unit 2

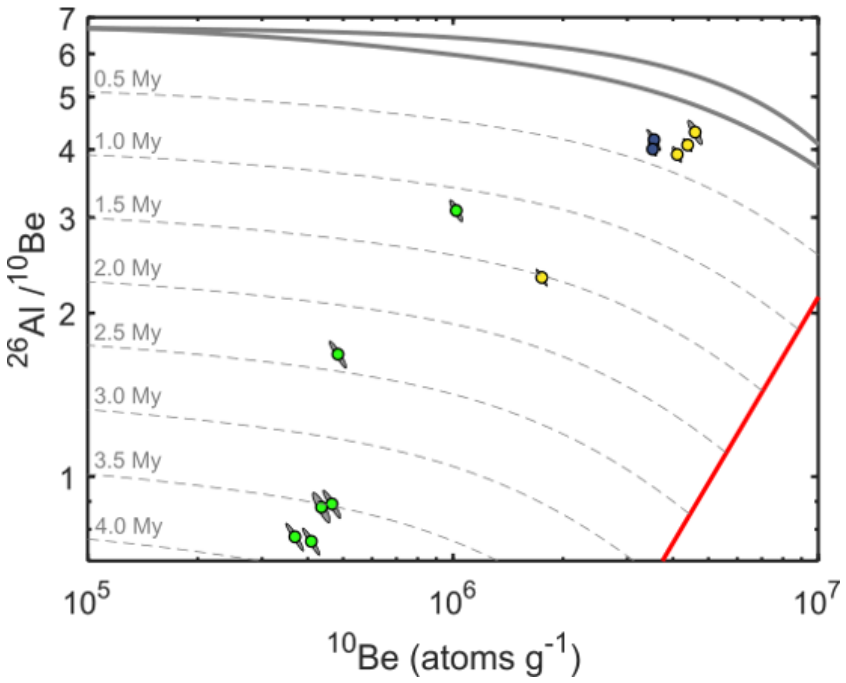


Figure 4.9: Two-isotope diagram of Victoria Core samples with 95% confidence intervals shown as ellipses, with labeled burial isochrons (grey dashed lines). Samples are colored in green, yellow, and blue for Units 1, 2, and 3, respectively.

samples have isotopic ratios ranging from 4.30-3.92 and an average burial time of 325 ka. These values do not fall within the simple exposure line, indicating a burial period, and suggest a younger age than Unit 1. One sample lies outside of this range and show a much older burial age of approximately 1.5 Ma. This sample was collected near the boundary between Unit 1 and 2 and may have experienced mixing between the two units. The core surface samples (blue circles) have an average ratio of 4.08 and an average burial time of 430 ka. While the two-isotope diagram provides substantial preliminary age estimates, a few assumptions are not accounted for, such as the influence of inherited nuclide concentration. This may explain why samples from the surface unit appear to be buried longer than in Unit 2. Based on work from Hall et al. (2002) and Sletten et al. (2003), we expect the near-surface units to be much younger in age and to fall closer to the simple exposure island. Furthermore, the ages of all units may be significantly younger if a large portion of the sample's concentration is from inherited nuclides from before

deposition. The inherited concentration must be accounted for or the age of the samples will be overestimated.

## 4.5 Description of Burial Models

### 4.5.1 Model Set-Up

We use the interpretation of the depositional environment based on stratigraphic and geochemical evidence and mechanisms of glacial deposition to guide the model setup (Figure 4.10):

(t0) Exposure of surface sediment prior to advance of Victoria Upper Glacier (VUG).

(t1) Unit 1 is interpreted as a basal till formed by an advancing wet-based VUG. This unit remains ice-covered until VUG retreats.

(t2) Retreat of VUG exposed Unit 1 at the surface

(t3) Unit 2 is deposited during retreat of VUG as water reworked glaciofluvial sediment. Unit 2 is exposed at the surface for a long enough period for a desert pavement and strongly oxidized surface to form.

(t4) Unit 2 is covered by advance of a now cold-based VUG

(t5) Unit 3 is deposited as a sublimation till as VUG retreats.

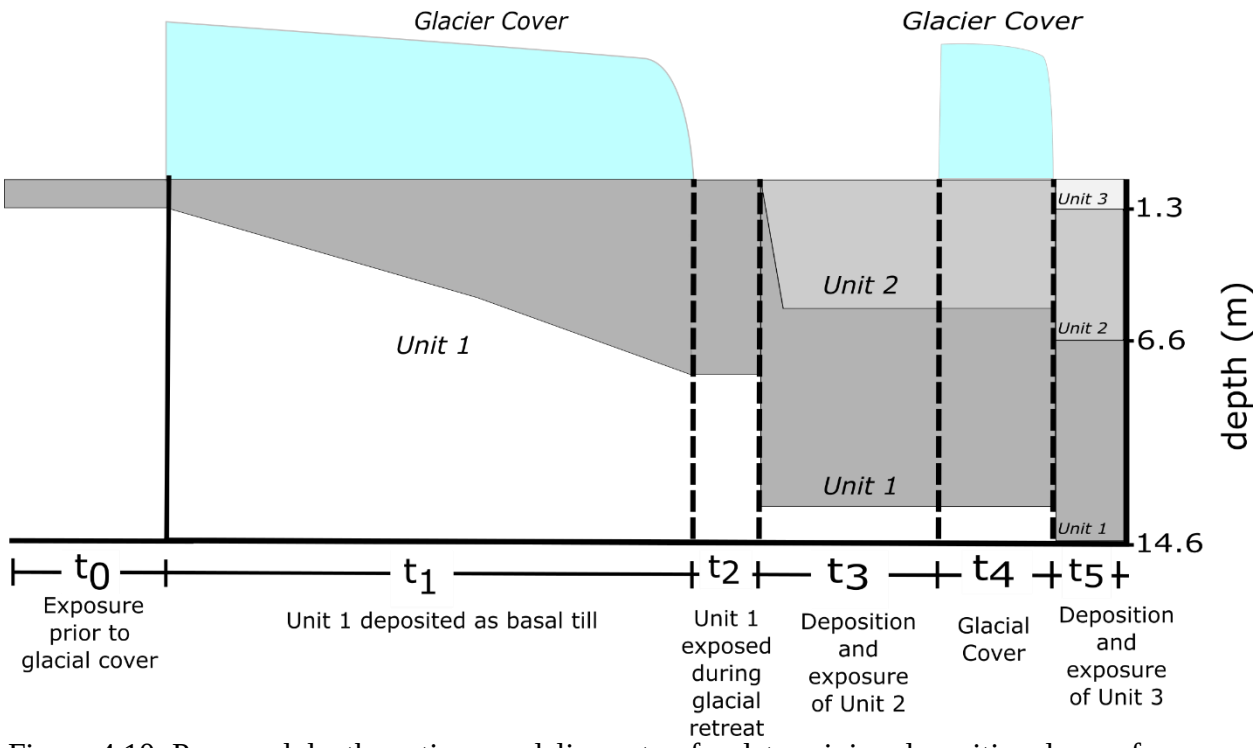


Figure 4.10: Proposed depth-vs-time modeling setup for determining depositional age of glaciogenic deposits in the Victoria Valley core. Nuclide production and decay are calculated for periods of exposure at the surface, complete shielding by glacier cover, and burial by subsequent deposits.

There are a few assumptions included in this model setup based on the stratigraphic and glacial history of the region. Based on the lack of any visible sedimentary structures, it is assumed that Unit 2 was deposited over a short enough period for the time of sediment accumulation to be negligible, and we model the deposition as a single bulk deposition of sediment (i.e., instantaneous deposition). Bulk deposition of Unit 2 and subsequent exposure is further supported by evidence of only a single desert pavement and strongly oxidized paleosurface capping this unit. It is also assumed that erosion is negligible due to the long-term stability of the MDV surface. The MDV are well-known for having low erosion rates and the cold-based glacial advance at $t_4$ should have little impact on the overriding surface, as is

supported by the preserved paleosurface of Unit 2. Similarly, prior studies in the MDV have found relict moraines and glacial drifts overlying undisturbed desert pavement, suggesting relict desert pavement can survive cold-based glaciation within minimal erosion (Brook et al., 1993; Brown et al., 1991; Calkin, 1971). Furthermore, the Victoria Valley core samples in this study have been buried for most of their history and have only had a short period of exposure at the surface where minimal erosion may occur. A third assumption is that during periods of glacier cover, the sediment was completely shielded and only experienced decay of cosmogenic nuclides. Cosmogenic nuclide production is negligible at depths greater than 30.0 m (Granger and Muzikar, 2001), and we assume that VUG was thicker than 30.0 m based on present-day thickness. When accounting for inherited nuclide concentrations, it is assumed that samples from individual units started with the same inherited concentration. For example, all samples collected from Unit 1 start with the same initial $^{26}$Al and $^{10}$Be, and all samples from Unit 2 start with the same initial concentration. However, samples from Unit 1 and 2 may have different initial concentrations. The final assumption is that the uppermost unit, Unit 3, has only been exposed on the surface for approximately 10,000 years (Hall et al., 2002; Sletten et al., 2003) which is too short for substantial nuclide accumulation. Therefore, the unknown time and inherited concentrations of Unit 3 are removed from our argument parameters, and it is assumed that all measured nuclide concentrations for that unit were inherited from prior exposure near the surface.

### 4.5.2 Model Equations and Setup

We create a burial model whose arguments are the unknown parameters (inherited concentration and exposure/burial time of each unit) that predicts the $^{26}$Al and $^{10}$Be concentrations of each sample. The model then compares how well the computed concentrations

match the measured concentrations and uses constrained nonlinear optimization methods to find the best fit between the calculated and measured values. The $^{26}$Al and $^{10}$Be concentration can be predicted for the above scenarios by solving the differential equation that governs cosmogenic nuclide production and decay:

$$\frac{dN_{i,j}}{dt} = P_j(z_i(t)) - N_i\lambda_j \tag{4.1}$$

Where i is the sample number, j is the nuclide measured ($^{26}$Al or $^{10}$Be), N is the concentration (atoms g$^{-1}$), P is the production rate (atoms g$^{-1}$ yr$^{-1}$) at depth, z, and λ is the decay constant (yr$^{-1}$). The deposition is modeled as instantaneous bulk deposits and is calculated using an integrated production formula for complex burial histories:

$$N_{i,j,k} = N_{i,j,(k-1)}e^{-\lambda t_k} + \frac{P_j(z_{i,k})}{\lambda_j}(1 - e^{-\lambda_j t_k}) \tag{4.2}$$

Where *i* denotes the sample number, *j* denotes the isotope ($^{26}$Al or $^{10}$Be), $t_k$ is the duration of time period k (yrs), *N* is the concentration (atom g$^{-1}$), *P* is the production rate (atoms g$^{-1}$ yr$^{-1}$), *z* is the depth (g cm$^{-2}$), and $\lambda$ is the decay constant (yr$^{-1}$). The first part of this equation calculates the decay of the nuclide concentration present at the start of the time period, and the second part calculates new accumulation during the duration of the time period.

### 4.5.3 Misfit and Constraints

The model accounts for a total of 4 unknown times: $t_1$, $t_2$, $t_3$, and $t_4$, ($t_5$ is assigned an age of 10,000 years) and 6 unknown initial concentrations. A chi-squared test is used to determine the misfit between the measured and calculated concentrations:

$$M = \Sigma_i \Sigma_j \left(\frac{N_{i,j,k} - N_{i,j}^M}{\sigma N_{i,j}^M}\right)^2 \quad (4.3)$$

Where M is the misfit between the measured and the calculated, $N_{i,j,k}$ is the calculated concentration at a depth, $N_{i,j}^M$ is the measured concentration, and $\sigma N_{i,j}^M$ is the error of the measured concentration. The uncertainty is determined using a 10,000-point Monte Carlo simulation considering the $^{26}$Al and $^{10}$Be measurements with gaussian standard errors. We constrain results to be values greater than zero and the inherited concentration of Unit 1 to fall within the simple exposure region.

## 4.6 Model Results

Using the optimization scheme and initial guesses described above with a 10,000-point Monte Carlo simulation to determine error using a 98% confidence interval, the deposits' ages and periods of glacial cover are determined. We ignore sample 6 (VV3-603-613) as an outlier that may have been influenced by potential mixing or may not have the same inherited concentration as the rest of the unit. The ages of each unit are calculated by adding each successive time period. As explained in the model setup, it is believed that Unit 2 was deposited quickly; however, it is possible to test scenarios where deposition may have occurred more slowly. This requires a different solution for the differential equation, where it is assumed,

deposition occurs at a constant rate over the time of exposure at the surface. These results show a significantly larger misfit and are provided in Supplemental Material 4.D. Figure 4.11 shows the best fit between the calculated and measured values along the core's depth, and Table 4.4 shows the model results.

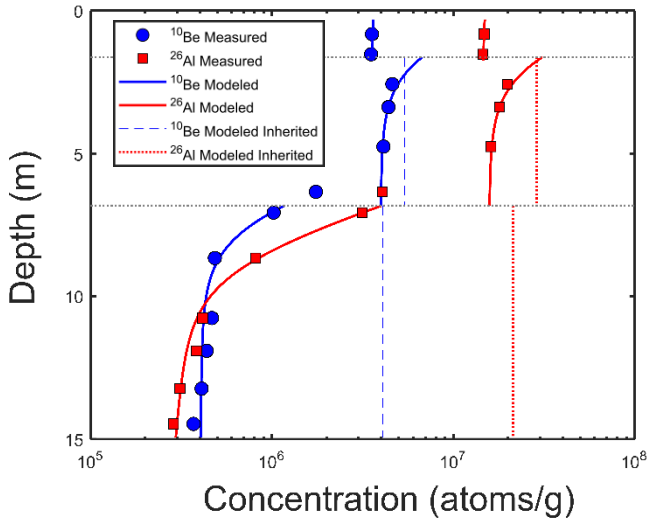


Figure 4.11: Measured and modeled $^{10}$Be and $^{26}$Al concentrations for forward model. The dashed lines represent the calculated inherited concentration of each unit.

Unit 1 is formed as a basal till during the advance of wet-based Victoria Upper Valley that covered the sediment for a minimum of 3.9 Ma ($t_1$). As Victoria Upper Glacier retreated, Unit 1 was exposed at the surface for approximately 0.13 Ma ($t_2$), and subsequently buried rapidly by Unit 2 about 0.68 Ma ago, which was exposed at the surface for 0.40 Ma ($t_3$). This longer surface exposure is consistent with a more strongly oxidized surface unit. Unit 2 was then shielded by another advance of a now cold-based Victoria Upper Glacier, which lasted 0.20 Ma. Finally, Unit 3 was deposited after glacial retreat and is the present-day surface unit.

Table 4.4: Model results forward model.

| Model Results | | |
|---|---|---|
| Time Period | Model Age Output ($10^6$) | Error ($10^6$) |
| $t_1$ | 3.90 | 0.09 |
| $t_2$ | 0.13 | 0.01 |
| $t_3$ | 0.40 | 0.05 |
| $t_4$ | 0.20 | 0.05 |
| $t_5$ | 0.01 | N/A |
| $N_{i,Be,Unit1}$ | 4.10 | 0.05 |
| $N_{i,Al,Unit1}$ | 21.00 | 0.23 |
| $N_{i,Be,Unit2}$ | 5.40 | 0.21 |
| $N_{i,Al,Unit2}$ | 29.00 | 2.20 |

## 4.6 Discussion

### 4.6.1 Interpreting Cosmogenic Nuclide Ages and Inherited Concentrations

As described earlier, we propose that Unit 1 is composed of paleosurface sediment that was entrained during glacial advance based on the presence of randomly oriented carbonate coatings found throughout the entirety of Unit 1. Furthermore, these carbonate coatings are limited to a single side of each clast, indicating these coatings formed on the MDV surface rather than as part of a lake deposit, where carbonate coatings would most likely coat the entire clast. Based on the best-fit model scenario and constraining the initial inherited concentration of the sediment that makes up Unit 1 to fall long the simple exposure curve, glacial ice is predicted to have covered the sediment for at least 3.9 Ma. This model provides a minimum estimate of ice cover since we cannot account for prior exposure/burial scenarios. We can also estimate a minimum time of how long the sediment was exposed prior to $t_1$ glacial cover. To do this, we look at the lowermost samples in Unit 1 and assume those sample have been the least affected by any cosmogenic nuclide accumulation after deposition and mostly reflect the decay of the inherited concentration. We can calculate the time of exposure needed to reach those

concentrations and determine ~0.65 Ma years of exposure during this time. Overall, this suggests that before deposition of Unit 1 ~ 0.7 Ma ago, the surface sediment that make up this unit experienced a relatively short period of exposure (at least 0.65 Ma) and comparably long periods of glacial cover (at least 3.9 Ma). This suggests that during the majority of the Plio-Pleistocene, Victoria Upper Glacier was larger than present-day and represented a glacial maximum during that time. To cover the core site, VUG advances a minimum of 5 km from its present-day position. Furthermore, based on our interpretation of Unit 1 as wet-based glacial deposits, this timing of this glacial cover indicates wet-based conditions existed in Victoria Upper Valley during the Plio-Pleistocene.

## 4.6.2 Previous Dating in the MDV

### *4.6.2.1 Glacial Moraines*

Comparison of glacial drifts among the various Dry Valleys is difficult due to variation in elevation, climate, and stochastic processes involving glacial deposition. Most of the work that has been done to date MDV moraine deposits has been focused in the southern, higher elevation valleys (Beacon Valley, Arena Valley, and Kennar Valley, and Vernier Valley) (Brook et al., 1993; Brown et al., 1991; Staiger et al., 2006a; Swanger et al., 2011b) where glacial processes may differ from lower elevation valleys due to colder and drier climate. Furthermore, most studies have focused on discrete surface deposits at terminal moraines rather than widespread glacial deposits that blanket the surface of the MDV. While the ages of surface terminal moraines provide strong evidence of the extent and timing of past glacial maximums or long-term retreat, they do not offer much context for glacial fluctuations or burial of past glacial deposits. Similarly, it is difficult to correlate the characteristics of drifts deposits that have been exposed at the surface since deposition and therefore weathered and altered to the drift

characteristics found within the core. Samples in this core have been buried and shielded from these weathering processes and may not be as mature as the surface deposits. Despite the uncertainty, deposits valley-wide can be roughly correlated based on time of deposition. Figure 4.12 shows locations and ages of past dating of moraines in the MDV, with a more detailed look at how these ages correlate to one another in Table 4.5. In higher elevation valleys, dated moraines provide evidence of overall glacial thinning of EAIS outlet glaciers since the Pliocene. Similarly, a moraine sequence from Stocking Glacier, an alpine glacier in Taylor Valley, has been retreating since Marine Isotope Stage (MIS) 11 (370-420 Kya) (Swanger et al., 2017). While the data presented could not address potential fluctuations of outlet glaciers since the Pliocene, most studies suggested changes were minimal in these regions. Furthermore, no deposits from these studies have identified deposits as being from wet-based glaciations. However, in Victoria Valley, Victoria Upper Glacier is believed to have fluctuated multiple times based on multiple glacial drifts and glacial benches identified within the valley(Prentice et al., 1998a). Using cores collected in the MDV to date glaciogenic sediment and using a model that accounts for periods of glacial cover and burial by subsequent deposits allows for a more robust interpretation and understanding of glacial fluctuations in the MDV than dating surface moraines.

This study provides evidence that long periods of potentially wet-based glacial cover occurred prior to depositing Unit 1 at around 0.7 Ma ago and provides the first dates on glacial events and glacial deposits in Upper Victoria Valley. Deposits dated from Lower Victoria Valley are slightly younger than Unit 2, with a minimum exposure age of approximately 0.3 Ma ago (McGowan et al., 2014). However, these deposits from Lower Victoria Valley most likely represent the growth of the Victoria Lower Glacier fed by the Wilson Piedmont Glacier, which

may behave differently than Victoria Upper Glacier. Because of the sporadic and sparse dating in the lower valleys, it is difficult to precisely correlate these ages to any established drifts in the region. Each valley has its own established set of named drifts (Table 4.5), often with poorly constrained age estimates due to lack of large-scale dating. Nonetheless, we correlate Unit 1 to Insel Drift (previously undated) in Victoria Valley. Insel drift is the oldest deposit in the valley and may correlate with Taylor IVb Drift (2.7 -3.0 Ma) (Bockheim and McLeod, 2013; Brown et al., 1991; Denton et al., 1971) in the upper elevation southern valleys, and potentially the Peleus till in Wright Valley (Prentice et al., 1993; Schiller et al., 2019). Unit 2 is more difficult to correlate with any specific drifts and can potentially correlate to Bull Drift in Victoria Valley and either Taylor III or Taylor IVa drift. An age of 0.66 Ma is significantly younger than previous estimates for Bull Drift (> 2 Ma) (Bockheim and McLeod, 2013); however, these ages were based on radiometric dating primarily from Wright and Taylor Valley

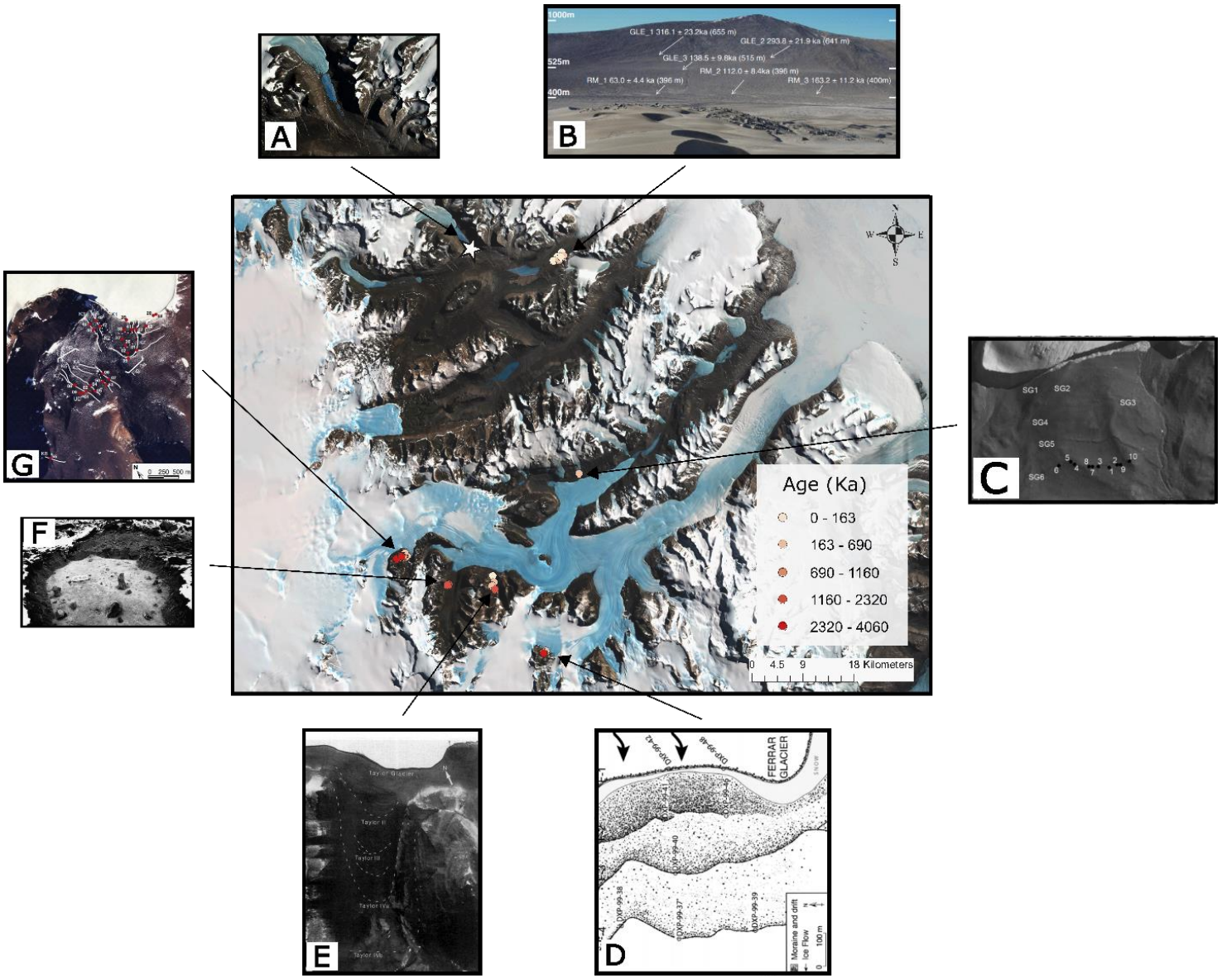


Figure 4.12: Compilation of all dated glacial deposits in the MDV, including this study. Most deposits date to the Pleistocene, with only a few dating to the Pliocene. Data is compiled from: A) this study, B) McGowan et al. (2014), C) Swanger et al. (2017), D) Staiger et al. (2006a), E) Brown et al. (1991) and Brook et al. (1993), F) Schäfer et al. (2000), and G) Swanger et al. (2011a)

*4.6.2.2 Wet-based Glaciation in the MDV*

The timing of wet-based glacial cover in Victoria Valley during the Plio-Pleistocene is consistent with other proposed wet-based depositional units in the MDV. While no other studies have dated wet-based events in Victoria Valley, a number of studies have identified potential wet-based glacial deposits in the neighboring Wright Valley (Bockheim and McLeod, 2008; Denton et al., 1993; Hall, 1992; Prentice et al., 1993; Prentice and Krusic, 2005; Prentice et al., 1998b; Schiller et al., 2019; Smellie et al., 2014; Stroeven and Prentice, 1997). Wright Valley is separated from Victoria by a low threshold (elevation change < 50 m) and connected through Bull Pass, suggesting glacial events in these valleys most likely interact with each other. Evidence for a wet-based glacial event in Wright Valley is determined primarily from the presence of Peleus till, which is proposed to be a subglacial till deposited during the Pliocene by a thick, wet-based EAIS outlet glacier and has been mapped out extensively in central Wright Valley (Prentice et al., 1993). The exact age of this unit is not well constrained. The Peleus till was initially constrained to have been deposited at a minimum 3.9 Ma ago based on the ages of Hart Ash deposited in Wright Valley that overlie the till (Hall, 1992; Hall et al., 1993; Prentice et al., 1993). However, recent work by Schiller et al. (2019) questions the age of the Hart Ash, proposing the age was overestimated by at least 1.0 Ma, and the ash was deposited approximately 2.9 Ma ago. Prentice and Krusic (2005) provided an upper limit on the age of Peleus till to be about 5.5 Ma based on Prospect fjord episode in Wright Valley. Further evidence from Wright Valley by Stroeven and Prentice (1997) provides strong indications of wet-based glaciation originating from an expansion of Wright Upper Glacier based on the identification of lodgment till and underlying striated pavement from the Sirius Group in Mt. Fleming. The timing of this event is also based on the age of Hart Ash previously described.

Table 4.5: Dated moraine deposits in the MDV. The dashed line between Vida and Bull Drift represents an uncertain age *boundary* between the two drifts. Similarly aged deposits in different valleys are likely to be from the same glacial event.

| | Figure 4.12 ID | | | | | | | | Named Drifts | | | |
|---|---|---|---|---|---|---|---|---|---|---|---|---|
| | A | B | C | D | E1* | E2* | F | G | | | | |
| | *This Study* | *McGowen et al., 2014* | *Swanger et al., 2017* | *Staiger et al., 2006* | *Brooke et al., 1993* | *Brown et al., 1991* | *Schafer et al., 2000* | *Swanger et al., 2011* | Victoria Valley (Previously Undated) | Taylor Valley/Arena Valley/Beacon Valley | Wright Valley (not all dated by moraine deposits) | Vernier Valley |
| **Glacier Type** | Outlet/Alpine | Piedmont | Alpine | Outlet | Outlet | Outlet | Outlet | Outlet | | | | |
| | Ages (Ka) | | | | | | | | | | | |
| | | 63<br>112<br>138<br>163 | | | 113<br><br>197 | 117 | | 20 | Packard Drift | Taylor II | Alpine IIa | Ferrar 1 |
| | | 294<br>316 | 391 | | 337 | 518 | | 290<br>320 | Vida Drift | Taylor III | Alpine IIb | Ferrar 2 |
| | 680 | | | 690<br>1160 | 1145 | 702 | | 590<br>1000 | Bull Drift | Taylor IVa | Alpine III | Ferrar 3 |
| | 2700-4500 (period of wet-based glaciation) | | | 4060 | | 2196 | 2280<br>2320 | 1800<br>3100<br>3900 | Insel Drift (wet based?) | Taylor IVb | Alpine IV or Peleus till** (wet-based?) | Ferrar 4 |

* Brooke et al., 1991 and Brown et al., 1993 analyze the same samples

** Ages for Peleus till based on ash deposits, not moraine deposits

### 4.6.3 Climate Implications

Our analysis indicates that wet-based glaciers existed in Victoria Valley during the late Pliocene to early Pleistocene, and that sediment in Unit 1 experienced at 3.9 Ma years of glacial cover and at least 0.65 Ma of exposure at the surface prior to its deposition at 1 Ma, suggesting a Plio-Pleistocene glacial event. After the Pliocene to early Pleistocene, VUG transitioned into its present-day cold-based glacier. The results from this study suggest a similar timing of large-scale glaciation found in connecting Wright Valley. These dates support that wet-based glaciation occurred during warmer and wetter conditions of the Plio-Pleistocene, and that this phenomenon was seen across multiple valleys (Prentice and Krusic, 2005; Raymo et al., 2006). During the Pliocene and early Pleistocene, models predict that global climate was 2-3°C warmer than present (Austermann et al., 2015; Dowsett et al., 2012; Patterson et al., 2014), which may have had an influence on MDV glacial dynamics. We suggest that the warmer and wetter climate was the cause of wet-based glaciation rather than increased glacial thickness, since outlet glaciers in the MDV are not often thick enough for basal melting. This is also consistent with evidence from the Antarctic Drilling Project (ANDRILL) of wet-based glacial fluctuations during the Pliocene. Dated stratigraphic units from within the AND-2A core suggest deposition during a temperate glacial regime from distant wet-based glaciers post 4.0 Ma (Fielding et al., 2011; Scopelliti et al., 2013). After the Pliocene, the MDV most likely looked more like present-day cold and dry conditions with cold-based glaciers with smaller, but not insignificant fluctuations.

## 4.7 Summary & Conclusions

This study analyzed a 15-meter permafrost core collected in Victoria Upper Valley containing glacial deposits from advance and retreat of Victoria Upper Glacier. Stratigraphic, sedimentological, and geochemical evidence from within the core support three glaciogenic

deposits. Based on the interpretation of these deposits, cosmogenic nuclides, $^{26}Al$ and $^{10}Be$, are used to constrain the timing of these depositional events using forward modeling. This study provides age constraints on the glacial history of Victoria Valley:

(1) The stratigraphic record and geochemical evidence support three distinct glacial deposits that have been identified at 14.60-6.60 m (Unit 1), 6.60-1.30 m (Unit 2), and 1.30-0.0 m (Unit 3). Unit 1 is interpreted as a subglacial till that formed during the advance of a wet-based glacier based on subangular to rounded clasts, randomly orientated carbonate coatings on gravels throughout the entire section, and high salt accumulations, including nitrate content. This is the first direct evidence of wet-based glacial deposits in Victoria Valley. Unit 2, a distinctly well-sorted sandy unit, is interpreted as a glaciofluvial deposits that occurred during the retreat of the wet-based glacier, and Unit 3 represents deposition by a cold-based glacier.

(2) Based on the interpretation of the exposure history of the core's glaciogenic deposits, the time of sediment deposition and periods of glacial cover are determined through a forward model using cosmogenic nuclides, $^{26}Al$ and $^{10}Be$. The model suggests glacial cover for at least 3.9 Ma years and at least 0.65 Ma years of sediment exposure prior to deposition of Unit 1 at approximately 0.7 My ago, suggesting a Plio-Pliestocene wet-based glacial event. Unit 2 was deposited during the retreat of this glacier and was rapidly deposited ~ 0.66 Ma ago and exposed at the surface for ~ 0.42 Ma. During the mid-to-late Pleistocene, a cold-based Victoria Upper Glacier, similar to the present day, advanced into Victoria Upper Valley, covering Unit 2 for ~ 0.23 Ma, and depositing Unit 3.

(3) The timing of wet-based glaciation in Victoria Valley is consistent with the timing of wet-based glacial deposits found in neighboring Wright Valley based on the interpretation and dating of Hart Ash. These ages both suggest that wet-based glaciation existed across multiple valleys during the warmer and wetter conditions during the Plio-Pleistocene.

## Supplemental Material 4.A Particle Size

| | | | | | < 2mm Fraction | | | |
|---|---|---|---|---|---|---|---|---|
| **Unit** | **Sample ID** | **Depth (cm)** | **% < 2mm** | **% > 2mm** | **Clay (< 2um)** | **Silt (2-50 um)** | **Sand (50-2000 um)** | **Mean** |
| Unit 3 | VV3-8-10 | 42.00 | 98.3% | 1.7% | 0.2% | 0.5% | 99.4% | 610.00 |
| | VV3-96-98 | 130.00 | 91.5% | 8.5% | 0.2% | 0.5% | 99.4% | 555.50 |
| | VV3-117-123 | 153.00 | 100.0% | 0.0% | 0.7% | 5.3% | 94.0% | 267.00 |
| | VV3-123-130 | 159.50 | 100.0% | 0.0% | 0.3% | 0.8% | 98.9% | 297.50 |
| Unit 2 | VV3-170-175 | 205.50 | 38.6% | 61.4% | N/A | N/A | N/A | N/A |
| | VV3-263-268 | 298.50 | 98.9% | 1.1% | 0.4% | 1.5% | 98.2% | 630.00 |
| | VV3-297-300 | 331.50 | 98.1% | 1.9% | 0.3% | 1.1% | 98.6% | 623.50 |
| | VV3-300-310 | 338.00 | 99.4% | 0.6% | 0.3% | 0.8% | 98.9% | 634.50 |
| | VV3-438-448 | 476.00 | 100.0% | 0.0% | 0.4% | 1.0% | 98.6% | 521.50 |
| | VV3-531-536 | 566.50 | 100.0% | 0.0% | 0.5% | 2.8% | 96.7% | 505.50 |
| | VV3-600-603 | 634.50 | 99.8% | 0.2% | 0.6% | 2.3% | 97.2% | 504.00 |
| | VV3-603-613 | 641.00 | 100.0% | 0.0% | 0.3% | 0.8% | 98.9% | 458.00 |
| Unit 3 | VV3-680-685 | 715.50 | 62.7% | 37.3% | 0.5% | 2.6% | 96.9% | 617.00 |
| | VV3-829-837 | 866.00 | 94.0% | 6.0% | 0.4% | 1.1% | 98.6% | 365.00 |
| | VV3-1039-1047 | 1076.00 | 91.7% | 8.3% | 0.4% | 0.9% | 98.7% | 404.50 |
| | VV3-1170-1175 | 1205.50 | 97.4% | 2.6% | 0.3% | 0.7% | 99.0% | 467.00 |
| | VV3-1285-1295 | 1323.00 | 99.7% | 0.3% | 0.4% | 1.1% | 98.6% | 485.50 |
| | VV3-1378-1383 | 1413.50 | 88.2% | 11.8% | 0.4% | 1.1% | 98.6% | 505.00 |

## Supplemental Material 4.B Carbonate Coatings

See excel file

## Supplemental Material 4.C Victoria Valley Core

See excel file

## Supplemental Material 4.D Slow Deposition

While evidence points to rapid deposition of sediment in unit 2, we can model this scenario as slow deposition to test for the misfit between measured and calculated values. We model slow deposition as constant accumulation rate over the entire exposure period. Slow deposition (constant deposition rate over entire period of exposure) is more complicated to solve than fast deposition since we add an unknown rate of deposition. The general equation used in this model is:

$$N_{i,j,k} = N_{i,j,(k-1)}e^{-\lambda t_k} + \frac{P_{j,sp}}{\lambda_j - \frac{\alpha}{\Lambda_{sp}}}\left(e^{-\frac{\alpha}{\Lambda_{sp}}t_k} - e^{-\lambda_j t_k}\right) + \frac{P_{j,m}}{\lambda_j - \frac{\alpha}{\Lambda_m}}\left(e^{-\frac{\alpha}{\Lambda_m}t_k} - e^{-\lambda_j t_k}\right)$$

Where *i* denotes the sample number, *j* denotes the isotope ($^{26}$Al or $^{10}$Be), sp denotes spallation, m denotes muon, $t_k$ is the duration of time period k (yrs), *N* is the concentration (atom g$^{-1}$), P is the production rate (atoms g$^{-1}$ yr$^{-1}$), $\lambda$ is the decay constant (yr$^{-1}$), α is the sedimentation rate ( α = z/t) (g cm$^{-2}$ yr$^{-1}$), and Λ is the attenuation length (g cm$^{-2}$). Modeled ages assuming slow deposition over the exposure period for Unit 2 deposition have a much worse fit than instantaneous deposition. Ages and model fit are shown in Table S4.1 and Figure S4.1.

Table S4. 1: Model results for slow deposition of Unit 2

| Model Results | | |
|---|---|---|
| | Slow Deposition | |
| | Value ($10^6$) | Error ($10^6$) |
| $t_1$ | 3..04 | 0.09 |
| $t_2$ | 0.08 | 0.01 |
| $t_3$ | 2.27 | 0.05 |
| $t_4$ | 0.04 | 0.05 |
| $t_5$ | 0.01 | N/A |
| $N_{i,Be,Unit1}$ | 4.89 | 0.05 |
| $N_{i,Al,Unit1}$ | 22.60 | 0.23 |
| $N_{i,Be,Unit2}$ | 7.60 | 0.21 |
| $N_{i,Al,Unit2}$ | 15.60 | 2.20 |

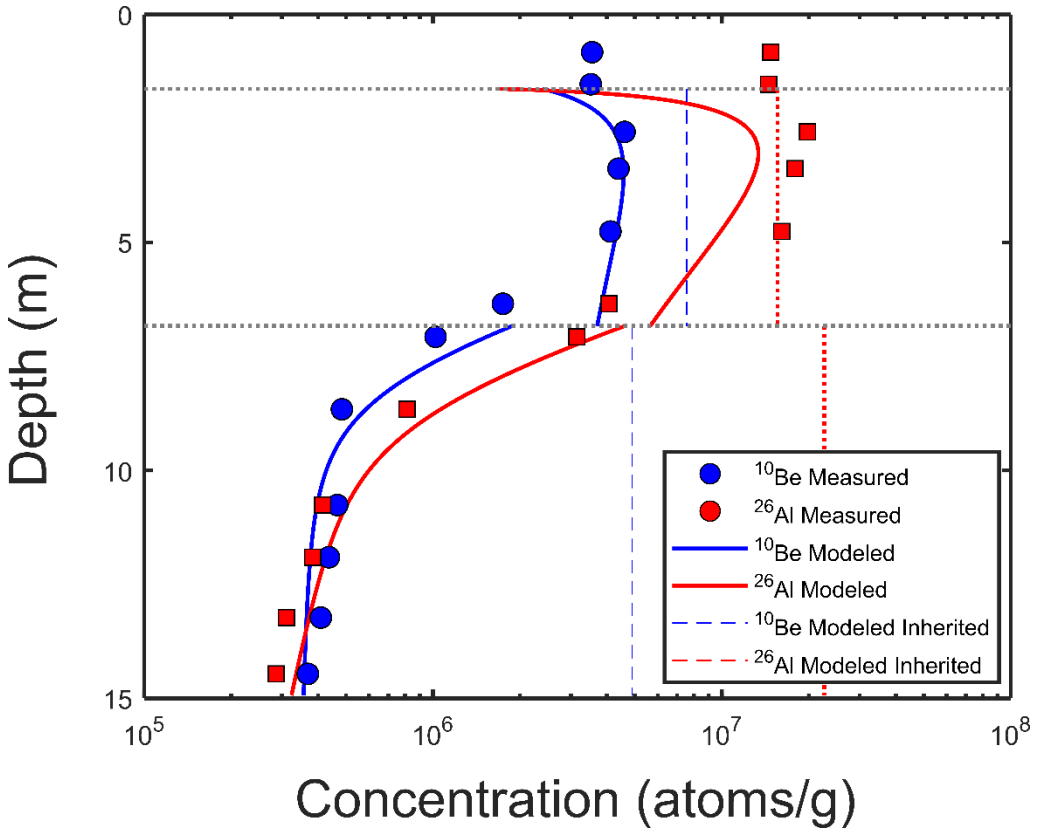


Figure S4. 1: Model fit for slow deposition of Unit 2

# Chapter 5 – Conclusions and Future Work

## 5.1 Summary and Conclusions

This dissertation uses ice-rich permafrost cores collected from the MDV to investigate long-term chemical weathering and the glacial history of the region. This work focuses on two cores: a 30-meter core collected in Beacon Valley to study chemical weathering in polar environments and a 15-meter core collected in Victoria Valley to better understand past glacial events in the region. This work characterizes, the mineralogy, stratigraphy, and chemistry of the Beacon Valley core, and provides evidence that chemical weathering, including dissolution, secondary salt precipitation, secondary clay formation, and cation exchange, are active processes even at subzero temperatures. In Victoria Valley, we provide evidence of three distinct glacial deposits, including a wet-based Plio-Pleistocene glaciation using the stratigraphic and geochemical evidence of glaciogenic deposits within the 15-meter core using a forward model and paired cosmogenic nuclides, $^{26}Al$ and $^{10}Be$.

In Chapter 2, evidence for chemical weathering based on salts, pH, and Mg isotopes shows weathering occurred in the upper 7.0 meters of ice-cemented permafrost, where up to 60% of Mg is derived from dolerite. In the lower 7.0-30 meters, less weathering occurs with an average of 5% of Mg sourced from dolerite weathering. The unfrozen water, modeled using ground temperature and soluble salts concentration, is one of the mains controls on the degree of weathering. This is supported in both the Mg isotopic data and pH values, where heavier Mg (sourced from dolerite) and higher pH (consumption of protons during dissolution) are more pronounced as a result of higher salt content and freezing point depression. Furthermore, an important finding of our study supports the concept of a ‘‘eutectic layer active zone”, where

unfrozen water (and chemical weathering) is present to the depth at which the maximum temperature exceeds the eutectic point of the dominant salt

Building upon the work of Chapter 2, Chapter 3 takes a more detailed look at the influence of secondary mineral formation (salt precipitation, clay minerals, and exchange processes) in permafrost environments. This work leverages the fact that the continuously frozen permafrost prevents leaching and locks weathering products in place. Each component of Mg involved in secondary mineral formation described above was isolated and the Mg isotopic composition of each component was analyzed. Both secondary salts and clay formation favored the heavy isotope, while the exchangeable Mg isotopic values reflect the composition of the exchanging reservoir (i.e., the permafrost ice). A key implication of this work was the fractionation factor determined between saponite, the most abundant clay formed in the Beacon Valley core, and the fluid phase of 0.83‰. Saponite is commonly formed during low-temperature alteration of oceanic crust and is a major Mg sink in the ocean budget; however, the flux of Mg lost to this process is poorly constrained. Using the fractionation factor between saponite and the fluid phase in the Beacon Valley core to represent the fractionation that occurs during low-temperature alteration of ocean crust, the Mg flux sink is calculated to be $0.16 \times 10^{12}$ mol/yr based on a simple mass balance calculation. The flux calculated in this study suggests a smaller flux than those previously calculated of $0.67 \times 10^{12}$ mol/yr and $1.0\text{-}1.7 \times 10^{12}$ mol/yr.

Finally, in Chapter 4, a 15-meter core collected from Victoria Valley is used to provide constraints on the timing of glacial events in Victoria Upper Valley. Stratigraphic, sedimentological, and geochemical evidence from within the core identified three glaciogenic deposits and revealed their depositional environment. Unit 1 is interpreted as a subglacial till formed during the advance of a wet-based glacier based on rounded clasts, randomly orientated

carbonate coatings on gravels throughout the entire section, and high salt accumulations including nitrate content. This is the first direct evidence of wet-based glacial deposits in Victoria Valley. Unit 2, a distinctly well-sorted sandy unit, is interpreted as a glaciofluvial deposits that occurred during the retreat of the wet-based glacier, and Unit 3 represents deposition by a cold-based glacier. Based on the interpretation of these deposits, cosmogenic nuclides, $^{26}Al$ and $^{10}Be$, are used to constrain the timing of these depositional events using forward modeling. A significant finding of this work is that there is evidence of a wet-based glacial event in Victoria Upper Valley that occurred during the Plio-Pleistocene that lasted for at least 3.9 Ma with 0.65 Ma years of sediment exposure prior to deposition of Unit 1 at approximately 0.7 Ma ago. The timing of this wet-based event is consistent with those described in neighboring valleys.

## 5.2 Future Work

Both the uniqueness of these core to preserve weathering products and the large amount of data collected during these projects provide ample opportunities to expand on this work. Considering Chapter 2 and 3, providing age constrains on the core would allow for calculations of the rate of different chemical weathering processes. This work is currently underway and will provide much need context on the timing of these processes.

Another key question we have not been able to answer from this work is why the Mg isotopic composition of Taylor Glacier ice (average = -0.93 ± 0.06‰) is isotopically lighter than seawater (-0.83 ± 0.09‰). Taylor Glacier is believed to ultimately be of marine origin and was assumed to have an isotopic composition equal to seawater. However, Taylor Glacier is significantly lighter, and resolving this discrepancy requires further investigation. One potential explanation may be an influence of carbonate dust on the surface of glaciers since carbonate

preferentially incorporates the light isotope into its structure. Analyzing Taylor Glacier samples from different ice cores and along a depth gradient may provide more insight into this phenomenon. Some of this work has already been completed, and we have found that the Mg isotopic composition of Taylor Glacier ice becomes heavier (and more like seawater Mg isotopic composition) with depth. This work can also be expanded to look at the Mg isotopic composition of other MDV glaciers to look for relationships between distance from the coast and Mg isotopic composition.

Another potential avenue to explore is a more detailed analysis of the mineralogy of the Beacon Valley core – specifically the clay-sized fraction. Saponite was identified within the core and expanded the scope of this work to help constrain the Mg flux during saponite formation during low-temperature alteration of oceanic crust. Therefore, a more detailed analysis of clays could further expand on these implications. The XRD analysis in this dissertation focused on the < 2 mm size fraction. Quantitative XRD analysis can be done by analyzing the clay-sized fraction to get better constraints on the clay minerals in the core. Analyzing more samples for quantitative XRD analysis would also be beneficial to future work on this core.

Using all the geochemical data samples along the depth of the core, chemical modeling can also help elucidate some of the weathering processes within the core. While chemical modeling was used to quantify the amount of unfrozen water found within the core, there is potential to look more closely at any brine migration (using soluble ions like Boron) or use pH and Mg isotopes to better constrain the amount of weathering on dolerite. This work is also currently underway, and more detailed work will be completed shortly.

Finally, there is significant work that can be done to improve the constraints on the timing of glaciation and age of glaciogenic deposits in Victoria Valley. A DVDP core collected near Lake Vida is the only other core that has been collected in Victoria Valley, and we can use similar forward modeling methods to try to add constraints on those deposits as well. This core is significantly further down-valley from Victoria Upper Glacier and may help estimate glacial advances in the region. Similarly, we can use exposure dating on surface samples of moraine deposits in Victoria Valley to compare to the ages we found within the core.

## References

Alberdi, M., Bravo, L.A., Gutiérrez, A., Gidekel, M. and Corcuera, L.J. (2002) Ecophysiology of Antarctic vascular plants. Physiologia Plantarum 115, 479-486.

Alt, J.C. (1995) Subseafloor processes in mid-ocean ridge hydrothermal systems. Geophysical Monograph-American Geophysical Union 91, 85-85.

Anderson, D.M., Gatto, L. and Ugolini, F.C. (1972) An Antarctic analog of Martian permafrost terrain. Antarctic Journal of the United States 7, 114-116.

Anderson, D.M. and Morgenstern, N. (1973) Physics, chemistry, and mechanics of frozen ground: a review, Permafrost: The North American Contribution to the Second International Conference, National Academy of Sciences, Washington, DC, pp. 257-288.

Anisimov, O.A., Vaughan, D.G., Callaghan, T.V., Furgal, C., Marchant, H., Prowse, T.D., Vilhjálmsson, H. and Walsh, J.E. (2007) Polar regions (arctic and antarctic). Climate change 15, 653-685.

Armstrong, R.L. (1978) K-Ar dating: Late Cenozoic McMurdo volcanic group and dry valley glacial history, Victoria Land, Antarctica. New Zealand journal of geology and geophysics 21, 685-698.

Armstrong, R.L., Hamilton, W. and Denton, G.H. (1968) Glaciation in Taylor Valley, Antarctica, older than 2.7 million years. Science 159, 187-189.

Arvidson, R.S., Guidry, M.W. and Mackenzie, F.T. (2011) Dolomite controls on Phanerozoic seawater chemistry. Aquatic Geochemistry 17, 735-747.

Arvidson, R.S., Mackenzie, F.T. and Guidry, M. (2006) MAGic: A Phanerozoic model for the geochemical cycling of major rock-forming components. American Journal of Science 306, 135-190.

Atkins, C. (2013) Geomorphological evidence of cold-based glacier activity in South Victoria Land, Antarctica. Geological Society, London, Special Publications 381, 299-318.

Atkins, C.B. and Dickinson, W.W. (2007) Landscape modification by meltwater channels at margins of cold‐based glaciers, Dry Valleys, Antarctica. Boreas 36, 47-55.

Austermann, J., Pollard, D., Mitrovica, J.X., Moucha, R., Forte, A.M., DeConto, R.M., Rowley, D.B. and Raymo, M.E. (2015) The impact of dynamic topography change on Antarctic ice sheet stability during the mid-Pliocene warm period. Geology 43, 927-930.

Bao, H., Barnes, J.D., Sharp, Z.D. and Marchant, D.R. (2008) Two chloride sources in soils of the McMurdo Dry Valleys, Antarctica. Journal of Geophysical Research: Atmospheres 113.

Bao, H., Campbell, D.A., Bockheim, J.G. and Thiemens, M.H. (2000) Origins of sulphate in Antarctic dry-valley soils as deduced from anomalous 17O compositions. Nature 407, 499-502.

Bartoli, G., Hönisch, B. and Zeebe, R.E. (2011) Atmospheric CO2 decline during the Pliocene intensification of Northern Hemisphere glaciations. Paleoceanography 26.

Berner, R.A. (1992) Weathering, plants, and the long-term carbon cycle. Geochimica et Cosmochimica Acta 56, 3225-3231.

Berner, R.A. (2004) A model for calcium, magnesium and sulfate in seawater over Phanerozoic time. American Journal of Science 304, 438-453.

Bigeleisen, J. and Mayer, M.G. (1947) Calculation of equilibrium constants for isotopic exchange reactions. The Journal of Chemical Physics 15, 261-267.

Blackburn, T., Edwards, G., Tulaczyk, S., Scudder, M., Piccione, G., Hallet, B., McLean, N., Zachos, J., Cheney, B. and Babbe, J. (2020) Ice retreat in Wilkes Basin of East Antarctica during a warm interglacial. Nature 583, 554-559.

Bockheim, J. (2002) Landform and soil development in the McMurdo Dry Valleys, Antarctica: a regional synthesis. Arctic, Antarctic, and Alpine Research, 308-317.

Bockheim, J. and McLeod, M. (2008) Early Pliocene expansion of the East Antarctic ice sheet, upper Wright valley, Antarctica. Geografiska Annaler: Series A, Physical Geography 90, 187-199.

Bockheim, J.G. (1995) Permafrost distribution in the southern circumpolar region and its relation to the environment: a review and recommendations for further research. Permafrost and Periglacial Processes 6, 27-45.

Bockheim, J.G. (2010) Evolution of desert pavements and the vesicular layer in soils of the Transantarctic Mountains. Geomorphology 118, 433-443.

Bockheim, J.G., Kurz, M.D., Soule, S.A. and Burke, A. (2009) Genesis of active sand-filled polygons in lower and central Beacon Valley, Antarctica. Permafrost and Periglacial Processes 20, 295-308.

Bockheim, J.G. and McLeod, M. (2013) Glacial geomorphology of the Victoria Valley System, Ross Sea Region, Antarctica. Geomorphology 193, 14-24.

Bolou-Bi, E.B., Vigier, N., Poszwa, A., Boudot, J.-P. and Dambrine, E. (2012) Effects of biogeochemical processes on magnesium isotope variations in a forested catchment in the Vosges Mountains (France). Geochimica et Cosmochimica Acta 87, 341-355.

Borchardt, G. (1989) Smectites. Minerals in soil environments 1, 675-727.

Bowers, T.S. and Taylor Jr, H.P. (1985) An integrated chemical and stable-isotope model of the origin of midocean ridge hot spring systems. Journal of Geophysical Research: Solid Earth 90, 12583-12606.

Bromley, A.M. (1985) Weather observations Wright Valley, Antarctica. New Zealand Antarctic Research Programme. Vanda Station.

Brook, E.J., Kurz, M.D., Ackert Jr, R.P., Denton, G.H., Brown, E.T., Raisbeck, G.M. and Yiou, F. (1993) Chronology of Taylor Glacier advances in Arena Valley, Antarctica, using in situ cosmogenic 3He and 10Be. Quaternary Research 39, 11-23.

Brown, E.T., Edmond, J.M., Raisbeck, G.M., Yiou, F., Kurz, M.D. and Brook, E.J. (1991) Examination of surface exposure ages of Antarctic moraines using in situ produced 10Be and 26Al. Geochimica et Cosmochimica Acta 55, 2269-2283.

Brown, J., Ferrians Jr, O., Heginbottom, J.A. and Melnikov, E. (1997) Circum-Arctic map of permafrost and ground-ice conditions. US Geological Survey Reston, VA.

Brown, J., Ferrians, O., Heginbottom, J. and Melnikov, E. (2002) Circum-Arctic map of permafrost and ground-ice conditions, version 2. Boulder, Colorado USA, National Snow and Ice Data Center.

Bull, C. (1962) Quaternary glaciations in southern Victoria Land, Antarctica. Journal of Glaciology 4, 240-241.

Calkin, P.E. (1964) Geomorphology and glacial geology of the Victoria Valley system, southern Victoria Land, Antarctica.

Calkin, P.E. (1971) Glacial geology of the Victoria Valley system, southern Victoria Land, Antarctica. Antarctic Snow and Ice Studies II, 363-412.

Campbell, I. and Claridge, G. (1969) A CLASSIFICATION OF FRIGIC SOILS-THE ZONAL SOILS OF THE ANTARCTIC CONTINENT. Soil science 107, 75-85.

Campbell, I.B. and Claridge, G. (1987) Antarctica: soils, weathering processes and environment. Elsevier.

Chinn, T. (1990) The dry valleys. Antarctica; the Ross Sea region DSIR Information Series, 137-153.

Claridge, G. and Campbell, I. (1968) Origin of nitrate deposits.

Claridge, G. and Campbell, I. (1977) The salts in Antarctic soils, their distribution and relationship to soil processes. Soil Science 123, 377-384.

Claridge, G. and Campbell, I. (1984) Mineral transformation during the weathering of dolerite under cold arid conditions in Antarctica. New Zealand journal of geology and geophysics 27, 537-545.

Colman, S.M. (1982) Chemical weathering of basalts and andesites; evidence from weathering rinds. USGPO.

Cook, C.P., van de Flierdt, T., Williams, T., Hemming, S.R., Iwai, M., Kobayashi, M., Jimenez-Espejo, F.J., Escutia, C., González, J.J. and Khim, B.-K. (2013) Dynamic behaviour of the East Antarctic ice sheet during Pliocene warmth. Nature Geoscience 6, 765-769.

Craig, D. and Loughnan, F. (1964) Chemical and mineralogical transformations accompanying the weathering of basic volcanic rocks from New South Wales. Soil Research 2, 218-234.

Cuozzo, N., Sletten, R.S., Hu, Y., Liu, L., Teng, F.-Z. and Hagedorn, B. (2020) Silicate weathering in antarctic ice-rich permafrost: Insights using magnesium isotopes. Geochimica et Cosmochimica Acta 278, 244-260.

Dansgaard, W. (1964) Stable isotopes in precipitation. Tellus 16, 436-468.

De Villiers, S., Dickson, J. and Ellam, R. (2005) The composition of the continental river weathering flux deduced from seawater Mg isotopes. Chemical Geology 216, 133-142.

Denton, G.H., Armstrong, R.L. and Stuiver, M. (1971) The late Cenozoic glacial history of Antarctica. The Late Cenozoic Glacial Ages, 267-306.

Denton, G.H., Prentice, M.L., Kellogg, D.E. and Kellogg, T.B. (1984) Late Tertiary history of the Antarctic ice sheet: Evidence from the Dry Valleys. Geology 12, 263-267.

Denton, G.H., Sugden, D.E., Marchant, D.R., Hall, B.L. and Wilch, T.I. (1993) East Antarctic Ice Sheet sensitivity to Pliocene climatic change from a Dry Valleys perspective. Geografiska Annaler. Series A. Physical Geography, 155-204.

Diaz, M.A., Adams, B.J., Welch, K.A., Welch, S.A., Opiyo, S.O., Khan, A.L., McKnight, D.M., Cary, S.C. and Lyons, W.B. (2018) Aeolian material transport and its role in landscape connectivity in the McMurdo Dry Valleys, Antarctica. Journal of Geophysical Research: Earth Surface 123, 3323-3337.

Diaz, M.A., Corbett, L.B., Bierman, P.R., Adams, B.J., Wall, D.H., Hogg, I.D., Fierer, N. and Lyons, W.B. (2020) Relative terrestrial exposure ages inferred from meteoric 10 Be and NO 3− concentrations in soils along the Shackleton Glacier, Antarctica. Earth Surface Dynamics Discussions, 1-35.

Dickinson, W.W. and Grapes, R.H. (1997) Authigenic chabazite and implications for weathering in Sirius group diamictite, Table Mountain, Dry Valleys, Antarctica. Journal of Sedimentary Research 67, 815-820.

Dickinson, W.W. and Rosen, M.R. (2003) Antarctic permafrost: An analogue for water and diagenetic minerals on Mars. Geology 31, 199-202.

Dickinson, W.W., Williams, G., Hill, M., Cox, S.C. and Baker, J.A. (2017) Granite erratics in Beacon Valley, Antarctica. Antarctic Science 29, 343-355.

Dolan, A.M., Haywood, A.M., Hill, D.J., Dowsett, H.J., Hunter, S.J., Lunt, D.J. and Pickering, S.J. (2011) Sensitivity of Pliocene ice sheets to orbital forcing. Palaeogeography, Palaeoclimatology, Palaeoecology 309, 98-110.

Doran, P.T., McKay, C.P., Clow, G.D., Dana, G.L., Fountain, A.G., Nylen, T. and Lyons, W.B. (2002) Valley floor climate observations from the McMurdo Dry Valleys, Antarctica, 1986–2000. Journal of Geophysical Research: Atmospheres 107.

Dowling, C.B., Lyons, W. and Welch, K.A. (2013) Strontium isotopic signatures of streams from Taylor Valley, Antarctica, Revisited: The role of carbonate mineral dissolution. Aquatic geochemistry 19, 231-240.

Dowsett, H.J., Robinson, M.M., Haywood, A.M., Hill, D.J., Dolan, A.M., Stoll, D.K., Chan, W.-L., Abe-Ouchi, A., Chandler, M.A. and Rosenbloom, N.A. (2012) Assessing confidence in Pliocene sea surface temperatures to evaluate predictive models. Nature Climate Change 2, 365.

Dutton, A., Carlson, A.E., Long, A., Milne, G.A., Clark, P.U., DeConto, R., Horton, B.P., Rahmstorf, S. and Raymo, M.E. (2015) Sea-level rise due to polar ice-sheet mass loss during past warm periods. science 349.

Eggleton, R.A., Foudoulis, C. and Varkevisser, D. (1987) Weathering of basalt: changes in rock chemistry and mineralogy. Clays and Clay Minerals 35, 161-169.

Elderfield, H. and Schultz, A. (1996) Mid-ocean ridge hydrothermal fluxes and the chemical composition of the ocean. Annual Review of Earth and Planetary Sciences 24, 191-224.

Elliot, D., Fleming, T., Haban, M. and Siders, M. (1995) Petrology and mineralogy of the Kirkpatrick basalt and Ferrar dolerite, Mesa range region, North Victoria Land, Antarctica. Contributions to Antarctic Research IV, 103-141.

Fielding, C.R., Browne, G.H., Field, B., Florindo, F., Harwood, D.M., Krissek, L.A., Levy, R.H., Panter, K.S., Passchier, S. and Pekar, S.F. (2011) Sequence stratigraphy of the ANDRILL AND-2A drillcore, Antarctica: A long-term, ice-proximal record of Early to Mid-Miocene climate, sea-level and glacial dynamism. Palaeogeography, Palaeoclimatology, Palaeoecology 305, 337-351.

Fitzsimons, S., Webb, N., Mager, S., MacDonell, S., Lorrain, R. and Samyn, D. (2008) Mechanisms of basal ice formation in polar glaciers: an evaluation of the apron entrainment model. Journal of Geophysical Research: Earth Surface 113.

Flint, R., Sanders, J. and Rodgers, J. (1960a) Symmictite: a name for nonsorted terrigenous sedimentary rocks that contain a wide range of particle sizes. Geological Society of America Bulletin 71, 507-510.

Flint, R.F., Sanders, J. and Rodgers, J. (1960b) Diamictite, a substitute term for symmictite. Geological Society of America Bulletin 71, 1809-1810.

Fountain, A.G., Nylen, T.H., Monaghan, A., Basagic, H.J. and Bromwich, D. (2010) Snow in the McMurdo Dry Valleys, Antarctica. International Journal of Climatology 30, 633-642.

Galy, A., Bar-Matthews, M., Halicz, L. and O'Nions, R.K. (2002) Mg isotopic composition of carbonate: insight from speleothem formation. Earth and Planetary Science Letters 201, 105-115.

Gérard, F., Ranger, J., Ménétrier, C. and Bonnaud, P. (2003) Silicate weathering mechanisms determined using soil solutions held at high matric potential. Chemical Geology 202, 443-460.

Gibson, E.K., Wentworth, S.J. and McKay, D.S. (1983a) Chemical weathering and diagenesis of a cold desert soil from Wright Valley, Antarctica: An analog of Martian weathering processes. Journal of Geophysical Research: Solid Earth 88.

Gibson, E.K., Wentworth, S.J. and McKay, D.S. (1983b) Chemical weathering and diagenesis of a cold desert soil from Wright Valley, Antarctica: An analog of Martian weathering processes. Journal of Geophysical Research: Solid Earth 88, A912-A928.

Graly, J.A., Licht, K.J., Druschel, G.K. and Kaplan, M.R. (2018) Polar desert chronologies through quantitative measurements of salt accumulation. Geology 46, 351-354.

Granger, D.E. and Muzikar, P.F. (2001) Dating sediment burial with in situ-produced cosmogenic nuclides: theory, techniques, and limitations. Earth and Planetary Science Letters 188, 269-281.

Green, W.J., Angle, M.P. and Chave, K.E. (1988) The geochemistry of Antarctic streams and their role in the evolution of four lakes of the McMurdo Dry Valleys. Geochimica et Cosmochimica Acta 52, 1265-1274.

Gunn, B.M. (1962) Differentiation in ferrar dolerites, Antarctica. New Zealand Journal of Geology and Geophysics 5, 820-863.

Hagedorn, B., Sletten, R.S., Hallet, B., McTigue, D.F. and Steig, E.J. (2010) Ground ice recharge via brine transport in frozen soils of Victoria Valley, Antarctica: Insights from modeling δ 18 O and δD profiles. Geochimica et Cosmochimica Acta 74, 435-448.

Hall, B.L. (1992) Surficial geology and geomorphology of eastern Wright Valley, Antarctica: Implications for plio-pleistocene ice-sheet dynamics. University of Maine.

Hall, B.L. and Denton, G.H. (2002) Holocene history of the Wilson Piedmont Glacier along the southern Scott Coast, Antarctica. The Holocene 12, 619-627.

Hall, B.L., Denton, G.H., Lux, D.R. and Bockheim, J.G. (1993) Late Tertiary Antarctic paleoclimate and ice-sheet dynamics inferred from surficial deposits in Wright Valley. Geografiska Annaler: Series A, Physical Geography 75, 239-267.

Hall, B.L., Denton, G.H., Overturf, B. and Hendy, C.H. (2002) Glacial Lake Victoria, a high-level Antarctic lake inferred from lacustrine deposits in Victoria Valley. Journal of Quaternary Science: Published for the Quaternary Research Association 17, 697-706.

Hallet, B. (1978) Solute redistribution in freezing ground, Proceeding of the Third International Conference on Permafrost, Edmonton, Alberta, pp. 86-91.

Hambrey, M.J. and Fitzsimons, S.J. (2010) Development of sediment–landform associations at cold glacier margins, Dry Valleys, Antarctica. Sedimentology 57, 857-882.

Hambrey, M.J. and Glasser, N.F. (2012) Discriminating glacier thermal and dynamic regimes in the sedimentary record. Sedimentary Geology 251, 1-33.

Heindel, R.C., Lyons, W.B., Welch, S.A., Spickard, A.M. and Virginia, R.A. (2018) Biogeochemical weathering of soil apatite grains in the McMurdo Dry Valleys, Antarctica. Geoderma 320, 136-145.

Heldmann, J., Pollard, W., McKay, C., Marinova, M., Davila, A., Williams, K., Lacelle, D. and Andersen, D. (2013) The high elevation Dry Valleys in Antarctica as analog sites for subsurface ice on Mars. Planetary and Space Science 85, 53-58.

Hendy, C., Sadler, A., Denton, G. and Hall, B. (2000) Proglacial lake‐ice conveyors: a new mechanism for deposition of drift in polar environments. Geografiska Annaler: Series A, Physical Geography 82, 249-270.

Higgins, J.A. and Schrag, D. (2010) Constraining magnesium cycling in marine sediments using magnesium isotopes. Geochimica et Cosmochimica Acta 74, 5039-5053.

Higgins, S.M., Hendy, C.H. and Denton, G.H. (2000) Geochronology of Bonney drift, Taylor Valley, Antarctica: evidence for interglacial expansions of Taylor Glacier. Geografiska Annaler: Series A, Physical Geography 82, 391-409.

Hindshaw, R.S., Tosca, R., Tosca, N.J. and Tipper, E.T. (2020) Experimental constraints on Mg isotope fractionation during clay formation: Implications for the global biogeochemical cycle of Mg. Earth and Planetary Science Letters 531, 115980.

Holland, H.D. (2005) Sea level, sediments and the composition of seawater. American Journal of Science 305, 220-239.

Hu, Y., Harrington, M.D., Sun, Y., Yang, Z., Konter, J. and Teng, F.Z. (2016) Magnesium isotopic homogeneity of San Carlos olivine: a potential standard for Mg isotopic analysis by multi‐collector inductively coupled plasma mass spectrometry. Rapid Communications in Mass Spectrometry 30, 2123-2132.

Huang, K.-J., Teng, F.-Z., Plank, T., Staudigel, H., Hu, Y. and Bao, Z.-Y. (2018) Magnesium isotopic composition of altered oceanic crust and the global Mg cycle. Geochimica et Cosmochimica Acta 238, 357-373.

Huang, K.-J., Teng, F.-Z., Wei, G.-J., Ma, J.-L. and Bao, Z.-Y. (2012) Adsorption-and desorption-controlled magnesium isotope fractionation during extreme weathering of basalt in Hainan Island, China. Earth and Planetary Science Letters 359, 73-83.

Jackson, M.L. (2005) Soil chemical analysis: Advanced course. UW-Madison Libraries Parallel Press.

Jones, L.M. and Faure, G. (1978) A study of strontium isotopes in lakes and surficial deposits of the ice-free valleys, southern Victoria Land, Antarctica. Chemical Geology 22, 107-120.

Keys, J.H. and Williams, K. (1981) Origin of crystalline, cold desert salts in the McMurdo region, Antarctica. Geochimica et Cosmochimica Acta 45, 2299-2309.

Kohl, C. and Nishiizumi, K. (1992) Chemical isolation of quartz for measurement of in-situ-produced cosmogenic nuclides. Geochimica et Cosmochimica Acta 56, 3583-3587.

Krusic, A., Prentice, M. and Licciardi, J. (2009) Climatic implications of reconstructed early–mid Pliocene equilibrium-line altitudes in the McMurdo Dry Valleys, Antarctica. Annals of Glaciology 50, 31-36.

Kurasawa, H. and MG JR, M. (1974) GEOLOGIC LOG OF THE LAKE VIDA CORE-DVDP 6.

Kushnir, J. (1980) The coprecipitation of strontium, magnesium, sodium, potassium and chloride ions with gypsum. An experimental study. Geochimica et Cosmochimica Acta 44, 1471-1482.

Lacelle, D., Davila, A.F., Pollard, W.H., Andersen, D., Heldmann, J., Marinova, M. and McKay, C.P. (2011) Stability of massive ground ice bodies in University Valley, McMurdo Dry Valleys of Antarctica: Using stable O–H isotope as tracers of sublimation in hyper-arid regions. Earth and Planetary Science Letters 301, 403-411.

Leslie, D., Lyons, W.B., Warner, N., Vengosh, A., Olesik, J., Welch, K. and Deuerling, K. (2014) Boron isotopic geochemistry of the McMurdo Dry Valley lakes, Antarctica. Chemical Geology 386, 152-164.

Li, W.-Y., Teng, F.-Z., Ke, S., Rudnick, R.L., Gao, S., Wu, F.-Y. and Chappell, B. (2010) Heterogeneous magnesium isotopic composition of the upper continental crust. Geochimica et Cosmochimica Acta 74, 6867-6884.

Li, W., Beard, B.L. and Johnson, C.M. (2011) Exchange and fractionation of Mg isotopes between epsomite and saturated MgSO 4 solution. Geochimica et Cosmochimica Acta 75, 1814-1828.

Li, W., Beard, B.L., Li, C. and Johnson, C.M. (2014) Magnesium isotope fractionation between brucite [Mg (OH) 2] and Mg aqueous species: Implications for silicate weathering and biogeochemical processes. Earth and Planetary Science Letters 394, 82-93.

Ling, M.X., Sedaghatpour, F., Teng, F.Z., Hays, P.D., Strauss, J. and Sun, W. (2011) Homogeneous magnesium isotopic composition of seawater: an excellent geostandard for Mg isotope analysis. Rapid Communications in Mass Spectrometry 25, 2828-2836.

Linkletter, G., Bockheim, J. and Ugolini, F. (1973) Soils and glacial deposits in the Beacon Valley, southern Victoria Land, Antarctica. New Zealand Journal of Geology and Geophysics 16, 90-108.

Liu, L., Sletten, R.S., Hagedorn, B., Hallet, B., McKay, C.P. and Stone, J.O. (2015) An enhanced model of the contemporary and long‐term (200 ka) sublimation of the massive subsurface ice in Beacon Valley, Antarctica. Journal of Geophysical Research: Earth Surface 120, 1596-1610.

Liu, X.-M., Teng, F.-Z., Rudnick, R.L., McDonough, W.F. and Cummings, M.L. (2014) Massive magnesium depletion and isotope fractionation in weathered basalts. Geochimica et Cosmochimica Acta 135, 336-349.

Low, P.F., Anderson, D.M. and Hoekstra, P. (1968) Some thermodynamic relationships for soils at or below the freezing point: 1. Freezing point depression and heat capacity. Water Resources Research 4, 379-394.

Luijendijk, E., Gleeson, T. and Moosdorf, N. (2020) Fresh groundwater discharge insignificant for the world's oceans but important for coastal ecosystems. Nature communications 11, 1-12.

Lunt, D.J., Foster, G.L., Haywood, A.M. and Stone, E.J. (2008) Late Pliocene Greenland glaciation controlled by a decline in atmospheric CO 2 levels. Nature 454, 1102-1105.

Lyons, W.B., Bullen, T.D. and Welch, K.A. (2017) Ca isotopic geochemistry of an Antarctic aquatic system. Geophysical Research Letters 44, 882-891.

Lyons, W.B., Deuerling, K., Welch, K.A., Welch, S.A., Michalski, G., Walters, W.W., Nielsen, U., Wall, D.H., Hogg, I. and Adams, B.J. (2016) The soil geochemistry in the Beardmore Glacier region, Antarctica: Implications for terrestrial ecosystem history. Scientific reports 6, 1-8.

Lyons, W.B. and Mayewski, P.A. (1993) The geochemical evolution of terrestrial waters in the Antarctic: The role of rock-water interactions. Physical and Biogeochemical Processes in Antarctic Lakes 59, 135-143.

Ma, L., Teng, F.-Z., Jin, L., Ke, S., Yang, W., Gu, H.-O. and Brantley, S.L. (2015) Magnesium isotope fractionation during shale weathering in the Shale Hills Critical Zone Observatory: Accumulation of light Mg isotopes in soils by clay mineral transformation. Chemical Geology 397, 37-50.

Marion, G. (1997) A theoretical evaluation of mineral stability in Don Juan Pond, wright valley, victoria land. Antarctic Science 9, 92-99.

Marion, G., Catling, D., Zahnle, K. and Claire, M. (2010) Modeling aqueous perchlorate chemistries with applications to Mars. Icarus 207, 675-685.

Marion, G.M. and Grant, S.A. (1994) FREZCHEM: A chemical-thermodynamic model for aqueous solutions at subzero temperatures. DTIC Document.

Marra, K.R., Madden, M.E.E., Soreghan, G.S. and Hall, B.L. (2017) Chemical weathering trends in fine-grained ephemeral stream sediments of the McMurdo Dry Valleys, Antarctica. Geomorphology 281, 13-30.

Maurice, P.A., McKnight, D.M., Leff, L., Fulghum, J.E. and Gooseff, M. (2002) Direct observations of aluminosilicate weathering in the hyporheic zone of an Antarctic Dry Valley stream. Geochimica et Cosmochimica Acta 66, 1335-1347.

Mayfield, K.K., Eisenhauer, A., Ramos, D.P.S., Higgins, J.A., Horner, T.J., Auro, M., Magna, T., Moosdorf, N., Charette, M.A. and Gonneea, M.E. (2021) Groundwater discharge impacts marine isotope budgets of Li, Mg, Ca, Sr, and Ba. Nature Communications 12, 1-9.

McElroy, C. and Rose, G. (1987) Geology of the Beacon Heights area, southern Victoria Land. Antarctica: New Zealand Geological Survey Miscellaneous Series Map 15.

McGowan, H.A., Neil, D.T. and Speirs, J.C. (2014) A reinterpretation of geomorphological evidence for Glacial Lake Victoria, McMurdo Dry Valleys, Antarctica. Geomorphology 208, 200-206.

Mehra, O. and Jackson, M. (1960) Iron oxide removal from soils and clays by a dithionite–citrate system buffered with sodium bicarbonate, Clays and clay minerals: proceedings of the Seventh National Conference. Elsevier, pp. 317-327.

Meyer, H., Derevyagin, A.Y., Siegert, C. and Hubberten, H.-W. (2002) Paleoclimate studies on Bykovsky Peninsula, North Siberia-hydrogen and oxygen isotopes in ground ice. Polarforschung 70, 37-51.

Michalski, G., Bockheim, J., Kendall, C. and Thiemens, M. (2005) Isotopic composition of Antarctic Dry Valley nitrate: Implications for NOy sources and cycling in Antarctica. Geophysical Research Letters 32.

Moncrieff, A. (1989) Classification of poorly-sorted sedimentary rocks. Sedimentary Geology 65, 191-194.

Morse, J.W. and Mackenzie, F.T. (1990) Geochemistry of sedimentary carbonates. Elsevier.

Murrmann, R.P. (1973) Ionic mobility in permafrost, Proceedings of the Second International Conference on Permafrost, Yakutsk, pp. 352-359.

Naish, T., Powell, R., Levy, R., Florindo, F., Harwood, D., Kuhn, G., Niessen, F., Talarico, F. and Wilson, G. (2007) A record of Antarctic climate and ice sheet history recovered. Eos, Transactions American Geophysical Union 88, 557-558.

Naish, T., Powell, R., Levy, R., Wilson, G., Scherer, R., Talarico, F., Krissek, L., Niessen, F., Pompilio, M. and Wilson, T. (2009) Obliquity-paced Pliocene West Antarctic ice sheet oscillations. Nature 458, 322-328.

Nesbitt, H. and Wilson, R. (1992) Recent chemical weathering of basalts. American Journal of Science 292, 740-777.

Nezat, C.A., Lyons, W.B. and Welch, K.A. (2001) Chemical weathering in streams of a polar desert (Taylor Valley, Antarctica). Geological Society of America Bulletin 113, 1401-1408.

Nielsen, S.G., Rehkämper, M., Teagle, D.A., Butterfield, D.A., Alt, J.C. and Halliday, A.N. (2006) Hydrothermal fluid fluxes calculated from the isotopic mass balance of thallium in the ocean crust. Earth and Planetary Science Letters 251, 120-133.

O'Neil, J.R. (1986) Theoretical and experimental aspects of isotopic fractionation. Reviews in Mineralogy 16, 1-40.

Opfergelt, S., Burton, K., Georg, R., West, A., Guicharnaud, R., Sigfusson, B., Siebert, C., Gislason, S. and Halliday, A. (2014) Magnesium retention on the soil exchange complex controlling Mg isotope variations in soils, soil solutions and vegetation in volcanic soils, Iceland. Geochimica et Cosmochimica Acta 125, 110-130.

Opfergelt, S., Georg, R., Delvaux, B., Cabidoche, Y.-M., Burton, K. and Halliday, A. (2012) Mechanisms of magnesium isotope fractionation in volcanic soil weathering sequences, Guadeloupe. Earth and Planetary Science Letters 341, 176-185.

Ostroumov, V., Hoover, R., Ostroumova, N., Van Vliet-Lanoë, B., Siegert, C. and Sorokovikov, V. (2001) Redistribution of soluble components during ice segregation in freezing ground. Cold regions science and technology 32, 175-182.

Pagani, M., Liu, Z., LaRiviere, J. and Ravelo, A.C. (2010) High Earth-system climate sensitivity determined from Pliocene carbon dioxide concentrations. Nature Geoscience 3, 27.

Patterson, M., McKay, R., Naish, T., Escutia, C., Jimenez-Espejo, F., Raymo, M., Meyers, S., Tauxe, L., Brinkhuis, H. and Expedition, I. (2014) Orbital forcing of the East Antarctic ice sheet during the Pliocene and Early Pleistocene. Nature Geoscience 7, 841.

Pettit, E.C., Whorton, E.N., Waddington, E.D. and Sletten, R.S. (2014) Influence of debris-rich basal ice on flow of a polar glacier. Journal of Glaciology 60, 989-1006.

Péwé, T.L. (1960) Multiple glaciation in the McMurdo Sound region, Antarctica: A progress report. The Journal of Geology, 498-514.

Pollard, D., DeConto, R.M. and Alley, R.B. (2015) Potential Antarctic Ice Sheet retreat driven by hydrofracturing and ice cliff failure. Earth and Planetary Science Letters 412, 112-121.

Prentice, M., Bockheim, J., Wilson, S., Burckle, L., Hodell, D., Schlüchter, C. and Kellogg, D. (1993) Late Neogene Antarctic glacial history: evidence from central Wright Valley. The Antarctic Paleoenvironment: A Perspective on Global Change: Part Two 60, 207-250.

Prentice, M. and Krusic, A. (2005) Early Pliocene alpine glaciation in Antarctica: terrestrial versus tidewater glaciers in Wright Valley. Geografiska Annaler: Series A, Physical Geography 87, 87-109.

Prentice, M.L., Kleman, J.L. and Stroeven, A.P. (1998a) The composite glacial erosional landscape of the northern McMurdo Dry Valleys: Implications for Antarctic Tertiary glacial history. Wiley Online Library.

Prentice, M.L., Kleman, J.L. and Stroeven, A.P. (1998b) The composite glacial erosional landscape of the northern McMurdo Dry Valleys: Implications for Antarctic Tertiary glacial history. Ecosystem Dynamics in a Polar Desert: the Mcmurdo Dry Valleys, Antarctica 72, 1-38.

Quinn, J., Graff, T. and Ming, D. (2020) X-ray Amorphous Components of Antarctica Dry Valley Soils: Weathering Implications for Mars.

Raymo, M.E., Lisiecki, L. and Nisancioglu, K.H. (2006) Plio-Pleistocene ice volume, Antarctic climate, and the global δ18O record. Science 313, 492-495.

Riordan, A. (1973) The climate of Vanda Station, Antarctica. Climate of the Arctic, 268-275.

Ross, C.S. and Hendricks, S.B. (1945) Minerals of the montmorillonite group: Their origin and relation to soils and clays. US Government Printing Office.

Rustad, J.R., Casey, W.H., Yin, Q.-Z., Bylaska, E.J., Felmy, A.R., Bogatko, S.A., Jackson, V.E. and Dixon, D.A. (2010) Isotopic fractionation of Mg2+ (aq), Ca2+ (aq), and Fe2+ (aq) with carbonate minerals. Geochimica et Cosmochimica Acta 74, 6301-6323.

Ryu, J.-S., Vigier, N., Decarreau, A., Lee, S.-W., Lee, K.-S., Song, H. and Petit, S. (2016) Experimental investigation of Mg isotope fractionation during mineral dissolution and clay formation. Chemical Geology 445, 135-145.

Ryu, J.-S., Vigier, N., Derry, L. and Chadwick, O.A. (2021) Variations of Mg isotope geochemistry in soils over a Hawaiian 4 Myr chronosequence. Geochimica et Cosmochimica Acta 292, 94-114.

Schaefer, C.E.G., Michel, R.F., Delpupo, C., Senra, E.O., Bremer, U.F. and Bockheim, J.G. (2017) Active layer thermal monitoring of a Dry Valley of the Ellsworth Mountains, Continental Antarctica. Catena 149, 603-615.

Schäfer, J.M., Baur, H., Denton, G.H., Ivy-Ochs, S., Marchant, D.R., Schlüchter, C. and Wieler, R. (2000) The oldest ice on Earth in Beacon Valley, Antarctica: new evidence from surface exposure dating. Earth and Planetary Science Letters 179, 91-99.

Schauble, E.A. (2011) First-principles estimates of equilibrium magnesium isotope fractionation in silicate, oxide, carbonate and hexaaquamagnesium (2+) crystals. Geochimica et Cosmochimica Acta 75, 844-869.

Scherer, R., Bohaty, S., Dunbar, R.B., Esper, O., Flores, J.A., Gersonde, R., Harwood, D., Roberts, A. and Taviani, M. (2008) Antarctic records of precession-paced insolation-

driven warming during early Pleistocene Marine Isotope Stage 31. Geophysical Research Letters 35.

Schiller, M., Dickinson, W., Iverson, N. and Baker, J. (2019) A re-evaluation of the Hart Ash, an important stratigraphic marker: Wright Valley, Antarctica. Antarctic Science 31, 139-149.

Scopelliti, G., Bellanca, A., Monien, D. and Kuhn, G. (2013) Chemostratigraphy of the early Pliocene diatomite interval from MIS AND-1B core (Antarctica): Palaeoenvironment implications. Global and Planetary Change 102, 20-32.

Scopelliti, G., Bellanca, A. and Neri, R. (2011) Petrography and carbonate isotope stratigraphy from MIS AND-1B core, Antarctica: Evidence of the early Pliocene warming event. Global and Planetary Change 76, 22-32.

Scott, R.F. (1907) The voyage of the Discovery. Charles Scribner's Sons.

Seki, O., Foster, G.L., Schmidt, D.N., Mackensen, A., Kawamura, K. and Pancost, R.D. (2010) Alkenone and boron-based Pliocene pCO 2 records. Earth and Planetary Science Letters 292, 201-211.

Shalev, N., Bontognali, T.R., Wheat, C.G. and Vance, D. (2019) New isotope constraints on the Mg oceanic budget point to cryptic modern dolomite formation. Nature communications 10, 1-10.

SHAW, J. (1977) Till body morphology and structure related to glacier flow. Boreas 6, 189-201.

Sletten, R., Hallet, B. and Fletcher, R. (2003) Resurfacing time of terrestrial surfaces by the formation and maturation of polygonal patterned ground. Journal of geophysical research: Planets 108.

Smellie, J.L., Rocchi, S., Wilch, T.I., Gemelli, M., Di Vincenzo, G., McIntosh, W., Dunbar, N., Panter, K. and Fargo, A. (2014) Glaciovolcanic evidence for a polythermal Neogene East Antarctic ice sheet. Geology 42, 39-41.

Staiger, J., Marchant, D., Schaefer, J., Oberholzer, P., Johnson, J., Lewis, A. and Swanger, K. (2006a) Plio-Pleistocene history of Ferrar Glacier, Antarctica: Implications for climate and ice sheet stability. Earth and Planetary Science Letters 243, 489-503.

Staiger, J.W., Gosse, J., Little, E.C., Utting, D.J., Finkel, R., Johnson, J.V. and Fastook, J. (2006b) Glacial erosion and sediment dispersion from detrital cosmogenic nuclide analyses of till. Quaternary Geochronology 1, 29-42.

Stefánsson, A., Gíslason, S.R. and Arnórsson, S. (2001) Dissolution of primary minerals in natural waters: II. Mineral saturation state. Chemical Geology 172, 251-276.

Stone, J. (2004) Extraction of Al and Be from quartz for isotopic analysis. UW Cosmogenic Nuclide Lab Methods and Procedures.

Stroeven, A.P. and Prentice, M.L. (1997) A case for Sirius Group alpine glaciation at Mount Fleming, South Victoria Land, Antarctica: a case against Pliocene East Antarctic ice sheet reduction. Geological Society of America Bulletin 109, 825-840.

Stuiver, M., Yang, I.C., Denton, G.H. and Kellogg, T.B. (1981) Oxygen isotope ratios of Antarctic permafrost and glacier ice. Dry valley drilling project 33, 131-139.

Swanger, K.M., Babcock, E., Winsor, K. and Valletta, R.D. (2019) Rock glaciers in Pearse Valley, Antarctica record outlet and alpine glacier advance from MIS 5 through the Holocene. Geomorphology 336, 40-51.

Swanger, K.M., Lamp, J.L., Winckler, G., Schaefer, J.M. and Marchant, D.R. (2017) Glacier advance during marine Isotope stage 11 in the McMurdo dry valleys of Antarctica. Scientific reports 7, 41433.

Swanger, K.M., Marchant, D.R., Schaefer, J.M., Winckler, G. and Head III, J.W. (2011a) Elevated East Antarctic outlet glaciers during warmer-than-present climates in southern Victoria Land. Global and Planetary Change 79, 61-72.

Swanger, K.M., Marchant, D.R., Schaefer, J.M., Winckler, G. and Head, J.W. (2011b) Elevated East Antarctic outlet glaciers during warmer-than-present climates in southern Victoria Land. Global and Planetary Change 79, 61-72.

Talarico, F.M., McKay, R.M., Powell, R.D., Sandroni, S. and Naish, T. (2012) Late Cenozoic oscillations of Antarctic ice sheets revealed by provenance of basement clasts and grain detrital modes in ANDRILL core AND-1B. Global and Planetary Change 96, 23-40.

Tamppari, L., Anderson, R., Archer Jr, P., Douglas, S., Kounaves, S., McKay, C., Ming, D., Moore, Q., Quinn, J. and Smith, P. (2012a) Effects of extreme cold and aridity on soils and habitability: McMurdo Dry Valleys as an analogue for the Mars Phoenix landing site. Antarctic Science 24, 211.

Tamppari, L., Anderson, R., Archer, P., Douglas, S., Kounaves, S., McKay, C., Ming, D., Moore, Q., Quinn, J. and Smith, P. (2012b) Effects of extreme cold and aridity on soils and habitability: McMurdo Dry Valleys as an analogue for the Mars Phoenix landing site. Antarctic Science 24, 211-228.

Teng, F.-Z. (2017) Magnesium isotope geochemistry. Reviews in Mineralogy and Geochemistry 82, 219-287.

Teng, F.-Z., Li, W.-Y., Rudnick, R.L. and Gardner, L.R. (2010) Contrasting lithium and magnesium isotope fractionation during continental weathering. Earth and Planetary Science Letters 300, 63-71.

Teng, F.-Z., Wadhwa, M. and Helz, R.T. (2007) Investigation of magnesium isotope fractionation during basalt differentiation: implications for a chondritic composition of the terrestrial mantle. Earth and Planetary Science Letters 261, 84-92.

Teng, F.Z., Li, W.Y., Ke, S., Yang, W., Liu, S.A., Sedaghatpour, F., Wang, S.J., Huang, K.J., Hu, Y. and Ling, M.X. (2015) Magnesium isotopic compositions of international geological reference materials. Geostandards and Geoanalytical Research 39, 329-339.

Teng, F.Z. and Yang, W. (2014) Comparison of factors affecting the accuracy of high-precision magnesium isotope analysis by multi-collector inductively coupled plasma mass spectrometry. Rapid Communications in Mass Spectrometry 28, 19-24.

Thompson, L.G. (1973) Analysis of the concentration of microparticles in an ice core from Byrd station, Antarctica. Research Foundation and the Institute of Polar Studies, The Ohio State ….

Tice, A.R., Yuanlin, Z. and Oliphant, J. (1985) The effects of soluble salts on the unfrozen water contents of the Lanzhou, PRC, silt. Journal of Glaciology and Geocryology 2.

Tipper, E., Galy, A., Gaillardet, J., Bickle, M., Elderfield, H. and Carder, E. (2006) The magnesium isotope budget of the modern ocean: constraints from riverine magnesium isotope ratios. Earth and Planetary Science Letters 250, 241-253.

Tipper, E.T., Calmels, D., Gaillardet, J., Louvat, P., Capmas, F. and Dubacq, B. (2012a) Positive correlation between Li and Mg isotope ratios in the river waters of the Mackenzie Basin

challenges the interpretation of apparent isotopic fractionation during weathering. Earth and Planetary Science Letters 333, 35-45.

Tipper, E.T., Gaillardet, J., Louvat, P., Capmas, F. and White, A.F. (2010) Mg isotope constraints on soil pore-fluid chemistry: evidence from Santa Cruz, California. Geochimica et Cosmochimica Acta 74, 3883-3896.

Tipper, E.T., Lemarchand, E., Hindshaw, R.S., Reynolds, B.C. and Bourdon, B. (2012b) Seasonal sensitivity of weathering processes: Hints from magnesium isotopes in a glacial stream. Chemical Geology 312, 80-92.

Toner, J.D. and Sletten, R.S. (2013) The formation of Ca-Cl-rich groundwaters in the Dry Valleys of Antarctica: Field measurements and modeling of reactive transport. Geochimica et Cosmochimica Acta 110, 84-105.

Toner, J.D., Sletten, R.S. and Prentice, M.L. (2013) Soluble salt accumulations in Taylor Valley, Antarctica: implications for paleolakes and Ross Sea Ice Sheet dynamics. Journal of Geophysical Research: Earth Surface 118, 198-215.

Ugolini, F. (1986) Processes and rates of weathering in cold and polar desert environments. Rates of chemical weathering of rocks and minerals, 193-235.

van Breemen, N., Mulder, J. and Driscoll, C. (1983) Acidification and alkalinization of soils. Plant and soil 75, 283-308.

von Strandmann, P.A.P., Burton, K.W., James, R.H., van Calsteren, P., Gislason, S.R. and Sigfússon, B. (2008) The influence of weathering processes on riverine magnesium isotopes in a basaltic terrain. Earth and Planetary Science Letters 276, 187-197.

von Strandmann, P.A.P., Opfergelt, S., Lai, Y.-J., Sigfússon, B., Gislason, S.R. and Burton, K.W. (2012) Lithium, magnesium and silicon isotope behaviour accompanying

weathering in a basaltic soil and pore water profile in Iceland. Earth and Planetary Science Letters 339, 11-23.

Webb, P., Harwood, D., McKelvey, B., Mercer, J. and Stott, L.D. (1984) Cenozoic marine sedimentation and ice-volume variation on the East Antarctic craton. Geology 12, 287-291.

Wentworth, S.J., Gibson, E.K., Velbel, M.A. and McKay, D.S. (2005) Antarctic Dry Valleys and indigenous weathering in Mars meteorites: Implications for water and life on Mars. Icarus 174, 383-395.

White, A. (2003) Natural weathering rates of silicate minerals. Treatise on geochemistry 5, 605.

White, A.F., Schulz, M.S., Stonestrom, D.A., Vivit, D.V., Fitzpatrick, J., Bullen, T.D., Maher, K. and Blum, A.E. (2009) Chemical weathering of a marine terrace chronosequence, Santa Cruz, California. Part II: Solute profiles, gradients and the comparisons of contemporary and long-term weathering rates. Geochimica et Cosmochimica Acta 73, 2769-2803.

Wimpenny, J., Colla, C.A., Yin, Q.-Z., Rustad, J.R. and Casey, W.H. (2014) Investigating the behaviour of Mg isotopes during the formation of clay minerals. Geochimica et Cosmochimica Acta 128, 178-194.

Wimpenny, J., Gíslason, S.R., James, R.H., Gannoun, A., Von Strandmann, P.A.P. and Burton, K.W. (2010) The behaviour of Li and Mg isotopes during primary phase dissolution and secondary mineral formation in basalt. Geochimica et Cosmochimica Acta 74, 5259-5279.

Witherow, R.A., Lyons, W.B. and Henderson, G.M. (2010) Lithium isotopic composition of the McMurdo Dry Valleys aquatic systems. Chemical Geology 275, 139-147.

Yang, W., Teng, F.-Z. and Zhang, H.-F. (2009) Chondritic magnesium isotopic composition of the terrestrial mantle: a case study of peridotite xenoliths from the North China craton. Earth and Planetary Science Letters 288, 475-482.

Zhang, T., Barry, R.G., Knowles, K., Heginbottom, J. and Brown, J. (1999) Statistics and characteristics of permafrost and ground‐ice distribution in the Northern Hemisphere. Polar Geography 23, 132-154.

Zhou, Y., Sawyer, A.H., David, C.H. and Famiglietti, J.S. (2019) Fresh submarine groundwater discharge to the near‐global coast. Geophysical Research Letters 46, 5855-5863.